Ultrahigh Pressure Capillary Liquid Chromatography-Mass Spectrometry for Metabolomics and Lipidomics

by

Matthew J. Sorensen

A dissertation submitted in partial fulfillment
of the requirements for the degree of
Doctor of Philosophy
(Chemistry)
in the University of Michigan
2021

Doctoral Committee:

Professor Robert T. Kennedy, Chair
Professor Ormond A. MacDougald
Professor Subramaniam Pennathur
Professor Brandon T. Ruotolo

Matthew J. Sorensen

sorenm@umich.edu

ORCID iD: 0000-0002-9140-1760

Acknowledgements

Countless people have helped me get to where I am at today. I would first like to thank my PhD advisor, Professor Robert Kennedy. Bob has pushed me to work hard and challenged me to think outside the box. He has taught me a lot about the fundamentals of separations, helped me improve my writing skills, helped in countless ways in brainstorming and troubleshooting research ideas, and overall has taught me what it means to be a good analytical scientist.

I would like to thank my committee members, Professors Ormond MacDougald, Brandon Ruotolo, Sub Pennathur, and Brent Martin. They were supportive throughout my graduate school progress and challenged me to think critically about the data that was generated and the experiments that were planned or carried out. Their broad expertise was greatly appreciated and valued, and helped to approach problems from different perspectives.

I would also like to thank my numerous collaborators at Michigan that I was fortunate to work with throughout my time here, including Professor Martin Myers, Professor Jonathan Flak, Professor Darleen Sandoval, Dr. Simon Evers, and Alison Affinati for work with catecholamine determination in plasma and liver; Professor Jun Wu and Drs. Heejin Ju and Alexander Nights for work with acetylcholine determination in adipose tissues; Thomas White and his work with microfabricated push-pull probes for *in vivo* neurochemical monitoring; and Professor Ryan Bailey, Colleen Riordan, and Marina Sarcinella for work with lipid nanodiscs.

I would also like to thank our collaborators at UNC Chapel Hill. Professor Jim Jorgenson and Dr. Kelsey Miller were very helpful in teaching me how to pack columns, several tips on capillary LC, and working together on various lipid projects. I'd also like to thank them for

welcoming me to Chapel Hill when I visited and allowing us to take some instruments when Jim retired. They have been put to good use!

I would like to thank my many undergraduate professors and mentors who taught me a lot about chemistry and motivated me to pursue graduate work. Specifically, I would like to thank Professor Dwight Stoll who allowed me to work in his lab for a number of years and taught me a lot about analytical chemistry and instrumentation. I would also like to thank Professor Jared Anderson who allowed me to conduct research in his lab for a summer, and his graduate student Dr. Kevin Clark who mentored me.

I am grateful for all the Kenney lab members, past and present, whom I had the pleasure to not only work with but enjoy many events outside of lab. I would like to thank Dr. Daniel Steyer for showing me around Ann Arbor during my visitation and also helping out in the lab. I'd like to thank Professor Jim Grinias and Dr. Alec Valenta for being great mentors, particularly when I first started out. I'd like to thank Brady Anderson for being very helpful with capillary LC, metabolomics, and fixing Haskel pumps. I'd like to thank Kelcie Zegalia for the many fruitful discussions and troubleshooting ideas mostly regarding capillary LC-MS. I'd like to thank Dr. Brian Shay for many helpful discussions, troubleshooting ideas, and instrument repairs. I'd like to thank Dr. Sugyan Dixit for help writing code for data processing. I'd like to acknowledge Heidi Baum, Drs. Maureen Kachman, TM Rajendiran, Stephanie Wernisch, and Charles Evans at the metabolomics core. I'd also like to thank Dr. Jen LaBarre for making my time at Brehm at least somewhat enjoyable.

I would like to acknowledge my sources of funding and institutions that donated materials that helped in my graduate studies. I'd like to thank the national institutes of health and the national science foundation for funding sources. I'd like to thank New Objective for donating nESI spray

tips and PicoClear unions. I'd like to thank Waters Corporation, specifically Kevin Wyndham, Martin Gilar, and Tom Walter for donating particles and for other helpful discussions regarding chromatography particles.

I would like to thank my family for providing constant support throughout my graduate school. I've been blessed with great parents and a great brother and sister who make time away from lab enjoyable. I would not be where I am at without them.

Finally, I would like to thank my girlfriend Mandy for providing countless hours of support and for always being there for me. My life has undoubtedly improved since meeting you and I can't wait to see what our future holds.

Table of Contents

List of Tables

List of Figures

List of Appendices

List of Abbreviations

A	Eddy diffusion coefficient
a	Reduced eddy diffusion coefficient
Ach	Acetylcholine
ACM	Acetominophen
AcylCoA	Acyl-Coenzyme A
B	Longitudinal diffusion coefficient
b	Reduced longitudinal diffusion coefficient
BEH	Bridged ethyl hybrid
BPI	Base peak intensity
BzCl	Benzoyl chloride
C	Mass transfer resistance coefficient
c	Reduced mass transfer resistance coefficient
C18	n-Octadecyl
Caff	Caffeine
CE	Cholesteryl ester
Ch	Choline
Chol	Cholesterol
Cer	Ceramide
Cyt	Cytidine
DA	Dopamine
Da	Dalton
DDA	Data dependent acquisition
DG	Diacylglycerol
D_m	Diffusion coefficient in the mobile phase
DOPAC	3,4-Dihydroxyphenylacetic acid
d_p	Particle diameter
EIC	Extracted ion chromatogram
ESI	Electrospray ionization
FA	Fatty acid
FT-ICR	Fourier transform ion cyclotron resonance
FWHM	Full width at half maximum
GC	Gas chromatography
h	Reduced plate height
h_{min}	Reduced plate height minimum
HETP or H	Height equivalent to a theoretical plate or plate height
HexCer	Hexosyl ceramide
HILIC	Hydrophilic interaction liquid chromatography
HiP	High pressure equipment company

H_{min}	Plate height minimum
HPLC	High performance/pressure liquid chromatography
i.d.	Inner diameter
k'	Retention factor
L	Column length
LPC	Lysophosphatidylcholine
LPE	Lysophosphatidylethanolamine
LPG	Lysophosphatidylglycerol
m/z	Mass to charge ratio
MG	Monoacylglycerol
MS	Mass spectrometry
MS/MS	Tandem mass spectrometry
N	Theoretical plates
n_c	Peak capacity
NE	Norepinephrine
nESI	Nanoelectrospray ionization
NMR	Nuclear magnetic resonance
NP	Normal phase
o.d.	Outer diameter
OT	Open tubular
P	Pressure
PA	Phosphatidic acid
PAC	Pillar array column
PC	Phosphatidylcholine
PE	Phosphatidylethanolamine
PEEK	Polyether ether ketone
PG	Phosphatidylglycerol
Phe	Phenylalanine
PI	Phosphatidylinositol
PIP	Phosphatidylinositol phosphate
Pro	Proline
PS	Phosphatidylserine
PSD	Particle size distribution
Psi	Pounds per square inch
Q-ToF	Quadrupole-Time of flight
RP	Reversed phase
R_S	Resolution
RSD	Relative standard deviation
SEM	Scanning electron microscopy
SFC	Supercritical fluid chromatography
SM	Sphingomyelin
t_0	Dead time
TG	Triacylglycerol
t_G	Gradient time
Trp	Tryptophan
t_R	Retention time

Tyr	Tyrosine
u	Mobile phase linear velocity
UHPLC	Ultrahigh pressure/performance liquid chromatography
u_{opt}	Velocity that produces H_{min}
UV	Ultraviolet
v	Reduced linear velocity
v/v	Volume by volume
Val	Valine
w/v	Weight by volume
$W_{4\sigma}$	Peak width at the base
η	Viscosity
σ	Standard deviation
°C	Degrees Celsius
1D	One-dimensional
2D	Two-dimensional
^{1}D	First dimension
^{2}D	Second dimension
5-HT	Serotonin

Abstract

Metabolites and lipids are important compounds involved in various cellular processes. The comprehensive analysis of all metabolite and lipid species, termed metabolomics and lipidomics, respectively, is challenging due to the large size, chemical diversity, and concentration range of the metabolome and lipidome. Liquid chromatography coupled with mass spectrometry (LC-MS) is a powerful tool for metabolomics and lipidomics due to its sensitivity, selectivity, and amenability to a broad range of compounds. The goal of this thesis is to evaluate and demonstrate improvements in capillary LC-MS based metabolomics and lipidomics primarily using custom-built chromatography instrumentation capable of operating at 35 kpsi compared to what is currently commercially available.

Lipid separations were evaluated from plasma extracts using one- and two-dimensional liquid chromatography coupled with mass spectrometry. Use of 50 cm columns with 1.7 µm C18 particles provided up to a 95% increase in peak capacity compared to commercial limitations. We evaluated the effect of column and gradient length on the number of lipids detected from plasma and found a roughly linear relationship between peak capacity and lipids detected, illustrating the benefits of improved separation performance in lipidomic assays. An offline two-dimensional LC-MS system was developed utilizing HILIC in the first dimension to fractionate lipids from plasma based on their class, followed by re-injection on the 50 cm capillary columns. The 2D method demonstrated high orthogonality, achieved a peak capacity of approximately 1900 in 600 min, and detected roughly double the number of lipids compared to the one-dimensional work.

We evaluated the potential for fast yet high efficiency metabolite separations using porous C18 particles down to 1.1 µm and pressures up to 35 kpsi. Use of these particle sizes is possible with 35 kpsi available and are useful for high throughput metabolomics measurements. Columns were evaluated using isocratic and gradient separations of standards and metabolite extracts from plasma. Peak capacities of roughly 100 – 400 were achieved in 8 – 40 min with interfacing to MS, demonstrating relatively fast and high-resolution separations. We evaluated the effect of different LC-MS variables on mass spectral feature detection. Lower flow rates (down to 700 nL/min) and larger injection volumes (up to 1 µL) increased the features detected, demonstrating practical benefits for metabolomics assays.

Finally, gradient LC-MS operation up to 50 kpsi is achieved and peak capacities over 1000 are demonstrated. Gradient kinetic plots were constructed to guide choice of column length, particle size, and gradient time. Use of 100 cm capillaries packed with 1.7 µm particles achieved a peak capacity of ~1000 in about 4 h. Separations at 50 kpsi are achieved but not feasible for routine use with current hardware. Instrument modifications are evaluated and discussed for routine, leak-free operation at 50 kpsi.

The work described in this thesis describes approaches for improving LC-MS based metabolomics and lipidomics through improvements in separations primarily at 35 kpsi and using 1.1 – 1.7 µm particles packed in 20 – 100 cm long columns. This work illustrates practical applications of ultrahigh pressures in liquid chromatography and discusses advantages of such instrumentation in LC-MS based assays.

Chapter 1. Introduction

1.1. Metabolomics and lipidomics

1.1.1. Motivation for studying lipids and metabolites

Lipids and metabolites are relatively small molecules (< 2000 Da) involved in a variety of functions within living organisms. Lipids and metabolites are often closely related to the observed phenotype and are often considered the end product of the flow of information in an organism, also known as the central dogma. Studying the dynamics of metabolites and lipids can thus give insight into disease states and to help understand physiological mechanisms in systems biology. Figure 1-1 shows an illustration of the central dogma, with each sector including the associated "omics" technology, and thus forming what is often referred to as the "omics cascade".

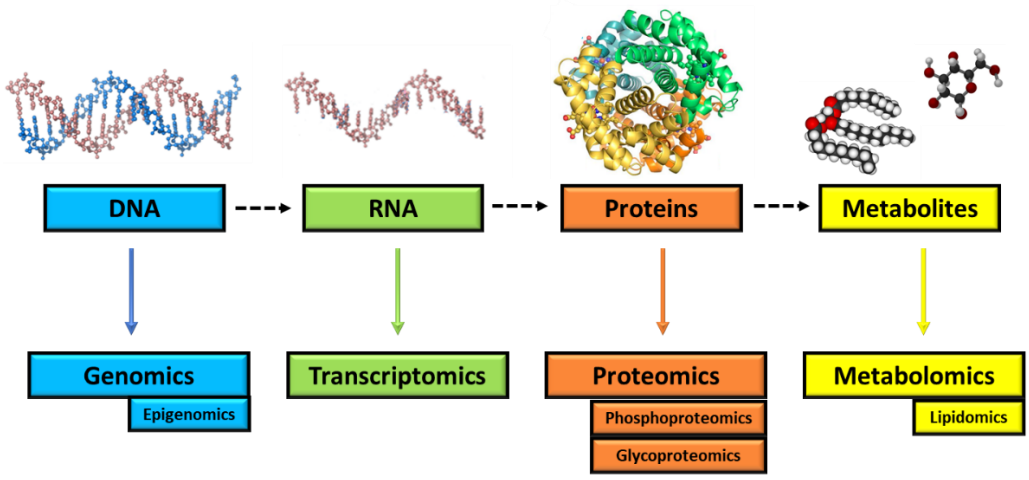

Figure 1-1. Schematic representation of the central dogma – the flow of information through a living organism – and their complementary -omics technologies with notable sub-disciplines. Adopted from Arújo et. al.[1]

The comprehensive analysis of metabolites is termed metabolomics. Lipidomics is a sub-field of metabolomics devoted to the comprehensive study of lipids and is often independent of metabolomics due to the complexity of the lipidome and the differences in biological functions and physicochemical properties of lipids. Metabolomics and lipidomics analyses can be performed in what's termed targeted or untargeted manners. In a targeted analysis, a set number of compounds are studied and quantified.[2] Generally, these analyses are hypothesis-driven with expectation of the target analytes being up-regulated or down-regulated. The goal of an untargeted analysis is to identify and quantify all the metabolites or lipids in the sample of interest; these studies are often hypothesis-generating. Metabolomics and lipidomics studies have been applied in many areas, including food science, plant biology, biofuels, environmental studies, and biomarker and drug discovery for animal and human health.[1,3–5] Diseases such as Alzheimer's, Parkinson's, diabetes, and chronic kidney disease have all been associated with altered metabolite or lipid profiles.[6,7]

1.1.2. Challenges of metabolomics

One of the biggest challenges in untargeted metabolomics and lipidomics arises from the large number of metabolites and lipids present in most biological or environmental samples. In humans for example, there are over 40,000 confirmed endogenous metabolites, and thousands more arising from external environments and activities.[8–10] Moreover, the diverse physicochemical properties and large concentration range of metabolites adds more challenges. Thus, no single analytical technique has been developed yet that can measure all metabolites in a single analysis.[11]

Identification and quantitation are also challenging in metabolomics. Targeted metabolomics offers better quantitation than untargeted approaches due to the use of standards and internal standards for calibration and to account for sample preparation errors and instrumental

drift. Additionally, methods can be modified to optimize resolution and signal intensity of the target analytes.

Untargeted methods, on the other hand, typically involve less method development and employ more general instrumental conditions to attempt to analyze as many compounds as possible. Identification remains a challenge due to the lack of standards available and the difficulty in implementing standards for all the potential compounds being measured. Additionally, unlike genomics or proteomics, metabolites are not comprised of smaller repeating units/monomers, and thus cannot be sequenced. Identification therefore typically relies on a combination of retention time data, accurate mass, tandem mass(es), drift time, chemical shift, and reference (external or internal) standards, depending on the analytical method of choice. These data are then imported into different databases, such as XCMS, LipidBlast, and the NIST standard reference database.[10,12–14]

1.1.3. Analytical strategies for metabolomics

A number of techniques are used in metabolomics. These techniques include spectroscopy, separation systems, and mass spectrometry (MS).[15,16] Spectroscopic instrumentation such as nuclear magnetic resonance (NMR), Raman, and infrared spectroscopy are useful tools for identification and quantitation of metabolites. NMR in particular has shown utility in various metabolomics studies and provides good information content such as structural identification and quantification, has good reproducibility, and is relatively high throughput.[17,18] The main disadvantage of spectroscopic techniques is the poor sensitivity, with detection limits typically on the ~mM to μM levels. In addition, efficient coupling of these instruments to separation systems for sample cleanup and preconcentration remains a challenge.

MS-based metabolomics typically offers better sensitivity than spectroscopic techniques, with detection limits down to picomolar or femtomolar levels being achieved.[19–21] A general overview of MS-based metabolomics is shown in Figure 1-2. MS-based metabolomics is a versatile technique that can be used for targeted analyses, typically employing triple quadrupole instrumentation, and untargeted analyses, using full-scan acquisition typically with time-of-flight (ToF) or orbital based (Orbitrap or FT-ICR) instruments. Furthermore, different ionization techniques such as electron impact, electrospray ionization (ESI), matrix assisted laser desorption/ionization, among others, in addition to positive and negative polarities, can be used depending on the properties of the analytes of interest. Lastly, MS is easily interfaced with separation techniques, which can provide enhanced metabolite and lipid coverage.

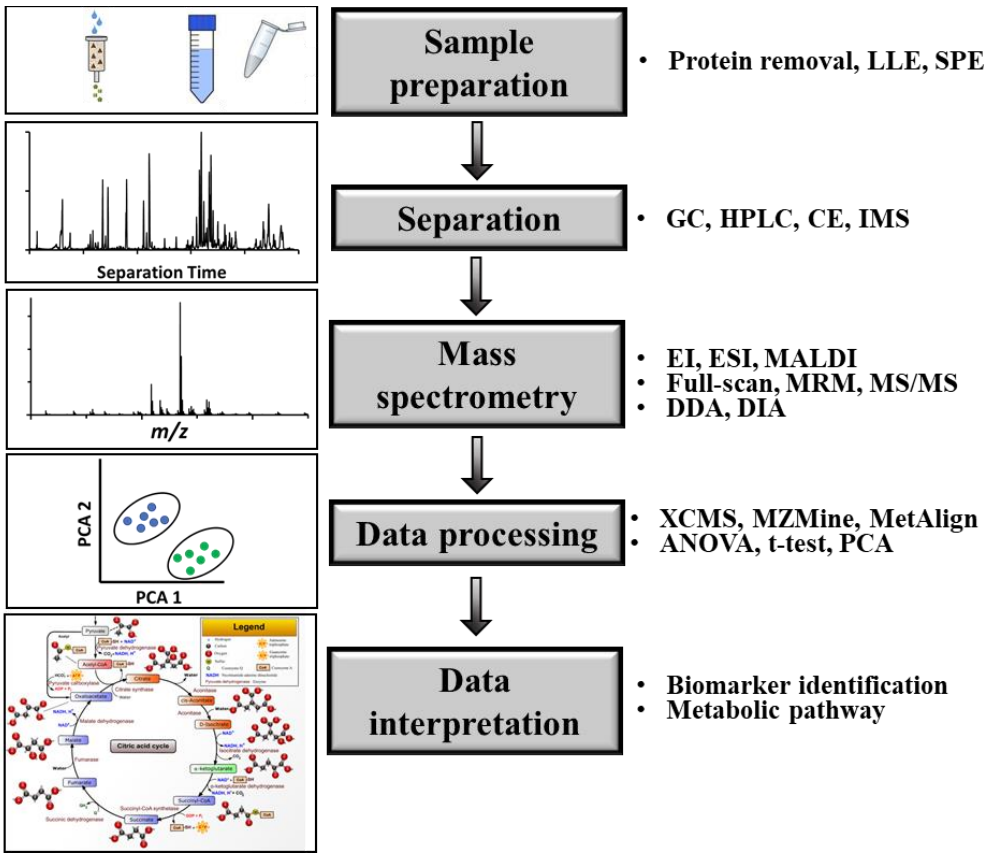

Figure 1-2. Typical workflow for MS-based metabolomics. Adapted from Wang et. al.[22]

Separations are an important step in most metabolomic assays as the majority of samples are very complex and potentially contain 10s of thousands to 100s of thousands of compounds. This complexity challenges the goals in achieving high metabolome coverage in untargeted workflows. Separations help by decreasing ionization suppression due to co-eluting species, separating isobaric and isomeric analytes, providing cleaner mass spectra for spectral matching and interpretation, and providing additional retention time information.[23–25] Ionization suppression is problematic for MS-based analysis of complex biological matrices such as plasma and can limit sensitivity.[26] Most separation techniques are amenable for online coupling with MS, allowing for relatively high throughput analysis. High efficiency separations are particularly desired for untargeted approaches where the goal is to achieve the highest number and confidence of identifications.

Gas chromatography (GC) is a popular technique for metabolite and lipid separations and is easily interfaced to MS for detection and identification;[27,28] however, the technique comes with numerous drawbacks. First, analytes must be volatile to be separated. Derivatization can be done to increase the volatility of certain compounds; however, this adds additional sample preparation steps, may not be amenable to all compounds, and may increase sample complexity due to undesired or incomplete derivatization. GC-MS analysis is also limited to thermally stable analytes, as thermally labile analytes may not be detected or have inaccurate quantitation.

Electrophoretic techniques are useful for separating charged species and can offer high separation efficiency, however interfacing to MS has remained a challenge. Additionally, target analytes are often limited to charged species and often necessitate derivatization. Nonetheless, metabolomics studies have been reported using electrophoretic techniques, most popular being capillary zone electrophoresis and micellular electrokinetic chromatography.[29–31]

Supercritical fluid chromatography (SFC) has been used for metabolite and lipid separations, with notable advantages including faster separations with minimal loss in performance and environmentally friendly mobile phases such as supercritical CO_2. SFC has been coupled to MS for both metabolomics and lipidomics applications.[32–34]

High performance liquid chromatography (HPLC) is perhaps the dominant approach for metabolite and lipid separations.[22,35,36] HPLC is amenable to most analytes, without the need for molecules to be volatile or charged. Furthermore, different modes of HPLC can be used depending on the physicochemical properties of the target analytes. The most common modes include reversed phase (RP) HPLC, which employs a hydrophobic stationary phase (most often n-octadecyl (C18)), and hydrophilic interaction HPLC (HILIC), which employs a hydrophilic interaction stationary phase (such as diol, amino-based, and amide-based functional groups). Additionally, both RP-LC and HILIC use a mixture of water and water-miscible organics (e.g., methanol or acetonitrile) as mobile phase, providing easy online coupling to MS most often through ESI or nanoESI (nESI) interfaces.

1.2. Chromatographic theory

1.2.1. Description of separation performance

Imperative to improving HPLC separations as a means to expand LC-MS based metabolomics is the need to understand what goes on inside the column and factors that influence analyte broadening during a separation. As an analyte moves through a chromatographic column, a Gaussian distribution, with an associated standard deviation (σ), is formed. This distribution, also known as a 'band' or 'zone', is a measure of the quality of the separation.[37] The overall quality of a separation, and thus the packing quality of the column, is often described by the height

equivalent of a theoretical plate (HETP), or simply termed the plate height, H, which relates the square of the band standard deviation, also known as the variance, to the column length (L):

$$H = \frac{\sigma^2}{L} \qquad \text{eq. 1-1}$$

Plate height provides good indication on the separation and packing quality of a given column, with values of the reduced plate heights (h, equal to H/d_p) less than 2 typically indicating a "well-packed" column. Plate height is not a good descriptor for total column performance, however, because it normalizes for column length. The efficiency of a column is thus described by the total number of theoretical plates (N) that are generated during the separation; N is a universal, dimensionless value that can be applied to most separations, not only chromatographic separations. Plate height and plate number are related through the column length:

$$N = \frac{L}{H} \qquad \text{eq. 1-2}$$

That is, longer columns will produce higher plate numbers assuming the packing quality is the same. The terminology of plate number and plate height dates to classic distillation procedures, where 'N' number of equilibrations are carried out successively. Hence, more equilibration events (higher N values) equate to a more efficient separation. Through substitution of equation 1 and 2, the efficiency of a column can be written in terms of the variance of a zone:

$$N = \frac{L^2}{\sigma^2} \qquad \text{eq. 1-3}$$

Lastly, the measured resolution between two peaks of interest is another good description of separation performance. The resolution of two peaks is described by:

$$R_s = \frac{t_{R,2} - t_{R,1}}{0.5(W_{4\sigma,1} + W_{4\sigma,2})} \qquad \text{eq. 1-4}$$

Resolution can thus be improved by employing longer columns and/or particle sizes to decrease $W_{4\sigma}$. It can also be improved by employing alternative stationary phase chemistries, mobile phase

compositions, changing column temperature, and a number of other variables.[38] Indeed, these variables should be investigated first in attempt to increase resolution between peaks; however, for complex mixture analysis with 100s – 1000s of compounds, resolution between all peaks is simply impossible.[39] Hence, increasing N is the most effective means at increasing resolution of complex mixtures such as those encountered in lipidomic and metabolomic analyses.

1.2.2. Theory of gradient separations

Gradient separations, where the mobile phase composition changes throughout the separation, are important for decreasing analysis time and expanding the polarity range when many different compounds need to be separated in a single run. In metabolomics and lipidomics, the samples may contain thousands of different compounds with a wide range of physicochemical properties. For example, the logP of the amino acid proline is -2.7, whereas the triacylglycerol 42:0 is 18.7, over 21 orders of magnitude difference.[40,41]

While theoretical plates and plate height are the best assessment of column performance for isocratic separations, they do not hold true for gradient separations. A useful best metric for assessing column performance under gradient elution conditions is the peak capacity, n_c. The peak capacity is defined as the total number of peaks that can be separated with unit resolution over the course of the separation.[42] An approximate estimate for peak capacity and the relationship between theoretical plates is shown through equation 1-5:

$$n_c = \frac{\sqrt{N}}{4} ln(\frac{t_G}{t_0}) \qquad \text{eq. 1-5}$$

Where t_G is the gradient time and t_0 is the dead time. As a result, with the square root relationship, doubling the number of plates should result in a ~1.4X increase in peak capacity, assuming other gradient parameters such as gradient slope remain constant. Additionally, increasing gradient time will increase peak capacity but with diminishing returns through the logarithmic relationship. For

reference, commercial HPLC typically achieves peak capacities of ~200 (discussed more in section 1.3). The peak capacity is empirically calculated through the following equation:

$$n_c = 1 + \frac{t_G}{W_{4\sigma}} \quad \text{eq. 1-6}$$

1.2.3. The van Deemter curve

In the mid 1950s, van Deemter described the effect of the linear velocity of the mobile phase, *u*, on the observed plate height.[43] It was found that a minimum in H (H_{min}) was found at intermittent velocities. This minimum was due to a balance between excessive longitudinal diffusion at very slow velocities, and resistance to mass transfer at high linear velocities. The van Deemter equation which fit experimental data was derived:

$$H = A + \frac{B}{u} + Cu \quad \text{eq. 1-7}$$

Where the A, B, and C terms account for eddy dispersion, longitudinal diffusion, and mass transfer, respectively. Other similar equations were expressed by others in the field, with minor differences accounting for factors such as velocity-dependent eddy dispersion and mass transfer arising from stagnant mobile phase, among others.[44–46] Furthermore, "reduced parameters" were developed which normalizes the plate height and linear velocity to better compare columns and experiments with different particle sizes and diffusion coefficients (D_m). The reduced plate height, *h*, and reduced linear velocity, *v*, are defined as:

$$h = \frac{H}{d_p} \quad \text{eq. 1-8}$$

$$v = \frac{ud_p}{D_m} \quad \text{eq. 1-9}$$

Despite continued refinements and studies on the understanding and description of band broadening in chromatographic beds,[47] the van Deemter model continues to be used for describing the quality of a packed column and the factors that cause nonidealities in the separation.

1.2.4. Effect of particle size on plate height

Over the latter half of the 20th century and continuing today, there has been a steady decrease in the size of particles used in HPLC columns.[48] Currently, particle diameters (d_p) below 2 µm are primarily used in most HPLC systems. Smaller particles reduce band broadening due to eddy dispersion and mass transfer (A and C terms above), described by the first and third term of equation 1-10:

$$H = \lambda d_p + \frac{2\gamma D}{u} + \frac{d_p^2 u}{D} \qquad \text{eq. 1-10}$$

Equation 1-10 is a simplified expression of the van Deemter equation for describing the plate height in a chromatographic column that is empirically found to be approximately correct.[49] The constants λ and γ are parameters relating to the quality and presence of the packing, respectively. From equation 4, the impact of particle diameter on plate height is evident. Theoretical van Deemter curves are shown in Figure 1-3 for columns packed with 5, 3, and 1 µm particles. Decreasing particle diameter leads to both smaller plate heights and faster optimal linear velocities (u_{opt}, velocity that produces H_{min}) – the ability to achieve both faster and better separations. This improvement comes at the expense of much higher inlet pressure. For reference, achieving a linear velocity of 1 cm/s on a 10 cm column would require 1800, 5000, and 34000 psi when using 5, 3, and 1 µm particles, respectively.

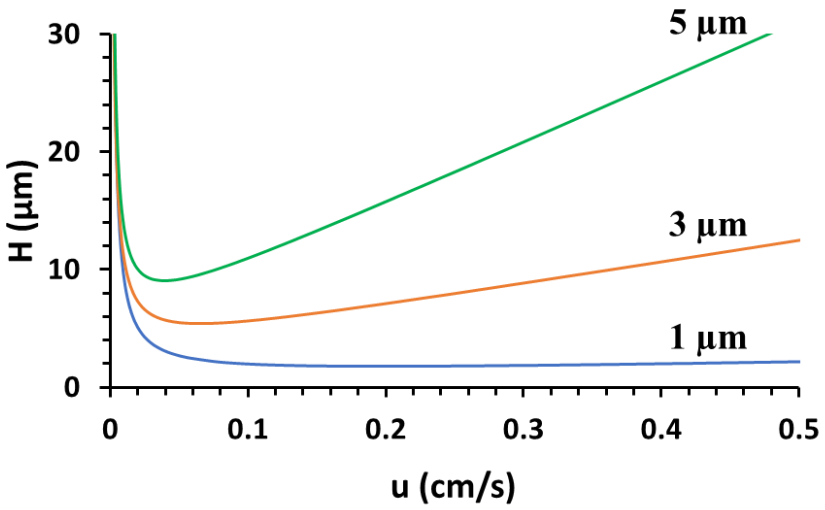

Figure 1-3. Theoretical van Deemter curves illustrating the benefit of utilizing smaller particle diameters in UHPLC. Smaller plate heights and higher optimal linear velocities are expected when using smaller particles.

1.2.5. Effect of smaller particles on column permeability

In the previous sections it was shown that implementing smaller diameter stationary phase particles can improve separation efficiency by decreasing band broadening due to eddy diffusion and resistance to mass transfer. To maintain a given column length, however, much higher back pressure is required to push solvent through a tube packed with such small particles, described through equation 1-11:

$$u = \frac{P d_p^2}{400 \eta L} \qquad \text{eq. 1-11}$$

Where η is the mobile phase viscosity and P is the inlet pressure. Therefore, if the pressure is not high enough, u becomes very slow, and thus the separation is limited by longitudinal diffusion. Additionally, because smaller particles reduce band broadening from mass transfer, the optimum mobile phase velocity, u_{opt}, is proportional to d_p. Taken together, the optimum pressure (e.g., pressure required to reach u_{opt} and h_{min}) is proportional to the cube of the particle diameter. Pressure can thus ultimately be a limiting factor for improvements in separation speed and efficiency when using packed columns.[49–51]

1.2.6. Kinetic plots for quantifying effect of pressure on separation performance

While the van Deemter curve is a good assessment of the quality of the packed column and factors leading to increases in plate height, it does not directly consider analysis time nor take into account column permeability, and thus does not say much about actual analysis time, total plates generated, and pressure limitations. Kinetic plots are helpful in identifying conditions that give a desired performance (theoretical plates) based on d_p, pressure limit, and analysis time.[52,53] Such plots therefore can help to understand when higher pressures are beneficial and should be implemented. Fig. 1-4A shows a kinetic plot illustrating the optimal particle size given a set pressure limit and analysis time.[49] For example, with an analysis time of 2 min, approximately 180,000 plates can be generated with the optimum particle size of 1 μm and 50 kpsi pressure limit. If only 10 kpsi pressure is available, the optimal particle size is 1.5 μm and only 80,000 plates are generated in the same 2 min analysis time. Particle size is often limited to those that are commercially available, and thus the plot in Fig 1-4A is not always practical. Another kinetic plot, sometimes called a Poppe plot, displays the plate time (time it takes to obtain 1 plate) versus plates and is useful for determining when certain particle size and column lengths are beneficial for different desired analysis times given a set pressure limit and particle size. Figure 1-4B shows such a plot for two different particle sizes (0.5 μm and 1.7 μm) and instrument pressure limits (12 kpsi and 50 kpsi). Going from left to right along a curve, column length increases such that dead time and column efficiency are increased. Column dead times are projected as a diagonal line for clarity. From this plot, it is clear how higher instrument pressure can lead to faster separations for a given plate number or higher plate numbers in a given time. For example, plate numbers for a 30 s dead time increase from 35,000 to 88,000 with 0.5 μm particles when 50 kpsi is available compared to 12 kpsi (green versus blue trace). When 1.7 μm particles are used, a more modest increase from

30,000 to 38,000 is achieved from 12 to 50 kpsi and a dead time of 30 s. However, at longer analysis times, e.g., 180 s, 1.7 µm particles are beneficial over 0.5 µm when 50 kpsi is available (blue vs. black trace). Thus, while higher pressures are almost always beneficial when column length or particle size can be varied, the extent of these improvements can vary.[54] Careful consideration of particle size and column length with the desired analysis time and plate count must be done to take advantage of higher pressure.

1.3. Practical uses of ultrahigh pressure liquid chromatography

1.3.1. Isocratic separations up to 100 kpsi

Many researchers have reported injection systems able to withstand very high inlet pressures, with some reports of over 100 kpsi.[51,55,56] These systems are often built around stainless steel valves and tubing that are commercially available, for example from High Pressure (HiP) equipment company. These injection systems typically employ a static-split flow injection scheme.

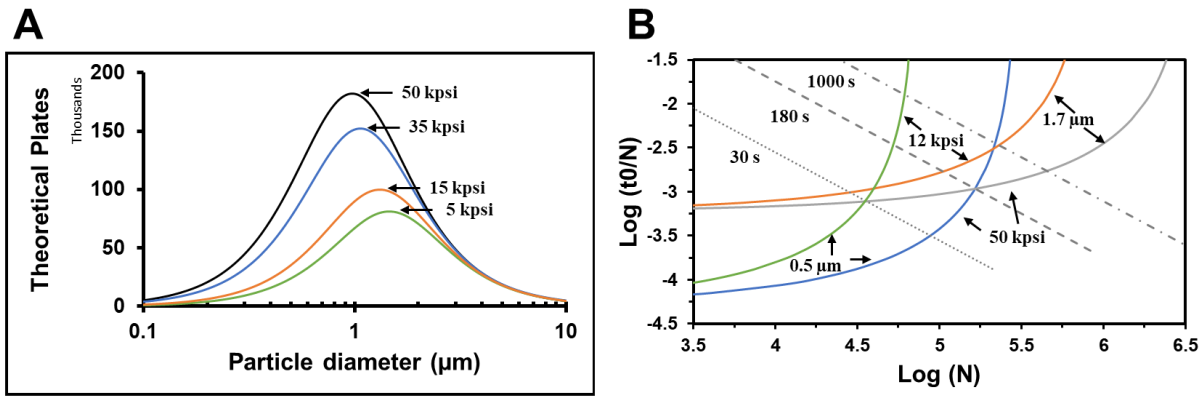

Figure 1-4. Kinetic plots illustrating the effect of operating pressure, particle diameter, column length, and analysis time on efficiency in HPLC. (A) For a set dead time of 2 min, the optimum particle diameter decreases and the number of theoretical plates achieved increases as instrument pressure increases. (B) "Poppe" style kinetic plot illustrating the effect of column length, instrument pressure, and a set particle diameter on time and efficiency. In both graphs, column length is varied along each curve, and minima and maxima occur with a balance between longitudinal diffusion and resistance to mass transfer. For details on kinetic plot construction see Appendix 2.

While these injectors offer very narrow injection bands that are good for column evaluation under isocratic conditions, they often require manual manipulation of valves and waste sample.

Early UHPLC studies heavily relied upon nonporous particles primarily due to their availability in small sizes. Separations were performed in fused silica capillaries from diameters of 10 – 150 μm to minimize heat generation which would otherwise cause axial and radial temperature gradients and significantly impede separation performance. Nonporous reversed-phase particles ranging from 1.0 to 1.5 μm were packed at ~60 kpsi in 40 – 50 cm × 30 μm capillaries and operated up to 100 kpsi, generating up to 310,000 plates for a small molecule test mixture with on-column amperometric detection.[55,56] Dead times were a few minutes, much faster than what would be possible at commercial pressures.

1.3.2. Studies on column packing

In order to realize the expected gains in separation efficiency discussed in section 1.2, columns must be well-packed, typically defined as an h_{min} below 2. While early work with nonporous particles laid the groundwork for UHPLC, the applications were limited due to the low loading capacity of these particles. With the introduction of sub-2 μm porous particles, differences in chromatographic performance were compared to nonporous particles.[57,58] Reduced plate heights as low as 1.6 were observed for 1.5 μm porous particles in 50 cm × 30 μm i.d. capillaries suggesting efficient packing. Higher C-terms were observed with porous particles at high linear velocities due to mass transfer contribution from the stagnant mobile phase. Additionally, the larger particle size distribution arising from synthesis of the porous particles poses potential limits to efficient column preparation.[59] Both the slurry solvent type and concentration influence the quality of the packed column. Using dispersive slurry solvents at low concentrations, packing is much slower, allowing time for smaller particles to travel to the wall, leading to radial heterogeneities that contribute to

poor performance.[60–62] Increasing slurry concentration and choosing slurry solvents that promote particle aggregation results in a more random and homogenous packing process, producing more efficient columns. At very high slurry concentrations, however, column performance again deteriorates due to the presence of large voids in the bed. Larger and a higher number of voids are more prevalent with smaller and smaller particle diameters. Implementation of sonication while packing has been investigated to mitigate the presence of packing voids. Meter long capillaries packed with a 200 mg/mL slurry of 2.0 μm bridged-ethyl hybrid silica particles (when the optimal is ~150 mg/mL without sonication) achieved reduced plate heights as low as 1.05 and 470,000 plates.[63] Further work remains on producing such long columns with even smaller particles (e.g., on the ~1 μm scale) as axial heterogeneities and large voids limit the packing efficiency using currently employed packing methods.[60,64]

1.3.3. Gradient separations at ultrahigh pressures

Reliable and automated gradient instrumentation capable of withstanding ultrahigh pressure is necessary to realize the capabilities suggested by the kinetic plots discussed above. Early ultrahigh pressure gradient systems were capable of operating up to 70 kpsi but had notable shortcomings, including split-flow, nonlinear gradients, and lack of automation.[56,65,66] Further improvements in system designs have allowed for automated sample injection and operation up to 45 kpsi with split-less and linear gradients.[67–69] Smaller tees and fittings likely contributed to the lower pressure limits. A schematic of a gradient system similar to that reported in Grinias et. al. is shown in Figure 1-5.[67] The system uses a commercial LC to load the gradient and inject sample on to a storage loop, followed by ultrahigh pressure separation using a second, independent pneumatic amplifier pump. This system is fully automated, produces linear gradients, and does not require split flow. Similar to most custom-built UHPLC systems, it operates at constant pressure

rather than constant flow, which can actually be beneficial as the flow is not limited by the highest viscosity in the gradient, thus decreasing analysis time without sacrificing peak capacity.[70] This system has been implemented and heavily utilized which has contributed to data throughout this thesis.

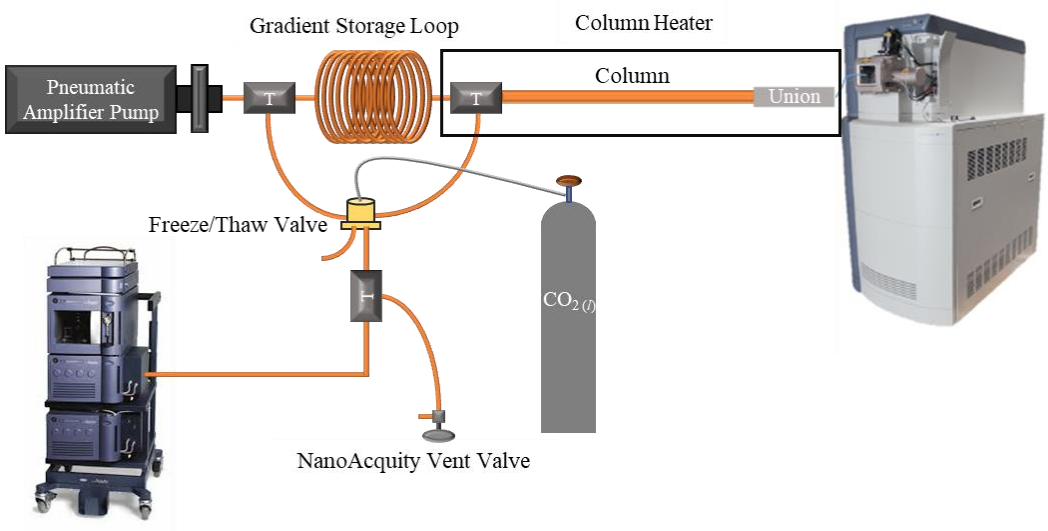

Figure 1-5. Schematic diagram of an LC-MS system for ultrahigh pressure gradient separations used in this thesis. Automated gradient loading and sample injection are performed with a commercial UHPLC, in this case a NanoAcquity. After, the mobile phase offline of the flow path is frozen by CO_2 and the pneumatic amplifier pump is initiated, pushing the sample on column followed by the preloaded gradient.

1.4. Dissertation overview

While highly efficient isocratic separations up to 100 kpsi have been demonstrated, and improvements in column packing using sub-2 µm particles have been described previously, the applications of these techniques have been sparse. This disparity is likely due to the difficulties in implementing reliable and robust gradient systems at such high pressures, synthesizing and efficiently packing small porous particles, and maintaining separation performance when using capillary systems and coupling with MS. The objective of this thesis is to describe the development of high-resolution separations coupled with mass spectrometry for untargeted metabolomic and lipidomic assays.

In chapter 2, gradient separations using the custom-built 35 kpsi system were performed and investigated for the separation and detection of lipids. Capillary columns between 15 – 50 cm long were packed with 1.7 µm C18 particles and evaluated for their ability to separate both lipid isomers and complex lipid extracts from human plasma. Lipids were detected using mass data of eluting peaks. Longer columns packed and operated at 35 kpsi outperformed shorter columns packed and run at lower pressures in terms of peak capacity and number of lipids detected. Peak capacities up to 410 were achieved, and roughly 480 lipids were detected from human plasma. Longer columns operated at shallow gradients also allowed for the best separation of both regional and geometrical isomers.

Chapter 3 extends the lipidomics work by developing a two-dimensional liquid chromatography system implementing the 50 cm microcolumns in the second dimension. Hydrophilic interaction liquid chromatography was employed in the first dimension to fractionate lipids based on their lipid class. Second dimension reversed phase chromatography using the custom-built UHPLC system allowed high-resolution separations of individual lipid species within each fraction. Effect of resuspension volume, injection volume, and gradient steepness were investigated to improve signal intensity and chromatographic resolution. Orthogonality measurements were also made to ensure a successful two-dimensional separation.

In chapter 4, separation of polar metabolites and the potential for capillary LC-MS based metabolomics utilizing porous C18 particles down to 1.1 µm diameter were evaluated. Using kinetic plots as a guide for choice of column length and particle size, 50 cm long columns with 1.7 µm particles and 20 cm long columns with 1.1 µm particles were packed, with the latter in theory providing equivalent performance in shorter times. Columns were tested by performing isocratic and gradient LC-MS analyses of small molecule metabolites and extracts from human plasma.

These columns provided peak capacities over 500 in 100 min for a complex plasma extract. To generate a given peak capacity, the 1.1 µm particles in 20 cm columns required roughly 75% of the time as 1.7 µm particles in 50 cm columns with both at 35 kpsi. The 1.1 µm particle packed columns generated a given peak capacity nearly 3 times faster than 1.7 µm particles in 15 cm columns at ~10 kpsi. To consider practical benefits for metabolomics, the effect of different LC-MS variables on mass spectral feature detection was also evaluated.

Finally, in chapter 5, instrument and column designs were considered for use at 50 kpsi and achieving peak capacities over 1000. Gradient kinetic plots were constructed to understand the expected peak capacity for different column lengths, particle sizes, and instrument pressure limits given a set gradient slope and length. Long columns with 1.7 µm d_p (100 cm) and 1.1 µm d_p (70 cm) were packed and evaluated at 35 – 50 kpsi under gradient lengths up to 8 h for a small molecule standard mixture. The 100 cm column with 1.7 µm d_p generated peak capacities of 790 – 1190 in 155 – 480 min. These values are much higher than what can be attained with commercial instrumentation and are some of the highest peak capacities per time reported in the literature. Improvements in packing protocols for efficiently preparing long columns with 1.1 µm particles are needed for fully realizing the benefits of such small particles. Instrument modifications for routine use at 50 kpsi are also discussed.

Chapter 2. Capillary Liquid Chromatography-Mass Spectrometry at 35 kpsi for the Separation of Lipids

Reproduced in part from Sorensen, M. J.; Miller, K. E.; Jorgenson, J. W.; Kennedy, R. T. *Journal of Chromatography A* **2020**, 1611, 460575.

2.1. Introduction

Lipids are important biological molecules with functions that include energy storage, cell signaling, and membrane formation.[71] A number of diseases such as Alzheimer's, Parkinson's, diabetes, and chronic kidney disease have been associated with altered lipid profiles.[6,7,72–74] Improved lipidomics methods are therefore of interest for better understanding of normal and pathological states and developing potential therapeutic targets. In this work we describe preparations and use of capillary LC columns up to 50 cm long operated at 35 kpsi for improved separation and coverage of complex lipid samples.

As described in the introduction of this thesis, analyzing the lipidome is challenging due to the diversity and complexity of the lipidome. Lipids can be divided into eight classes and many sub-classes spanning a wide range of physicochemical properties.[75] Additionally, they can be present in a wide concentration range within a biological system. A number of techniques are employed to characterize lipidomes, including spectroscopy, separations, and mass spectrometry (MS).[76] Direct infusion MS-based methods (e.g., shotgun lipidomics) are particularly powerful and popular due to their speed, sensitivity, ability to identify compounds, and mass resolving power.[77] Coupling separation techniques to MS can improve lipidome coverage by reducing ionization suppression[23] and separating isomeric and isobaric species.[24] Chromatographic data can also aid in lipid identification based on retention time.[12]

Although a variety of separation methods have been used for lipids,[78–80] high pressure and ultrahigh pressure liquid chromatography ((U)HPLC) is perhaps the dominant separation form used for lipid separations due to the wide range of lipid species amenable to this approach. A number of different HPLC modes have been used for lipid analysis, including reversed phase (RP),[81] normal phase (NP),[82] and hydrophilic interaction liquid chromatography (HILIC).[83,84] NP-LC and HILIC separate lipids primarily by their head group, effectively separating lipid classes. RP-LC predominantly separates lipids by hydrophobicity, allowing for separation by chain length, number of double bonds, and occasionally by the head group.

Studies suggest that separation performance can be a bottleneck for further gains in lipidomic coverage. A few reports utilizing long columns (e.g. 30 – 60 cm) operated at ultrahigh pressures, as described in the introduction of this thesis, have provided higher peak capacity for lipid separations.[85–87] Multidimensional separations such as 2D-LC offer even higher peak capacities than single dimension separations and have been shown to improve lipidomic coverage, likely due to alleviation of ionization suppression due to less co-elution and improved spectral quality.[88,89] Smaller diameter columns and nanoelectrospray ionization (nESI) emitters with low flow rates can also alleviate ionization suppression,[90] corroborated with a recent report showing increased lipidomic coverage using capillary LC-MS compared to a larger-bore 2.1 mm column.[40]

In this chapter, we investigated preparation of columns that could achieve the expected benefits of UHPLC operation of operating at 35 kpsi on lipid separations and lipidome coverage. The results demonstrate substantial peak capacity improvements for lipid separations at 35 kpsi when compared to 15 kpsi for the same stationary phases and mobile phase gradients. Our results also show a strong correlation between the chromatographic peak capacity and the number of lipids identified from a human plasma extract so that longer columns, which require higher pressure,

allowed more lipid identifications. Mass spectra of eluting peaks were cleaner due to less co-elution compared to lower resolution separations. Additionally, several different lipid isomers were investigated; longer columns operated at shallow gradients allowed for the best separation of both regional and geometrical isomers. These results demonstrate the benefits of using longer columns packed, using appropriate methods and operated at ultrahigh pressure for improving lipid separations and lipidome coverage.

2.2. Materials and methods

2.2.1. Chemicals and standards

HPLC grade water, acetone, methanol, and acetonitrile were purchased from VWR (Radnor, PA). Potassium chloride, acetic acid, HPLC grade 2-propanol, chloroform, formamide, formic acid and ammonium formate were purchased from Sigma Aldrich (St. Louis, MO). Potassium silicate (Kasil 2130) was purchased from PQ corporation (Valley Forge, IA). All lipids were purchased from Avanti Polar Lipids Inc (Alabaster, AL). A complete list of the lipids used in this work and their abbreviations are listed in Table 2-1. Abbreviations for all lipids were according to those reported by Liebisch et al.[91] A lipid standard mixture was prepared in mobile phase B. The mixture contained PC 14:0/16:0, PC 14:0/18:0, PC 16:0/18:0, PC 18:0/18:1, PC 18:1(9Z)/18:1(9Z), PC 18:1(9E)/18:1(9E), and PC 16:0/2:0, all at a concentration of 5 μM. The mixture also contained the Splash Lipidomix Mass Spec Standard (Avanti; Alabaster, AL), diluted 2:1 in the final mixture. This mixture contains 14 deuterium labeled lipids.

Table 2-1. List of lipid standards used in this work and their observed mass spectrometry response.

Lipid class	Abbreviation	Lipid species level	m/z	Adduct
Phosphatidylcholine	PC	15:0-18:1(d7)	753.61	$[M+H]^+$
Phosphatidylcholine	PC	18:1-18:1	786.60	$[M+H]^+$
Phosphatidylcholine	PC	16:0-2:0	538.35	$[M+H]^+$
Phosphatidylcholine	PC	14:0-16:0	706.54	$[M+H]^+$
Phosphatidylcholine	PC	14:0-18:0	734.56	$[M+H]^+$
Phosphatidylcholine	PC	16:0-18:0	762.60	$[M+H]^+$
Phosphatidylcholine	PC	18:0-18:1	788.62	$[M+H]^+$
Phosphatidylethanolamine	PE	15:0-18:1(d7)	711.57	$[M+H]^+$
Phosphatidylglycerol	PG	15:0-18:1(d7)	742.68	$[M+H]^+$
Lysophosphatidylcholine	LPC	18:1(d7)	529.40	$[M+H]^+$
Lysophosphatidyl ethanolamine	LPE	18:1(d7)	487.36	$[M+H]^+$
Cholesteryl Ester	CE	18:1(d7)	675.69	$[M+NH_4]^+$
Monoacylglycerol	MG	18:1(d7)	364.35	$[M+NH_4]^+$
Diacylglycerol	DG	15:0-18:1(d7)	605.59	$[M+NH_4]^+$
Triacylglycerol	TG	15:0-18:1(d7)-15:0	829.79	$[M+NH_4]^+$
Sphingomyelin	SM	18:1(d9) 18:1	738.66	$[M+H]^+$
Cholesterol	Chol	n/a (d7)	376.45	$[M-H_2O+H]^+$

2.2.2. Human plasma extraction

Pooled human plasma was provided by the Michigan Regional Comprehensive Metabolomics Resource Core. Lipids were extracted using a modification of Bligh and Dyer extraction protocol.[92] To 50 µL of plasma, 200 µL of 0.15 M KCl in water, 400 µL of methanol, 200 µL of chloroform, and 1 µL of acetic acid were added to an Eppendorf tube and mixed well. An additional 200 µL of water and 200 µL of chloroform were added, vortexed briefly, and

centrifuged at 12,100 × g for 5 min at room temperature. The organic layer was carefully collected and transferred to a glass HPLC vial, dried under nitrogen gas, and reconstituted in 400 µL of mobile phase B.

2.2.3. Column packing

Fused-silica capillaries with inner diameters of 100 µm and outer diameter of 360 µm were purchased from Polymicro Technologies, Inc. (Phoenix, AZ). Columns were prepared as previously described, with slight modifications.[55] Column outlet frits were prepared using the Kasil method.[93] An equal amount of potassium silicate and formamide were applied to a glass microfiber filter (Reeve Angel; Clifton, NJ) and the capillary tip was dabbed on the wetted paper to form the frit. The particles for all columns were 1.7 µm BEH (130 Angstrom) from Waters Corporation (Milford, MA). For the 15 cm columns operated at 15 kpsi, columns were packed at 15 kpsi using a 75 mg/mL slurry in acetone. After packing, columns were flushed at 20 kpsi for 1 h, depressurized, and an inlet frit was applied using the Kasil method. For the ultra-high performance columns, two packing methods were used to compare the effect that sonication has on column performance of gradient separations. For the non-sonicated columns, 75 mg/mL slurries containing 1.7 µm C18 BEH particles from Waters Corporation (Milford, MA) were prepared in acetone as this concentration has previously been reported as near optimal when not sonicating to balance between particle size segregation and void formation.[62] Columns of 25 and 50 cm in length were packed by steadily increasing the packing pressure to 30 kpsi in order to maintain packing flow rate and limit packing voids.[62] After, columns were flushed with 50/50 (v/v) acetonitrile/water at 40 kpsi for 1 h, and slowly depressurized for another hour before applying an inlet frit using the Kasil method. For the 50 cm sonicated columns, a 200 mg/mL slurry containing the same 1.7 µm C18 particles was prepared in acetone. The empty column was placed in a sonicator bath as

previously described.[63] After a couple centimeters of bed was formed, the pressure was immediately increased to 30 kpsi. The columns were flushed with 50/50 (v/v) acetonitrile/water at 50 kpsi for 1 h, depressurized for 1 h, and an inlet frit was applied using the Kasil method.

2.2.4. Instrument operation

A constant pressure pump UHPLC system (see Figure 5 in Introduction) was used to perform separations at 35 kpsi as previously described.[67,87] Mobile phase A was 60/40 (v/v) water/acetonitrile with 10 mM ammonium formate and 0.1% (v/v) formic acid. Mobile phase B was 85/10/5 (v/v/v) 2-propanol/acetonitrile/water with 10 mM ammonium formate and 0.1% (v/v) formic acid. One µL was injected on column using a Waters NanoAcquity UPLC. The column oven was set at 60 C. A 50–100% B gradient was used in all separations, with a 100% B hold for 10 column volumes. Gradients were loaded on to a gradient storage loop using a binary solvent manager of the NanoAcquity. Constant pressure separations were performed using a pneumatic amplifier pump (DSXHF-903 Haskel pump (Burbank, CA). Column volumes were calculated assuming a column porosity of 0.8. The peak capacity was calculated by dividing the elution window by the average peak width (4σ) of 12 lipid standards that eluted throughout the separation window. Plate heights were measured using the peak width at half maximum. Effluent from the column was connected to a Micromass Q-ToF Premier using a stainless-steel union connected to fused silica spray needle with a 75 µm inner diameter tapered to 30 µm. The scan rate was set to 0.3 s with a 0.1 s inter-delay. The MS was operated in full scan, positive ion mode with a mass window of 150–1000 m/z. External calibration was performed regularly using sodium formate. Source parameters were tuned by directly infusing 5 µM PC 18:1(9Z)/18:1(9Z)). The spray voltage was 1.75 kV, the source temperature was 100 °C, and sheath gas was 0.3 bar.

2.2.5. Lipid identification

Lipids were putatively identified at the lipid class level using LipidBlast software.[12,94] Mass spectra from 1 min elution windows were baseline subtracted and centered. The corresponding m/z values that were above 100 counts were input into the software. The mass accuracy was set at 10 mDa. Following in-silico identification, redundant species and salt adducts that corresponded to the same lipid were removed. If multiple lipids were matched for one m/z value (e.g., within 10 mDa mass units), only one lipid was considered an identification.

2.3. Results and discussion

In this work, we investigated the potential benefits of packing and operating capillary columns at 35 kpsi on lipid separations and lipidome coverage. We first compared the separation performance of a 25 cm and 50 cm column, packed under identical conditions as described in Section 2.3, to assess the impact that column length has on gradient separations of complex lipid extracts from human plasma. We then compared two 50 cm columns, one that was packed using sonication and high slurry concentrations, which was recently shown to improve column efficiency, particularly for longer columns,[63] and one packed without the use of sonication. Lastly, we compared these results with a 15 cm column operated at 15 kpsi, the current limits in commercial instrumentation. Altogether, for a given analysis time, longer columns packed with high slurry concentration and sonication and operated at 35 kpsi provided higher peak capacities, more lipid identifications and cleaner mass spectra from complex mixtures of lipids compared with shorter columns.

2.3.1. Column repeatability

Before performing detailed comparisons of individual columns under different conditions, we investigated the repeatability of the column packing and gradient LC-MS performance for the

different column dimensions studied in this chapter. Table 2-2 summarizes the retention time and peak capacity variation across three separate columns for each column length. In each condition, a gradient slope of 5% change in mobile phase (ΔB)/column volume was programmed and the instrument was operated at 15 kpsi for the 15 cm columns and 35 kpsi for the 25 and 50 cm columns. The results showed good repeatability in retention time and peak capacity for gradient separations of the standard lipid mixture. Retention time variation between columns was 1–3% RSD and peak capacity variation was 3–6% RSD. The sonicated columns in this chapter were evaluated at UNC Chapel Hill using a dedicated isocratic system with on-column electrochemical detection as previously described.[63] Reduced plate height curves of hydroquinone as the test analyte are displayed in Figure 2-1 and show high repeatability between columns.

Table 2-2. Summary of the performance of three separate columns for each column type evaluated in this work. For each column, 1 µL of the standard lipid mixture was injected and separated with a gradient slope of 5% ΔB/column volume at either 15 kpsi or 35 kpsi.

Column	Retention time variability (%RSD) (n = 3 columns)	Average peak capacity (n = 3 columns)	Peak capacity variation (%RSD)
25 cm x 100 µm (35 kpsi)	3%	115	6%
50 cm x 100 µm (35 kpsi)	3%	180	3%
15 cm x 100 µm (15 kpsi)	1%	79	6%

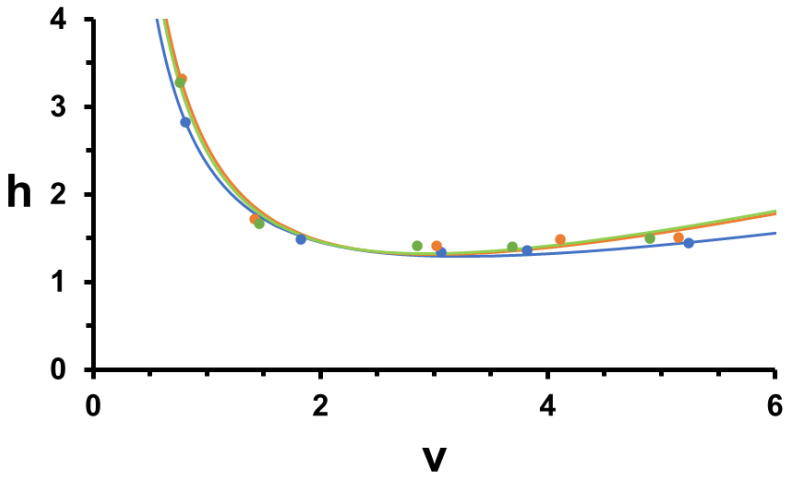

Figure 2-1 Reduced van Deemter plots of three 50 cm x 100 µm columns packed with sonication. Plate heights were determined using hydroquinone with amperometric detection as previously described.[63]

2.3.2. Effect of column length on lipid separations

In the first evaluation, we compared 25 cm and 50 cm columns that were prepared under identical packing conditions. Due to the shorter analysis times possible on the 25 cm column, method development was first carried out on this column using a standard lipid mixture to obtain a general understanding of lipid separations at 35 kpsi. Separation of the standard lipid mixture on the 25 cm column operated at 35 kpsi and 60 C is shown in Figure 2-2A. A 10X column volume was used as the gradient volume at 50–100% B, corresponding to a 5% ΔB per column volume. This gradient slope has previously provided good separation space and peak capacity for peptides.[67,95] Previous ultrahigh pressure work has shown that higher pressures in HPLC can alter separation selectivity and retention;[55,96] however, no significant differences between 15 kpsi and 35 kpsi operating pressure was seen in regard to retention or selectivity (discussed in more detail in Section 3.3). Similar to previous reports for RP-LC of lipids, separation is primarily based on the number and length of carbon chains attached to the glycerol backbone. For example, monoacylglycerols elute in the first portion of the chromatogram, whereas the more non-polar triacylglycerols and cholesteryl esters elute at the end.[97] The peak capacity for this 30 min

separation was 110 ± 5 (n = 3 injections). Figure 2-2B shows the separation of a lipid plasma extract on the 25 cm column with the same conditions as panel A. The peak capacity was 115 ± 7 (n = 3 injections). Using LipidBlast to analyze the data, 189 ± 29 (n = 3 injections) lipids were putatively identified at the lipid class level in full scan mode.[12,91] The higher number of lipids detected than peak capacity confirms that some lipids co-elute but are resolved by the mass spectrometer.

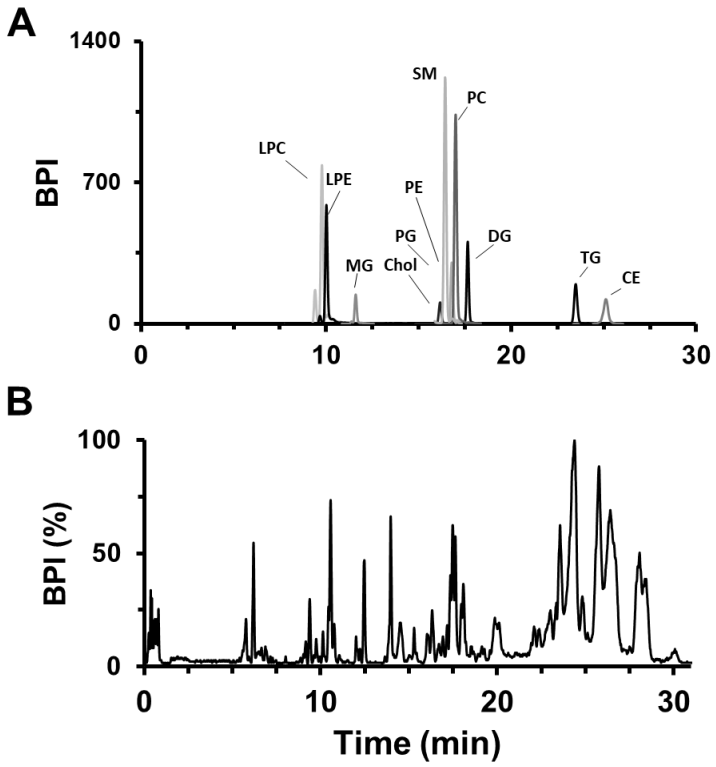

Figure 2-2. Chromatograms of (A) the lipid standard mixture displayed as overlaid extracted chromatograms and (B) lipid extract from human plasma displayed as a base peak intensity (BPI) chromatogram on a 25 cm × 100 µm column operated at 35 kpsi with a 50–100% B gradient at 60 °C. The gradient slope was 5% ΔB/column volume. Mobile phase A consisted of 60/40 ACN/water with 10 mM ammonium formate and 0.1% formic acid and mobile phase B was 85/10/5 IPA/ACN/water with 10 mM ammonium formate and 0.1% formic acid. See Table 2-1 for lipid abbreviations.

We sought to assess the impact that doubling the column length with columns packed under identical packing conditions has on peak capacity of complex lipid extracts with a variety of analysis times operated at 35 kpsi. A plot of the peak capacity as a function of the analysis time for the 25 cm and non-sonicated 50 cm columns is shown in blue and green traces, respectively, in

Figure 2-3. For the 25 cm column, the gradient slopes ranged from 10% to 0.5% ΔB/column volume. For the non-sonicated 50 cm column, the gradient slopes ranged from 5% to 1% ΔB/column volume. Again, all separations were performed at 35 kpsi for these two columns. Figure 2-4 shows the base peak intensity (BPI) chromatogram of a lipid plasma extract on the 25 and non-sonicated 50 cm columns with 2 h analysis time and 35 kpsi inlet pressure. The peak capacity on the non-sonicated 50 cm column was 265 ± 5 (n = 3 injection), which was only slightly higher than the 25 cm column of 237 ± 10 (n = 3 injection). For visual clarity, extracted ion chromatograms for three lipids eluting across the separation space are shown in Figure 2-4C to illustrate the similar peak widths between the two columns.

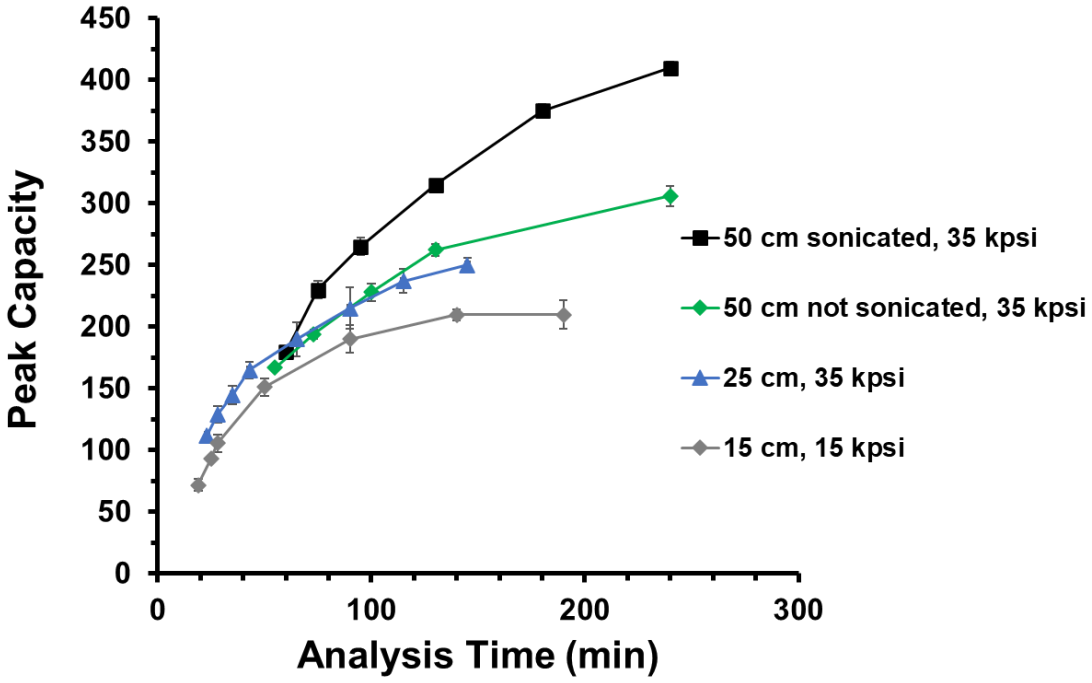

Figure 2-3. Peak capacity plotted as a function of analysis time for lipid separations on the different columns studied in this work. Analysis time was varied by changing the amount of mobile phase loaded on the storage loop effectively giving a longer, shallower gradient. Peak capacity was calculated by dividing the gradient time by the peak width at base of 12 lipid standards eluting throughout the separation window. Other conditions are the same as in Figure 2-2.

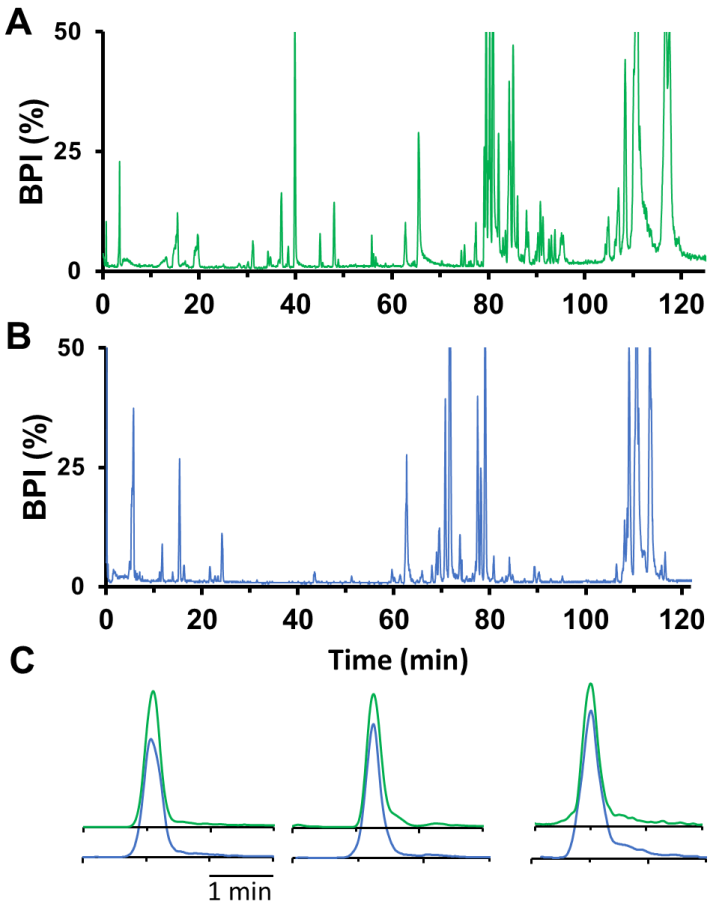

Figure 2-4. Base peak chromatograms of a lipid extract from human plasma on (A) 50 cm column and (B) 25 cm column packed under identical conditions at a constant analysis time of 120 min. The gradient slope was 0.6% ΔB/column volume for the 25 cm column and 2% ΔB/column volume for the 50 cm column. For clarity, the y-axis is zoomed to 50% height to focus on the peak widths at the base. Other conditions are the same as in Figure 2-2. Extracted ion chromatograms for three lipids eluting across the separation space are displayed in panel C showing similar peak widths between the 25 and 50 cm non-sonicated columns packed under identical packing conditions.

The modest improvement in peak capacity with length for columns packed under identical packing conditions may be related to packing quality for the longer column. Reduced van Deemter plots using phosphatidyl choline (PC) 18:1/18:1 as a test analyte showed worse performance for the 50 cm column compared to the 25 cm column (Figure 2-5). It should be noted that these studies were done with the same system used for gradient separations, not a dedicated isocratic system such as that used in Figure 2-1. Nonetheless, general trends can still be interpreted. The reduced plate height minimum (h_{min}) on the 25 cm column was 1.6, while on the 50 cm column h_{min} was 5.2. At 35 kpsi, the reduced plate heights were 4.0 and 6.6 on the 25 cm and 50 cm columns,

respectively. One explanation for this worse kinetic performance of the 50 cm column is the difficulty to pack longer columns. In particular, axial heterogeneities in the packing bed have been attributed to poor chromatographic efficiency for longer columns.[60]

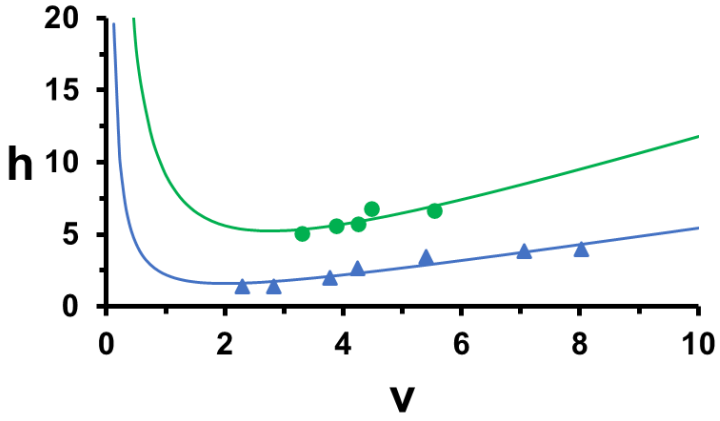

Figure 2-5. Reduced van Deemter curve of the 25 cm (blue triangles) and 50 cm (green circles) columns packed under identical packing conditions. Plate heights were measured using phosphatidyl choline 18:1/18:1 as a target analyte eluted at 90% B. Other conditions are the same as in Figure 2-2.

2.3.3. Effect of column packing procedures on lipid separations

The above findings indicated that the conditions used for packing the columns used did not generate equivalent performance per unit length in the tested columns, i.e., the conditions used were not ideal for longer columns. It was recently shown that sonication during column packing improves column efficiency, with reduced plate heights of 1.05 being reported for meter-long capillary columns.[63] Therefore, we compared two 50 cm long columns: one packed without sonication and one packed with sonication. Other slight differences between packing methods were employed based on previously reported packing methods as described in Section 2.3 of this chapter. For simplicity we refer to the two methods as “sonicated” and “not sonicated”. The black and green traces in Figure 2-3 show the peak capacity as a function of analysis time for the sonicated and not sonicated columns, respectively. It is clear that the sonicated column outperformed the non-sonicated column for gradient separations of complex lipid extracts. At short

and steep gradients, the improvement is not as drastic. Improvements in peak capacity at longer analysis times for longer columns is consistent with gradient elution theory and has previously been reported for peptide separations using 50 – 200 cm long columns.[67,98,99]

Example base peak chromatograms from the two 50 cm columns shows the improved separation for the sonicated column for a 4 h separation (Figure 2-6). The sonicated column provides narrower peaks and more baseline resolved peaks than the non-sonicated column. For the 240 min separation shown in Fig. 4, the peak capacity of the non-sonicated column was 306 ± 8 ($n = 3$ injections) and 407 ± 5 ($n = 3$ injections) for the sonicated column. Extracted ion chromatograms of three lipids from the plasma extract eluting across the separation space are shown in Fig. 2-6C to help visually see the improvement in peak width and shape between the two columns.

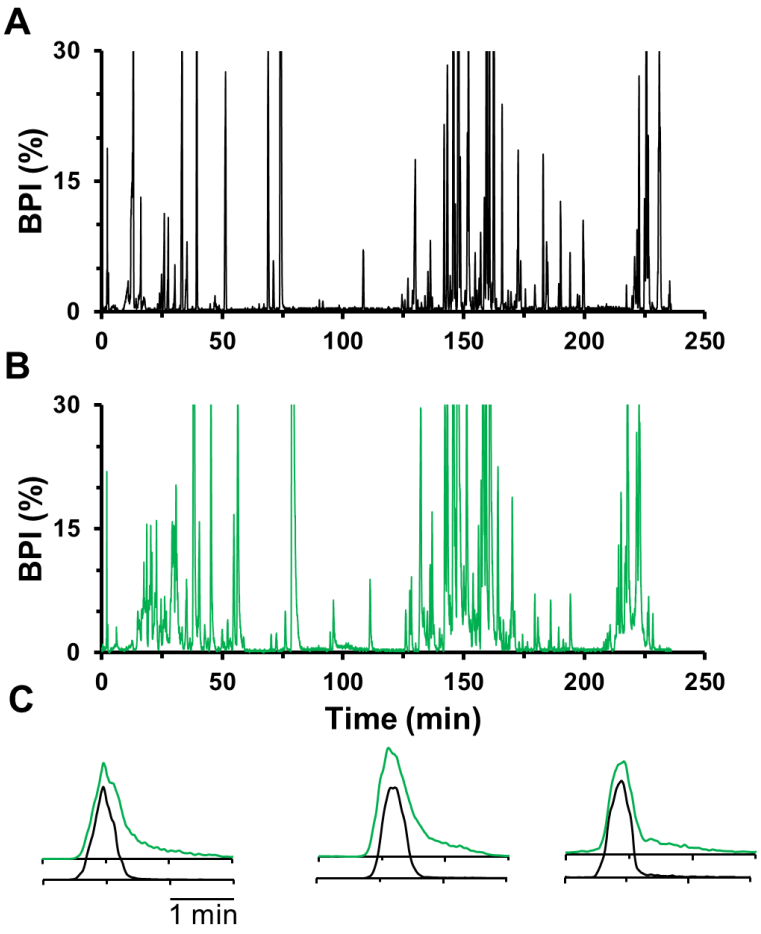

Figure 2-6. Representative chromatograms of a lipid extract from human plasma on the 50 cm columns studied in this work showing the influence of sonication during column packing of longer columns. Panel A is from the sonicated column and panel B is from the non-sonicated column. The 240 min gradient corresponded to a 1% ΔB/column volume. For clarity, the y-axis is zoomed to 30% height to focus on the peak widths at the base. Other conditions are the same as in Figure 2-2. Extracted ion chromatograms for three lipids eluting across the separation space displayed in panel C show improved peak width and peak shape for the sonicated column.

2.3.4. Comparison with commercial pressures

We also compared the performance of the system described here with what could be achieved with pressure limits of current state-of-the-art commercial instrumentation. For this study, we packed a 15 cm long column up to 20 kpsi and performed gradient separations at 15 kpsi. The separation performance of this column consistently under-performed the higher-pressure columns discussed previously. Figure 2-7 shows base peak chromatograms of a lipid extract from plasma on the 15 cm column at 15 kpsi and a sonicated 50 cm column at 35 kpsi with a constant

gradient slope of 2.5% ΔB/column volume. At these conditions, the peak capacity was 93 ± 2 ($n = 3$) for the 15 kpsi case and 265 ± 5 ($n = 3$) for the 35 kpsi case, albeit at a longer analysis time. Extracted ion chromatograms of three lipids from the plasma extract are shown in panel C with elution time windows of 8% of the total analysis time.

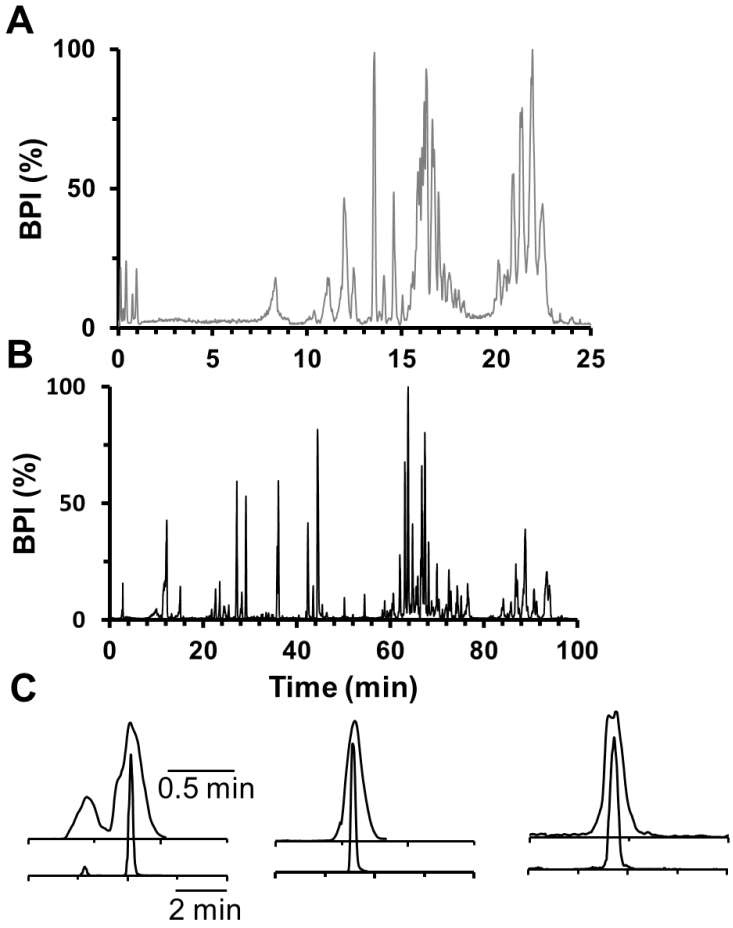

Figure 2-7. Base peak chromatograms of a lipid extract from plasma on (A) 15 cm column operated at 15 kpsi and (B) 50 cm column operated at 35 kpsi, both with a gradient slope of 2.5% ΔB/column volume. Other conditions are the same as in Figure 2-2. Extracted ion chromatograms in panel C for three lipids eluting across the separation space show improved peak width and peak shape for the 50 cm sonicated column compared to the 15 cm column. Retention windows are 8% of the total analysis time.

A comparison of the 15 cm and 50 cm columns at a constant analysis time for a lipid extract from plasma is shown in Figure 2-8. In general, lipids eluted slightly early for the same gradient profile when operated at lower pressures, similar observations for small molecules.[55,56] The peak

capacity of the standard lipid mixture as a function of analysis time for the 15 cm column operated at 15 kpsi in comparison to the higher pressure columns is shown in Figure 2-3. The peak capacity on the 15 cm column plateaued at a maximum of about 200, with no further gain achieved with increased analysis time. Longer columns and higher pressures are therefore particularly advantages at longer analysis times, offering up to 95% increase in peak capacity for the same analysis time. Improved performance with higher pressure limits is due to both being able to operate longer columns and possibly better packing. A recent study on peptide separations revealed that columns packed at 30 kpsi resulted in a 17% increase in peak capacity and a 16% increase in peptide identifications compared to those packed at 10 kpsi for 30 cm long columns despite both separations being performed with the same commercial UHPLC system at ~11 kpsi.[100]

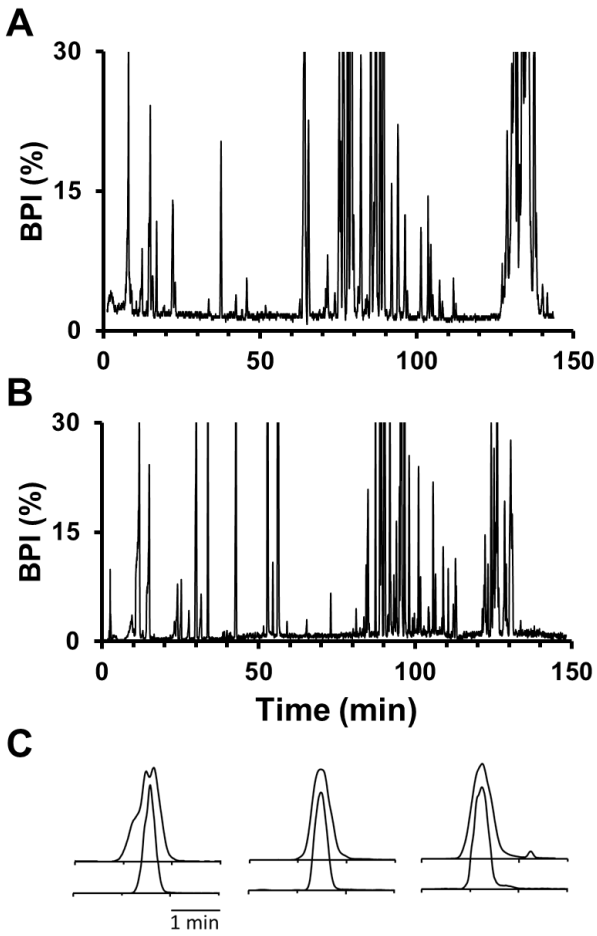

Figure 2-8. Base peak chromatograms of a lipid extract from plasma on A) 15 cm column operated at 15 kpsi and B) 50 cm sonicated column operated at 35 kpsi with a constant analysis time of 130 min. Other conditions are the same as Figure 2-2. Panel C shows extracted ion chromatograms for three lipids eluting across the separation space to help visualize the improvement in peak width and shape for the longer column operated at higher pressure.

2.3.5. Relationship between peak capacity and lipids detected

The above experiments illustrate that use of long, well-packed columns provides substantial increases in peak capacity for lipid separations. A critical goal of a lipidomic experiment is to enable identification or detection of large numbers of lipids. To evaluate the effect of using ultra-high pressure on ability to detect or identify discrete lipids in complex samples, we used LipidBlast software[12] to detect lipids in the samples at the class level,[91] e.g., fatty acid tails or double bond positioning are not differentiated. (All experiments were performed in positive ion

mode only because the only instrument we had available for these experiments was not functional in negative ion mode. In principle, use of negative mode would reveal even more identification from lipid classes, such as fatty acids, that are better detected that way.)

The results here show a roughly linear correlation between the chromatographic peak capacity and the number of lipids identified, independent of analysis time (Figure 2-9). For example, comparing the 15 cm and 50 cm sonicated column, with a constant 130 min analysis time, 206 ± 18 lipids ($n = 2$ injections) versus 480 ± 85 ($n = 2$ injections) lipids were detected, respectively. The peak capacities on the 15 cm and the 50 cm sonicated columns for those separations were 190 ± 10 ($n = 3$ injections) and 315 ± 5 ($n = 3$ injections), respectively (Figure 2-8). The lower number of detected lipids found with the shorter column may be mostly attributed to the lower peak capacity. It is also possible that other factors contributed as well. For example, to obtain a 130 min separation on the 15 cm column, a gradient slope of 0.2% ΔB/column volume was required. This shallow of a gradient may reduce signal intensity as peaks become broader, which could potentially limit the number of lipids detected.

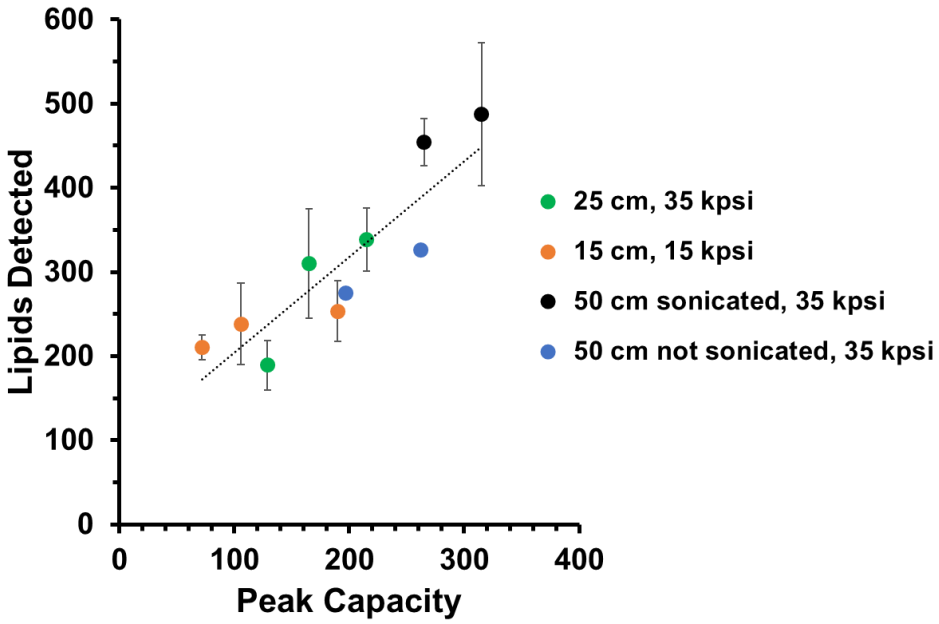

Figure 2-9. Detection of lipids from LipidBlast software is plotted as a function of the chromatographic peak capacity for various columns and conditions studied in this work. Error bars are mean standard error from duplicate injections for each condition.

Representative mass spectra from the beginning, middle, and end portions of the chromatogram of a lipid extract from plasma showed much cleaner spectra on a 100 min analysis on the sonicated 50 cm column compared to a 30 min analysis on the 15 cm column (Figure 2-10). Importantly, cleaner mass spectra can allow easier interpretation of data, leading to more identifications.[25]

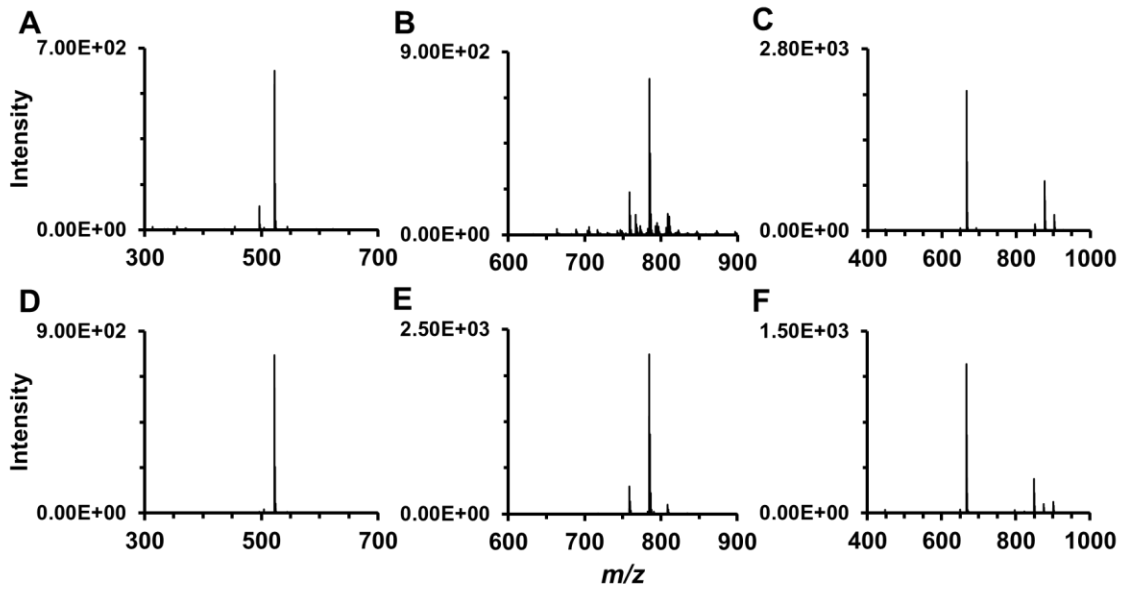

Figure 2-10. Example mass spectra of eluted lipids from a lipid extract from human plasma on a 15 cm (A, B, C) and 50 cm column (D, E, F). Averaged mass spectra are from a 0.2 min elution window of the base peak corresponding to LPC 18:1 – m/z 522.4 (A and D), PC 36:3 – m/z 784.6 (B and E), and CE 18:2 – m/z 666.6 (C and F). Other LC-MS conditions are the same as in Figure 2-2.

The linear relationship between the chromatographic peak capacity and the number of lipids identified by mass spectrometry illustrates the importance of high-resolution separations for lipidomics. The linear relationship between the chromatographic peak capacity and the number of lipids identified by mass spectrometry is in agreement with a previous study on peptide and protein separations.[101] A primary reason for this effect is likely reduction of ionization suppression. Ionization suppression has been well documented for lipids and it is likely that suppression due to co-elution is alleviated with higher peak capacity separations, leading to better signal for more lipids and therefore more lipid identifications.[23] This conclusion is supported by the observation that mass spectra from individual retention times were cleaner (Figure 2-10). While finding that improved peak capacity with longer improves number of identifications is possibly not surprising, there have been few reports of the effect of longer columns for LC-MS based lipidomics to demonstrate this effect. Further, several factors may prevent this effect from being realized. When

employing long, shallow gradients, signal intensity can diminish due to dilution, potentially offsetting the benefits of higher resolution separation for identification. It is also possible that while thousands of lipids may be present in a sample, a relatively small number is detectable in which case better peak capacity would not improve numbers identified; however, our result shows that further gains in peak capacity are likely desirable to further improve lipidome coverage. Also, since we used low flow rates, which can also reduce ionization suppression, it is possible that better chromatographic resolution would not further increase identification.[40] Our results here show that higher peak capacity is still beneficial when employing nanoESI.

The mass spectrometry method employed here does not allow for distinguishing of isomers as two or more unique identification. The increase in lipid identifications observed here could potentially be an under-estimate because more isomers are resolved. For example, PC 18:1 (Δ9-cis) and PC18:1 (Δ9-trans) are baseline resolved (see Section 3.6); however, because they have the same mass, they are identified as only one unique feature with the current MS conditions and software used in this work. Further work can be done using lipid identification software and MS/MS capabilities that allow full identification of different isomers to better understand the impact that higher resolution separations have in untargeted LC-MS based lipidomics. This was recently done for example using online ozonolysis to study the impact of ion mobility separation on lipid isomer analysis.[102]

2.3.6. Lipid isomer separations

In the last set of experiments, we evaluated resolution of certain lipid isomer pairs on the different columns and pressures studied here. A number of lipid isomers can exist for one lipid species, adding complexity to a lipidomics analysis.[24] Separation or partial separation of three sets of lipid isomers on the 25 cm and sonicated 50 cm column is shown in Figure 2-11. Panel A is PC

16:0/2:0 vs PC 2:0/16:0, panel B is PC 14:0/18:0 vs PC 18:0/14:0, and panel C is PC 18:1 (Δ9-cis) vs PC 18:1 (Δ9-trans). Panels A and B are examples of regioisomers in which bonding to the sn-1 and sn-2 positions on the glycerol backbone are switched. The subtle differences between PC 14:0/18:0 and PC 18:0/14:0 allowed only partial separation, while the larger difference between PC 2:0/16:0 and PC 16:0/2:0 allowed baseline resolution on both columns. Resolution increased in panels A and C on the 50 cm column. However, for the PC 14:0/18:0 pair, an increase in resolution was not seen between the 25 and 50 cm columns. Alternative stationary or mobile phases are likely required for separation of this more difficult lipid isomer pair. It is unlikely that the PC 2:0/16:0 pair is biologically relevant, however this pair provided insight into the separation limits of PC sn-1/sn-2 regioisomers. Cis/trans isomers have shown relevancy for example when monitoring the effect of dietary fat intake.[103] Other lipid isomers such as the fatty acid composition in the sn-1, 2, and 3 positions in triacylglycerols and diacylglycerols are of biological importance and should be investigated in future work.[104,105]

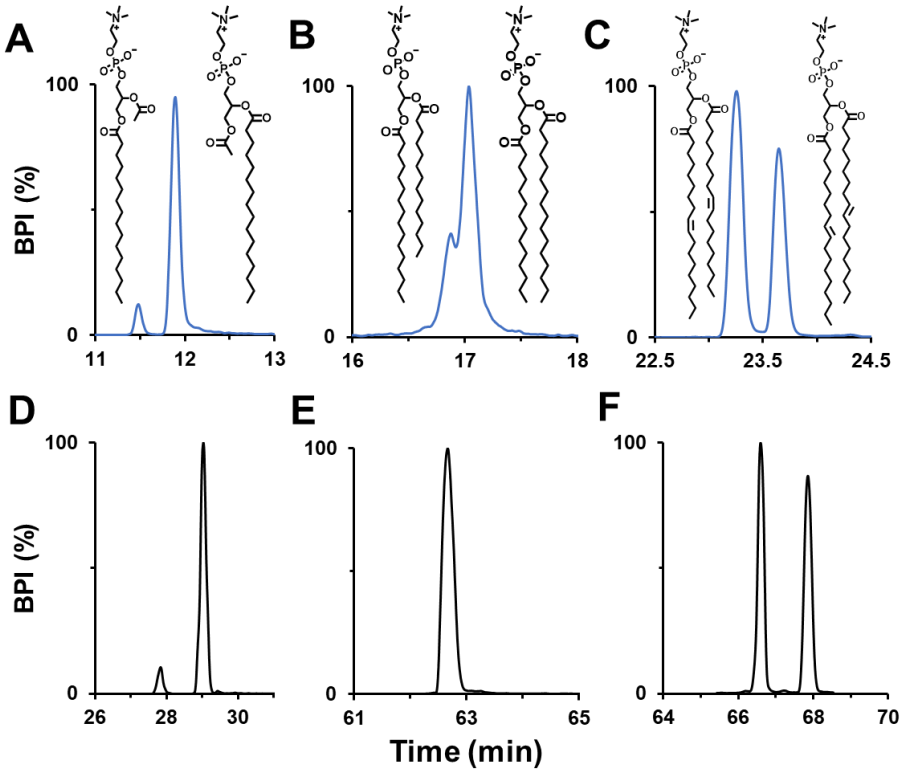

Figure 2-11. Separation of different lipid isomer pairs investigated in this work on a 25 cm (A, B, C) and 50 cm (D, E, F) column with both operated at 35 kpsi. A gradient slope of 3.3% ΔB/column volume was employed on each column. Other conditions are the same as Figure 2-2.

2.4. Conclusions

An ultrahigh-pressure liquid chromatography-mass spectrometry system operable up to 35 kpsi was evaluated for the separation of lipids from complex extracts from human plasma. Longer columns of 25 and 50 cm packed and operated at ultrahigh pressure outperformed 15 cm columns operated at 15 kpsi, with peak capacity improvements ranging from 20 – 95% at the same analysis time. Sonication while packing 50 cm columns was necessary to take full advantage of the longer column length. Use of 35 kpsi inlet pressure allowed for reasonable analysis times using 50 cm long columns and avoids excessive band broadening due to longitudinal diffusion. A linear increase in the number of lipid species detected was observed with an increase in the chromatographic peak capacity. Lastly, the resolution of both regional and geometrical isomers increased with longer columns and shallow gradients. These results demonstrate the benefits of

using longer columns packed and operated at ultrahigh pressure for improving lipid separations and lipidome coverage.

Chapter 3. Two-Dimensional Liquid Chromatography-Mass Spectrometry for Lipidomics Using HILIC x RPLC with Long Capillary Columns in the Second Dimension

3.1. Introduction

Lipidomics has emerged as an important technique for studying lipids from various biological and environmental samples. Applications of lipidomics include areas such as studying disease states, understanding physiological processes, pharmaceuticals, and food science.[106,107] While targeted lipidomics can be valuable for studying and quantifying certain lipids for hypothesis-driven studies, the limited scope of such studies is often not sufficient for fully understanding how lipids are involved within a given system.[2] Untargeted lipidomics, with the goal of identifying and quantifying all lipids in a sample, can give better insight into how lipids are associated within the system of interest and generate hypotheses based on the data generated.[108] Identifying and quantifying all lipids in a sample is challenging however due to the large number, wide concentration range, numerous isomers, and broad physicochemical properties of lipids in most biological or environmental samples. One analytical technique is not yet sufficient for analyzing an entire lipidome. In this work, we developed an offline two-dimensional liquid chromatography-mass spectrometry method utilizing hydrophilic interaction liquid chromatography followed by ultrahigh pressure capillary reversed phase chromatography coupled to mass spectrometry for lipidome analysis in human plasma.

A number of techniques have been implemented for untargeted lipidomics, including spectroscopy, mass spectrometry, and separations.[76] Advantages of LC-MS based lipidomics

include good sensitivity, amenability to a wide ranges of lipid classes, and relatively high throughput.[21,106,109,110] Various approaches have been pursued to increase the lipidome coverage in LC-MS based lipidomics. Improved peak capacity of the separation is an important route to improving lipidome coverage. Multidimensional separations are a powerful approach for increasing peak capacity.[111,112] The theoretical peak capacity of a two-dimensional (2D) separation for instance is the product of the first dimension (^{1}D) and second dimension (^{2}D) separation peak capacities, assuming the two separation mechanisms are orthogonal and the resolution of the first dimension is not compromised by the second dimension.[112] Multidimensional methods for lipids have been developed and demonstrated enhanced lipidome coverage provided by the improved separation performance relative to single dimensional analyses.[88,113–117]

Transfer of effluent from the first dimension can occur online, where fractions from the first dimension are transferred immediately to a rapid second dimension, or offline where fractions are collected and independently injected on the second dimension.[118,119] Online 2D-LC separations typically employ higher resolution 1D separations and have the advantage of being fast; however, they come with a number of disadvantages.[120] Online 2D-LC typically involves more complicated instrumentation, worse detection limits to additional chromatographic dilution and often times flow-splitting when coupled to MS, limited ^{2}D analysis time and peak capacity, and solvent incompatibility between the two dimensions.[121,122] Additionally, for rapid methods the second dimension uses high flow rates and results in peak widths less than 1 s, which is too narrow to be accurately characterized by current mass spectrometers. These effects can lead to inaccurate peak width measurement, mass measurement, reduced sensitivity, and quantification. It also reduces the effectiveness of MS/MS methods such as data dependent acquisition where multiple MS scan events need to occur within the elution of a given compound. The incompatibility with MS

constrains the possible applications of such on-line methods. Despite these drawbacks, various online 2D-LC-MS methods have been developed for lipidomics with good separation peak capacity and lipidome coverage with analysis times typically 2 – 4 h.[114,123–126]

Offline 2D-LC can overcome some of these challenges. Importantly, because the separations are independent, the ^{2}D analysis time is not limited by the ^{1}D peak width or sampling frequency. Thus, long gradients can be implemented in the second dimension, achieving high-resolution separations with peak widths that are compatible with MS, but at the expense of analysis time. The ^{1}D separation is typically faster for fractionation. Additionally, effluent from the first dimension can be dried down and resuspended in appropriate solvent for the second dimension. Finally, small resuspension volumes can preconcentrate fractions and provide enhanced signal intensity. Offline 2D-LC-MS approaches have typically provided broader lipidome coverage compared to online methods.[89,113]

An intermediate approach is stop-flow 2D-LC. These methods do not require fast ^{2}D dimension separations, but are still mostly considered online.[127] This approach is still limited by solvent compatibility and more intricate instrument configuration relative to offline 2D-LC. Stop-flow 2D-LC is popular for proteomics but has also been reported for lipidomics.[115,128]

Capillary LC with nanoESI-MS has also been implemented to increase lipidome coverage based on enhanced ionization efficiency and alleviation of ionization suppression associated with low flow rates.[40,129–131] Additionally, use of such small inner diameter columns reduces sample volume which can be beneficial for sample-limited analyses.[132–134] Such methods have been gaining much interest in the field of proteomics but little work has been reported for lipidomics.[133,135,136]

Another approach to improving lipidome coverage has been to use long columns packed with sub-2 µm particles and operated at ultrahigh pressures. It is well known that long columns packed with small particles can provide much higher theoretical plates; however, this approach requires much higher instrument operating pressure and thus is difficult to implement in a practical setting.[51,137] Recent reports of lipid separations have shown that use of long columns (e.g., 30 – 60 cm) packed with 1.7 µm C18 particles increased separation peak capacity for lipids, resolved more isomers, and detected more lipids in complex mixtures compared to lower resolution separations.[85–87,138]

The combination of the strategies mentioned above (multidimensional separations, capillary LC-MS, and use of long columns) has recently been employed for various proteomic workflows in both top-down and bottom-up approaches;[69,139–141] however, there has been limited use of such technologies in lipidomics or metabolomics.[116] Here, we describe an offline two-dimensional liquid chromatography-mass spectrometry method for untargeted lipidomics. We use a microbore bare silica HILIC column in the first dimension to separate lipid classes. Following evaporation and resuspension, each fraction was injected onto a 50 cm long x 100 µm bore column packed with 1.7 µm C18 particles operated at 35 kpsi interfaced to a quadrupole time-of-flight mass spectrometer. Our findings suggest large gains in peak capacity compared to one dimensional approaches with enhanced lipid coverage.

3.2. Materials and methods

3.2.1. Chemicals and standards

All solvents and chemicals were purchased from Sigma Aldrich (St. Louis, MO) unless otherwise stated. HPLC grade acetonitrile was purchased from Fisher Scientific (Waltham, MA). Potassium silicate (Kasil 2130) was purchased from PQ corporation (Valley Forge, IA). Palmitic

acid was purchased from Sigma Aldrich. All other lipids were purchased from Avanti Polar Lipids Inc (Alabaster, AL).

3.2.2. Human plasma extraction

Pooled human plasma was provided by the Michigan Regional Comprehensive Metabolomics Resource Core. For lipid extraction, 50 µL of plasma, 200 µL of 0.15 M KCl in water, 400 µL of methanol, 200 µL of chloroform, and 1 µL of acetic acid were added to an Eppendorf tube and vortexed well. An additional 200 µL of water and 200 µL of chloroform were added, vortexed briefly, and centrifuged at 12,100 × g for 5 min at room temperature. The organic layer was carefully collected and transferred to a glass HPLC vial, dried under nitrogen gas, and reconstituted in 100 µL of 90/10 (v/v) IPA/water for injection on the first dimension HILIC column.

3.2.3. First dimension HILIC-MS

Lipids were separated by HILIC in the first dimension using a 15 cm x 1 mm, 5 µm Spherisorb bare silica column (Waters; Milford, MA). A Waters NanoAcquity UPLC was used and coupled with a Micromass QToF Premier (Micromass/Waters; Milford, MA). The method was similar to a previously reported method for lipid class separations.[113,142] Mobile phase A was 5 mM ammonium acetate and mobile phase B was acetonitrile. The flow rate was 50 µL/min. A gradient elution program was used as follows: initial, 95% B; 40 min, 77% B; 42 min, 95% B; 55 min, 95% B. The column oven was set to 30 °C. The injection volume was 5 µL. Electrospray ionization was used in positive ionization mode at 3.5 kV. The source temperature was 100 °C, desolvation temperature 150 °C, cone gas 50 L/h, and desolvation gas 450 L/h. The MS was operated in full scan mode from m/z 100 – 1000 with a 1 s scan rate and 0.1 s inter-scan.

For fraction collection, effluent from the ^{1}D separation was collected in glass HPLC vials. Fractions were typically collected in 1 – 2 min portions, which amounted to 50 – 100 µL of volume. Solvent was evaporated with a stream of nitrogen and re-dissolved in reversed phase mobile phase (different compositions and volumes depending on fraction type).

3.2.4. Capillary column packing

Polyimide-coated, fused silica capillaries with inner diameters of 100 µm and outer diameter of 360 µm were purchased from Polymicro Technologies, Inc. (Phoenix, AZ). Columns of 50 cm x 100 µm i.d. were packed in-house with 1.7 µm C18 bridged ethyl hybrid particles (Waters; Milford, MA) as previously described.[87,143] Briefly, column outlet frits were prepared using the Kasil method.[93] An equal amount of potassium silicate and formamide were applied to a glass microfiber filter (Reeve Angel; Clifton, NJ) and the capillary tip was dabbed on the wetted paper to form the frit. A 200 mg/mL slurry was prepared in acetone and placed in an ultrahigh pressure packing apparatus. The column inlet was then secured and submerged in the slurry, with the rest of the column submerged in a sonication bath (Elma Schmidbauer GmbH; Singen, Germany). Packing was initiated by application of low pressure (~1000 psi) using a DSHF-300 pneumatic amplifier pump (Haskel; Burbank, CA). After ~2 cm of the column was packed, the pressure was immediately increased to 30 kpsi. Once ~60 cm was packed, the column was slowly depressurized. The column was flushed at 50 kpsi for 1 h using a DSXHF-903 pump (Haskel; Burbank, CA), slowly depressurized, cut to 50 cm, and an inlet frit was applied using the Kasil method.

3.2.5. Second dimension RPLC-MS

Reversed phase LC separations were carried out on collected fractions using capillary LC-MS. Gradient elution was performed using a custom-built UHPLC system operated at a constant

pressure of 35 kpsi using 50 cm x 100 µm, 1.7 µm C18 columns similar to previous reports.[87,144] Mobile phase A was 60/40 (v/v) water/acetonitrile with 10 mM ammonium formate and 0.1% (v/v) formic acid. Mobile phase B was 85/10/5 (v/v/v) isopropanol/acetonitrile/water with 10 mM ammonium formate and 0.1% (v/v) formic acid. For fractions containing only lysophospholipids the gradient was 50-70% B over 40 min. For PC and SM fractions, the gradient was 70-100% B over 70 min. For all other fractions, the gradient was 60-100% B over 60 min. The column temperature was 60 °C. Effluent from the column was transferred to either a Waters/Micromass QToF Premier or a Waters Xevo QToF using a stainless-steel union and a 30 µm i.d. spray tip (New Objective; Woburn, MA). For positive ionization mode, the spray voltage was 2 kV, cone voltage 30, the sheath gas was 0.5 bar, and the source temperature was 100 °C. For negative ionization mode, the spray voltage was 1.3 kV, cone voltage 22, and the sheath gas was 0.8 bar. Negative mode was used for fractions 1 and 5. The MS was operated in both full scan and MS/MS mode (MS^e and data-dependent acquisition). Scan rates were 0.3 s with 0.1 s inter-scan. External mass calibration was performed using sodium formate. Leucine enkephalin was used as the lock mass compound.

3.3. Results and discussion

3.3.1. First dimension HILIC separation

Previous work has shown that HILIC, which separates lipids primarily by polar headgroup, and RPLC were a useful and orthogonal combination for 2D-LC. Therefore, in this work we used this combination with HILIC HPLC (15 cm long x 1 mm bore packed with 5 µm bare silica particles) for fractionation in the first dimension. A set of 14 lipid standards were used for method development. As shown in Figure 3-1A, good separation of various lipid classes is achieved. Similar to previous reports, lipid separations utilizing bare silica particles is dominated by the lipid

head group, and consequently a majority of lipid classes can be separated.[83,113,142] Certain isomers such as sn-1/sn-2 isomers of lysoPC and lysoPE are also resolved; however, because they can be separated with higher resolution by RP in the second dimension, they were collected in the same fraction to minimize total analysis time. A 40-min separation offered good resolution between most lipid classes. Shortening the gradient to 20 or 30 min in attempt to increase throughput of the ^{1}D separation resulted in loss of resolution between sphingomyelin, phosphatidylcholine, and lysophosphatidylcholine (Figure 3-2).

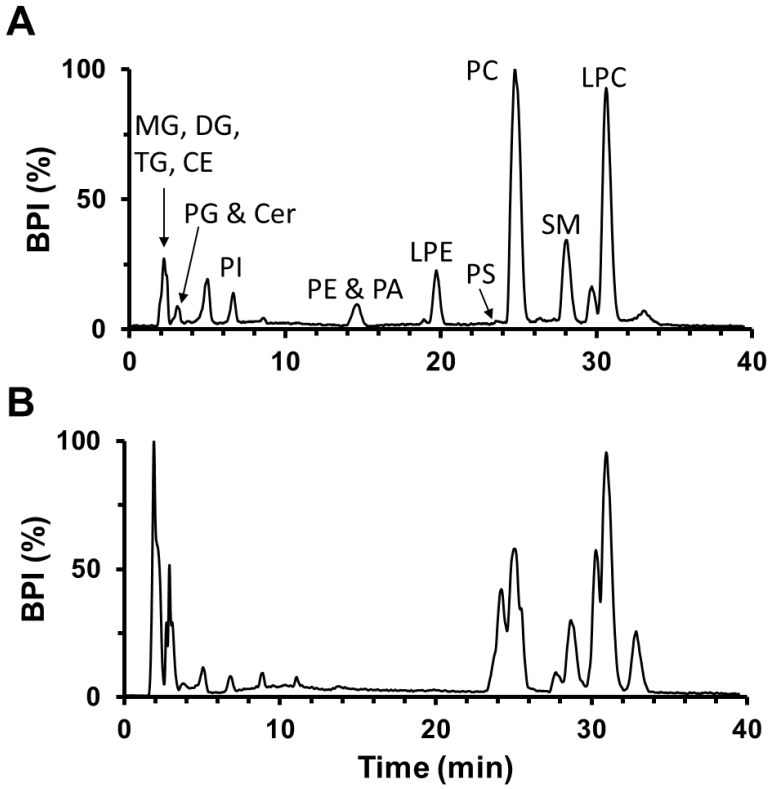

Figure 3-1. First dimension HILIC separation of (A) lipid standards and (B) human plasma extract. Conditions: 15 cm x 1 mm, 5 µm bare silica column; 50 µL/min; 30 °C; 5 µL injection volume; 95-77% B gradient over 40 min; mobile phase A was 5 mM ammonium acetate; mobile phase B was acetonitrile. MS was operated in full scan positive ion mode. All effluent went to MS during these separations.

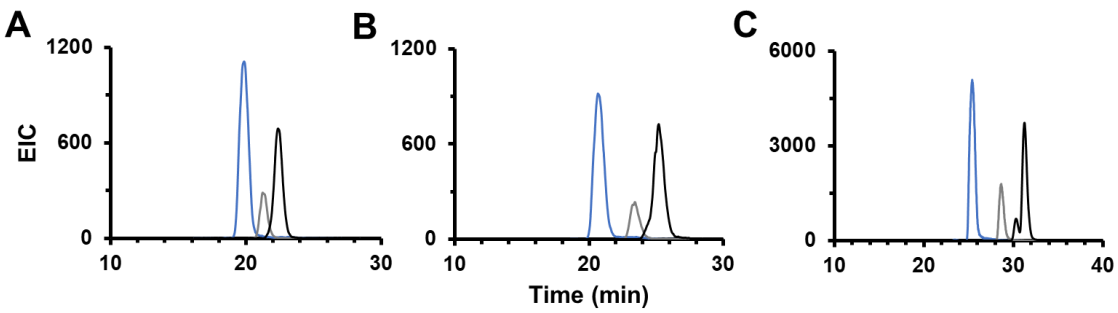

Figure 3-2. Effect of gradient steepness on the resolution of PC (blue), SM (gray), and LPC (black) lipid standards with HILIC. All method conditions were the same as in Figure 3-1 except that the gradient was over 20 min (A), 30 min (B), or 40 min (C).

Following relatively good separation of lipid standards, we applied the HILIC separation to a lipid extract from human plasma. Similar resolution and peak shapes compared to the standards were achieved for endogenous lipids present in the plasma (Figure 3-1B). Importantly, good repeatability of retention times was achieved with subsequent injections of the plasma extract, ensuring successful collection of each fraction (Table 3-1). Many lipid species within a lipid class co-eluted together because they possess the same head group. Fraction collection was based on the elution profiles of different classes and is summarized in Table 3-2. Other lipid classes not in the standard mixture were collected from the plasma extract (Table 3-2). The complexity of each fraction is illustrated in Figure 3-3 where many ions are detected for a given peak during online ESI-MS analysis.

Table 3-1. Retention time repeatability of the first dimension HILIC separation for three separation injections of a human plasma extract. Retention times of each fraction were based on the apex of each peak displayed in the MassLynx browser.

	Retention Time (min)				
	t0	PE	PC	SM	LPC
Run 1	1.92	13.60	25.20	28.86	31.03
Run 2	1.71	13.75	25.40	29.12	31.45
Run 3	1.94	13.90	25.46	29.15	31.41
Average	1.86	13.75	25.35	29.04	31.30
Std Dev	0.10	0.12	0.11	0.13	0.19
%RSD	5.6	0.9	0.4	0.4	0.6

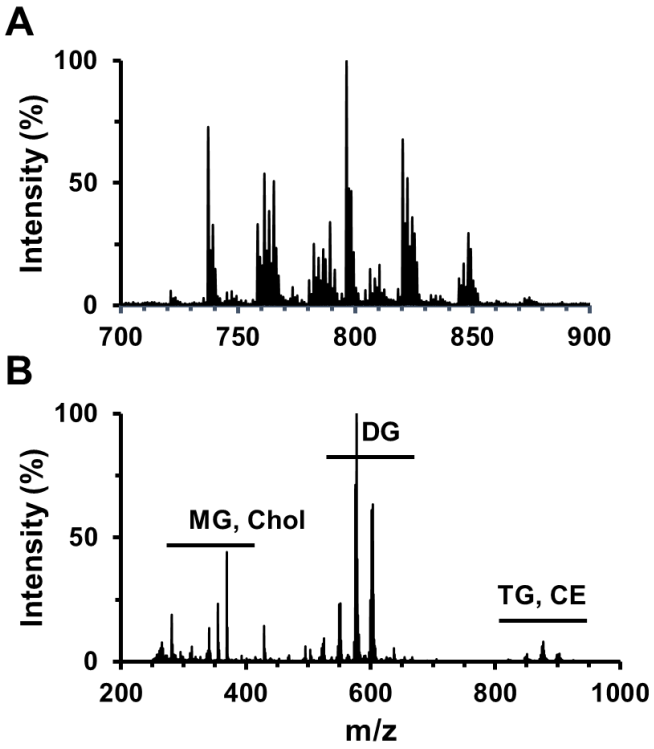

Figure 3-3. Example positive ion mode mass spectra of (A) fraction 7 (phosphatidylcholine) and (B) fraction 1 (acylglycerols, sterol esters, fatty acyls) following first dimension HILIC separation of human plasma with effluent diverted to the MS. Other LC-MS conditions are the same as in Figure 3-1.

Table 3-2. Timetable of fraction collection and associated lipid classes from first dimension HILIC separation. During fraction collection, all effluent was collected in the vial.

Fraction number	Lipid class(es) detected	Collection time (min)
1	TG, DG, MG, FA, Chol, CE, acylCoA, PIP	1.3 – 3
2	PG, Cer	3 – 5
3	PI, HexCer, LPG	5 – 8
4	PE, PA	13 – 16
5	LPE	18.5 – 21
6	PS	21.5 – 23
7	PC	23 – 26
8	SM	27 - 29.5
9	LPC	29.5 – 32.5

A disadvantage of employing bare silica columns is that most neutral and acidic lipids are not well separated. Fatty acids and neutral lipids such as acylglycerols and sterols/sterol esters elute in the dead time placing a greater burden on the separation of these components by reversed phase LC in the second dimension. Phosphatidic acids were retained but gave larger peak widths than the other lipid classes investigated (Figure 3-4). Recent work has shown that hydride stationary phases can give improved separation of acidic lipids, however this was not investigated in this work.[84] Nonetheless, phosphatidic acids were still able to be analyzed in this work and collected with the phosphatidylethanolamine fraction and detected following ^{2}D RP-LC-MS analysis.

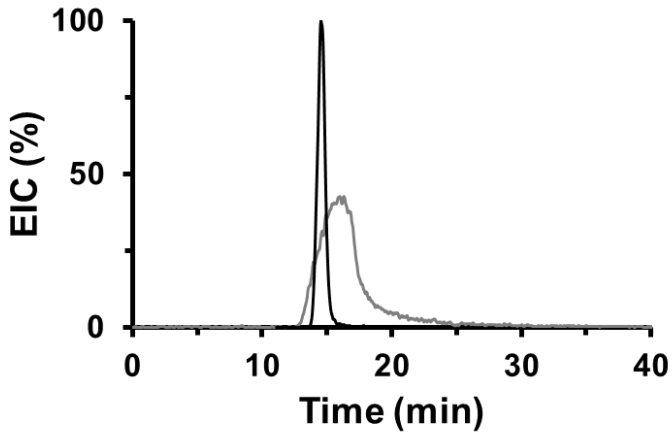

Figure 3-4. Poor peak shape of phosphatidic acid (gray) on the 1D bare silica column. Phosphatidylethanolamine (black), which co-eluted and was collected with phosphatidic acid, demonstrated better peak shape representative of most lipids on this column.

3.3.2. Evaluation of ^{2}D injection solvent

Following fraction collection, solvent was evaporated under nitrogen. Drying was rapid (~5 – 10 min), due to the low volume and high amount of acetonitrile in the ^{1}D mobile phase, and did not significantly contribute to the overall analysis time. Different compositions of reconstitution solvent were considered depending on the fraction type. For example, relatively polar fractions such as lysophospholipid fractions (e.g., lysophosphatidylethanolamine and lysophosphatidylcholine) could be resuspended in 100% mobile phase A (60/40 water/acetonitrile) without significant sample loss from insolubility and provided better peak shape compared to resuspension in stronger solvents. This approach was not possible, however, with the t_0 fraction that contained both fatty acids (1 acyl chain) and triacylglycerols (3 acyl chains). Resuspension of the t_0 fraction in 100% mobile phase B provided higher signal intensities for late eluting compounds; however, this injection solvent led to worse peak shapes for early eluting compounds such as fatty acids within this fraction (Figure 3-5). We chose 100% B as resuspension solvent for the t_0 fraction. It may be possible to overcome this compromise between peak shape for early eluting compounds and signal intensity for late eluting compounds by using alternative solvents

that provide good resuspension of nonpolar lipids while also providing good peak shape for early eluting polar lipids.[40]

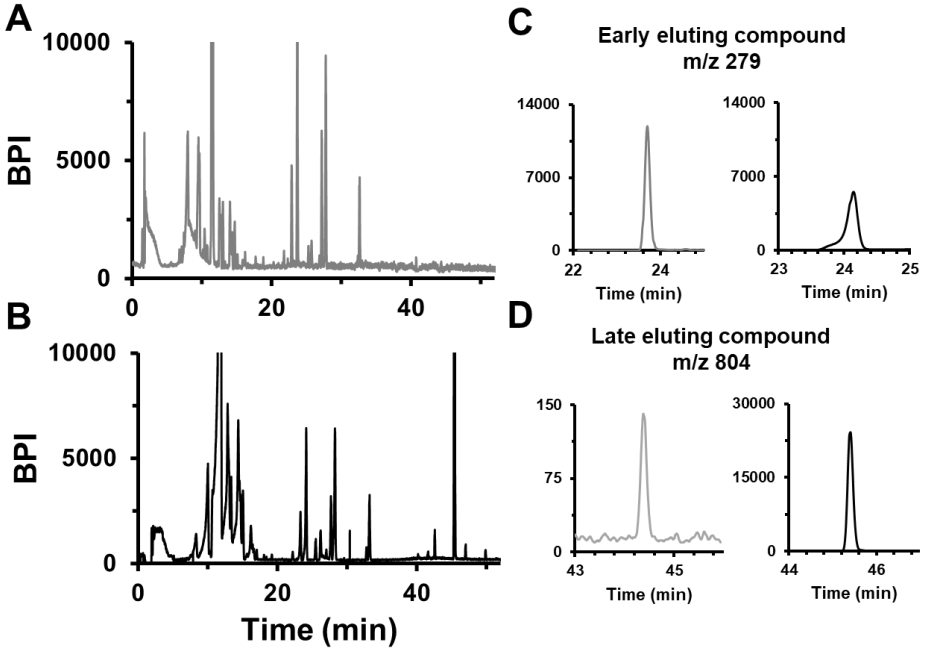

Figure 3-5. Effect of resuspension solvent on peak shape and signal intensity for the first fraction analyzed in negative mode. (A) 50/50 (v/v) mobile phase A/B was used or (B) 100% mobile phase B was used as resuspension buffer. Extracted ion chromatograms illustrate peak fronting for early eluting peaks with the stronger mobile phase injection solvent, but signal intensity for late eluting peaks was improved with the stronger mobile phase solvent. Other conditions: 50 cm x 100 µm, 1.7 µm C18 column; 35 kpsi operating pressure; 60 °C; mobile phase A was 60/40 water/acetonitrile with 10 mM ammonium formate and 0.1% formic acid; mobile phase B was 85/10/5 isopropanol/acetonitrile/water with 10 mM ammonium formate and 0.1% formic acid.

3.3.3. Evaluation of transfer from first to second dimension

One disadvantage of using an offline approach compared to online 2D-LC is the potential for analyte loss when transferring sample between the first and second dimensions. In this case, sample loss can arise from unsuccessful collection of the sample peaks, excessive or aggressive evaporation when drying the fractions, adsorption on collection vials, and failure to successfully resuspend the dried fractions in adequate solvent prior to the second dimension. We evaluated the sample recovery between the dimensions by comparing the signal of PC 18:1-18:1 standard injected directly onto the capillary column and injected on to the HILIC column, collected,

evaporated, resuspended in ^{2}D buffer, and subsequently injected on to the capillary column. Peak height was 2705 ± 225 (n = 2 injections) and 3033 ± 435 (n = 3 injections) and peak area was 545 ± 53 and 573 ± 58 for the for the 2D workflow versus direct injection, respectively, suggesting no significant sample loss. While we assume other lipids behaved similarly, trace amounts of the most nonpolar lipids such as triacylglycerols and cholesteryl esters were seen in multiple fractions, possibly due to solubility issues of TGs and CEs with the ^{1}D mobile phase, and especially considering the high concentration of these lipids in plasma (e.g., ~high µM to mM). Quantification could be problematic for these lipids as a result, and future work should investigate mitigation strategies.

3.3.4. Evaluation of ^{2}D injection amount

As discussed in the introduction, one advantage of using offline 2D-LC is that the ^{2}D separations are independent of the first dimension. Thus, there is greater freedom regarding the ^{2}D gradient time and injection volume that would otherwise be detrimental to the overall separation performance in online 2D-LC. We investigated different approaches for injecting larger amounts of each fraction on the ^{2}D column. One approach was sample preconcentration. By reconstituting the fraction in a smaller volume after solvent evaporation from the first dimension, a more concentrated sample can be injected. Figure 3-6A&B illustrates the gain in signal intensity for fraction 2 (phosphatidylglycerols and ceramides) with no preconcentration compared to a 2X preconcentrated sample (e.g., sample redissolved in 20 µL vs. 10 µL, respectively). Further preconcentration was attempted by redissolving in 5 µL; however, this approach was inconsistent likely due the difficulty in effectively dissolving the lipids dried in the glass vials. Additionally, this small of sample volume limits the number of possible replicates when using 1 – 2 µL injection volumes.

The second approach to maximizing the amount of lipids injected and detected was by simply increasing the injection volume. Although the column volume of the 50 cm x 100 µm capillary columns is ~3 µL, the high retention capacity of lipids on C18 columns allowed relatively large injection volumes (1 – 2 µL) without detrimental loss in separation performance. Example base peak chromatograms for fraction 8 (sphingomyelins) shows a larger number of observed peaks and enhanced signal when using a 2 µL injection volume compared to 1 µL (Figure 3-6C&D). These approaches for increasing the amount of sample injected on the second dimension were most beneficial for lower abundant fractions or fractions that do not produce as good of MS response.

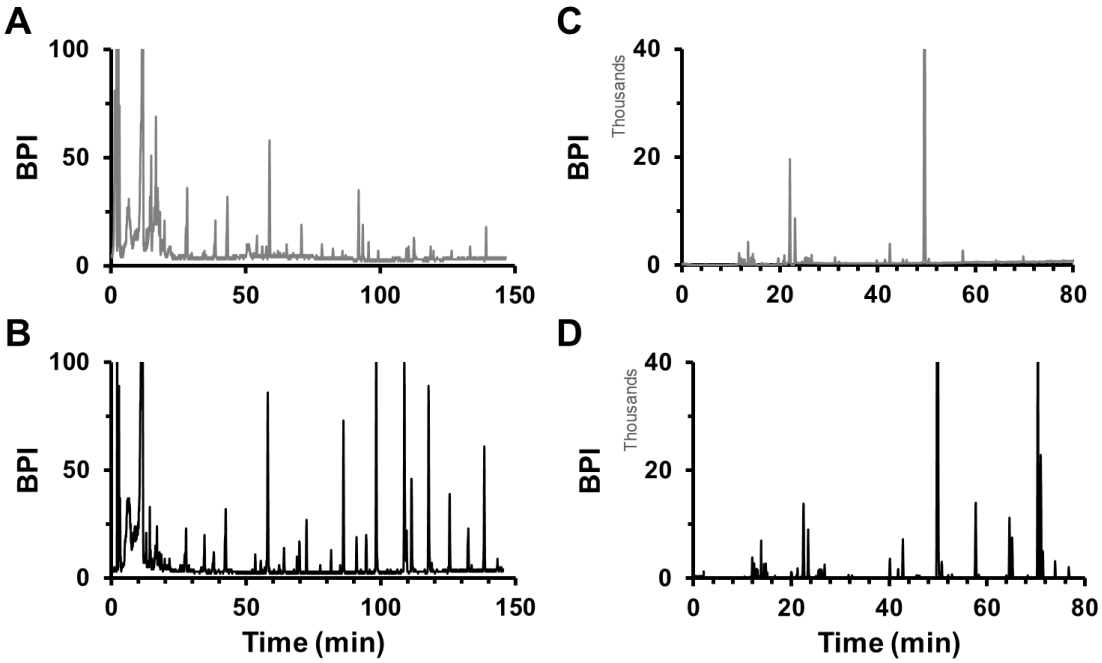

Figure 3-6. Effect of resuspension volume and injection volume on signal intensity for different fractions. Comparison of 20 µL (A) and 10 µL (B) resuspension volumes on signal intensity for fraction 2 (phosphatidylglycerols and ceramides). Comparison of 1 µL (C) and 2 µL (D) injection volumes on signal intensity for fraction 9 (sphingomyelins).

3.3.5. Evaluation of ^{2}D gradient length and steepness

A substantial disadvantage of online 2D-LC is that the ^{2}D gradient time is limited by the ^{1}D sampling time to maintain separation performance, often limiting the ^{2}D separation time to less

than ~2 min. In offline 2D-LC, the separations are independent and the ^{2}D gradient time can be modified to improve the separation for each fraction. We evaluated the effect of gradient time (e.g., gradient length) and gradient slope on resolution and signal intensity of the lipid fractions. Previous work has shown that longer gradient times (~2 – 3 h) and shallower gradients improve the resolution and the number of lipids identified in untargeted single dimensional LC-MS lipidomics.[85–87] This observation is likely due to alleviation of ionization suppression caused by co-elution and increased resolution of isobaric species. In attempt to limit each ^{2}D separation to ~1 h to keep total analysis time relatively short, we first compared 2-3 h gradient separations to shorter gradients. For a few fractions, a shorter gradient provided better signal intensity due to narrower peaks and higher peak heights from less chromatographic dilution (e.g., PG/Cer fraction, LPC fraction) compared to a ~2.5 h gradient (Figure 3-7). In some cases, the broader peaks caused by such shallow gradients caused a loss in detection for lower abundance isomers (e.g., LPC 18:0 in the inset of Figure 3-7A&B). For other fractions, however, a steeper gradient caused losses in resolution for certain critical pairs, and further method development was needed to resolve. Implementing a narrower Δ% B (e.g., 70 – 100% B) more amenable to the target compounds in each fraction allowed for shallower gradients to be used in roughly the same amount of time compared to wider gradient profiles (e.g., 50 – 100% B). This change provided good separation for isomeric and other critical pairs and was most evident in the fractions containing PCs and SMs (Figure 3-8).

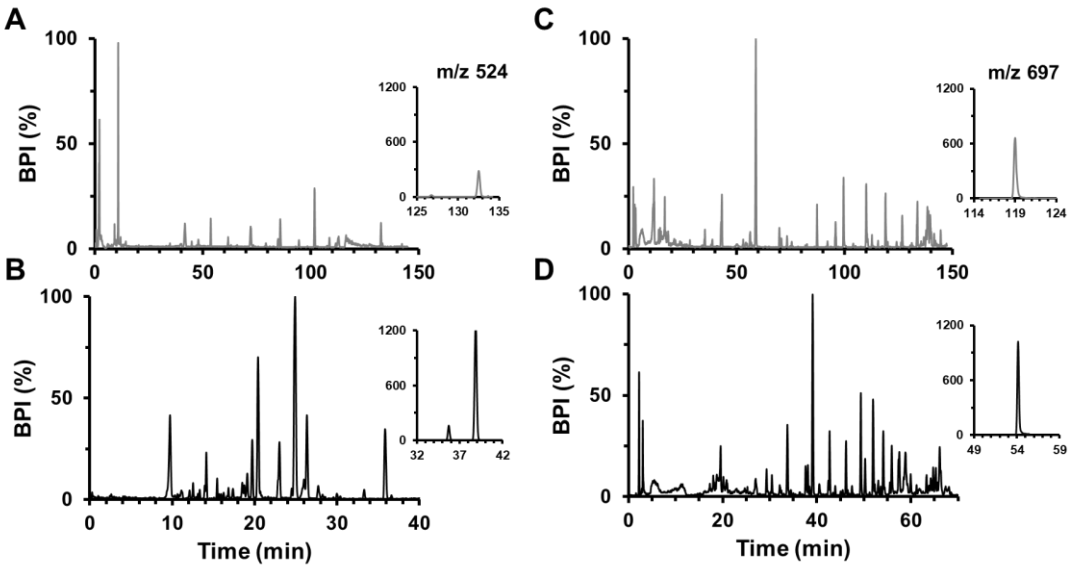

Figure 3-7. Comparison of gradient length for (A and B) fraction 9 (lysophosphatidylcholines) and (C and D) fraction 2 (phosphatidylglycerols/ceramides). For these fractions, a steeper gradient provided better signal intensities with narrower peak widths while still providing good resolution for most peaks. Extracted ion chromatograms show the decrease in signal intensity for the longer, shallower gradients, with an isomer of LPC 18:0 approaching the detection limit (inset of panel A).

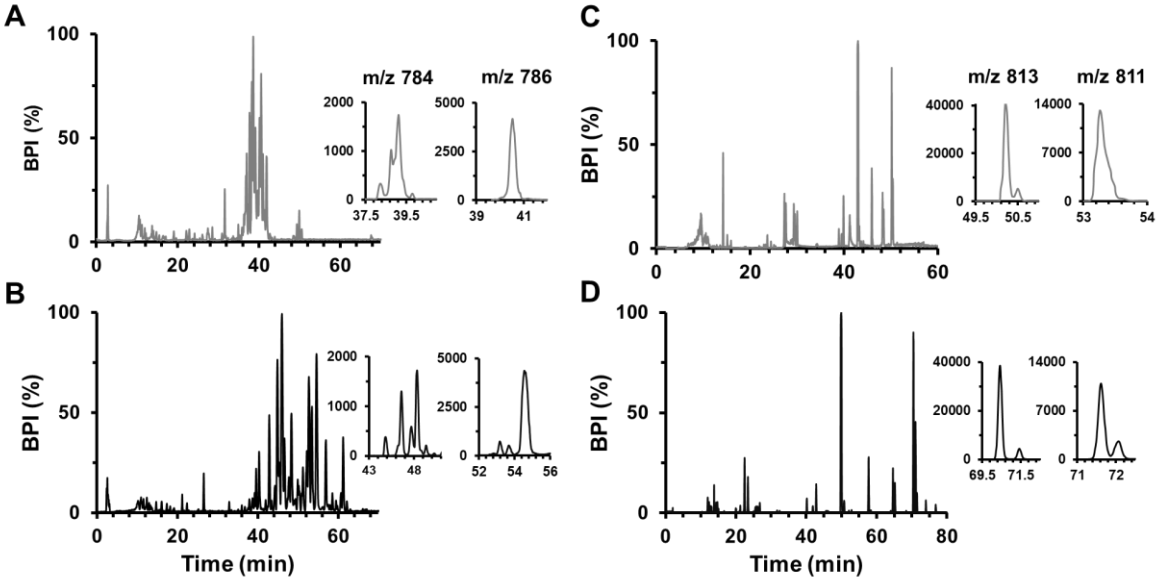

Figure 3-8. Effect of gradient steepness on chromatographic resolution for (A and B) fraction 7 (phosphatidylcholines) and (C and D) fraction 8 (sphingomyelins). A 50-100% B gradient (A) is compared with an 70-100% B gradient (B). Example EICs for m/z 784 and 786 are shown to illustrate the improvement in resolution of different isomers with a shallower gradient. A 60-100% B gradient over 50 min (C) is compared with an 70-100% B gradient over 70 min (D). EICs for m/z 813 and 811 are shown.

3.3.6. Orthogonality measurement

Employing orthogonal separation mechanisms in a multidimensional separation is crucial for obtaining the expected gain in peak capacity.[111,112] The idea and necessity of orthogonality in 2D separations has been studied in the past; consequently, empirical approaches for calculating orthogonality have been explored.[145–150] These evaluations are critical for accurately measuring the peak capacity of a multidimensional separation. In this work, we evaluated the orthogonality between the ^{1}D HILIC separation and the ^{2}D RP separations using the 'bin-containing' method.[145,149] In this approach, the separation space is divided into bins, and the fractional coverage is calculated by dividing the number of bins containing peaks by the total number of bins within the separation space. In this work, a bin was defined as 0.5 min, and a bin was considered at each point between the start and end of the gradient. Next, a base peak chromatogram was generated for each fraction and the maximum intensity normalized to 100% for each fraction (Figure 3-9A). A bin was considered "full" if the signal intensity was above 3% of the baseline. Results of this calculation are shown in Figure 3-9B. The coverage was determined to be 41%, which is considered highly orthogonal and so the product rule of peak capacity measurement for a 2D separation is a good approximation.[145] A ~40% coverage space is similar to previous lipidomics reports using online HILIC and RP-LC.[114] The total peak capacity of the 2D separation was 1870 with a separation time of approximately 505 min for the 9 fractions plus 40 min for the ^{1}D separation. The t_0 fraction was analyzed twice (once in positive ion mode and once in negative ion mode), which made the total analysis time 605 min but did not increase the separation peak capacity.

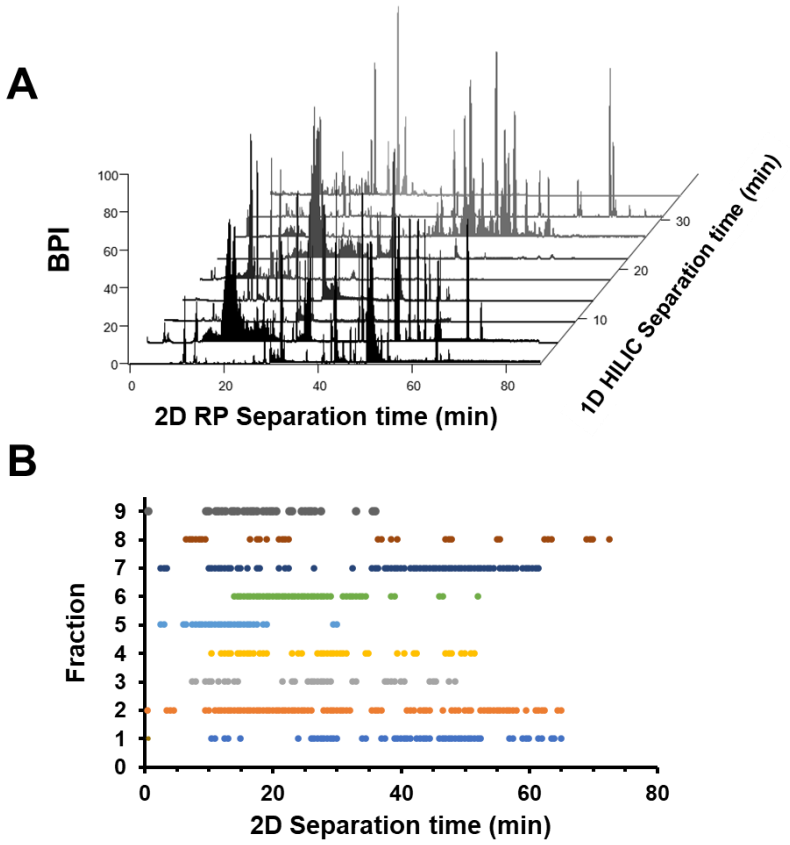

Figure 3-9. (A) Two-dimensional waterfall plot of the 9 fractions each displayed as base peak intensity chromatograms. (B) "Bin"-based fractional coverage plot used for orthogonality measurement.

3.3.7. Lipid identification

The previous sections described approaches for increasing the separation peak capacity and MS signal intensity of lipids from a human plasma extract. These metrics are important and can often improve identification of lipids from a complex matrix such as plasma; however, the total number of lipids detected and identified is the most important characteristic of an untargeted lipidomics method. We putatively identified or detected lipids from the human plasma extract using MS1 data and libraries from Lipid Blast[12] and the Metabolomics Workbench.[9] Approximately 1082 lipids were detected in human plasma using the 2D-LC-MS method. Of the 8 total lipid categories, glycerolipids, glycerophospholipids, fatty acyls, sterols, and sphingolipids

were detected. Among these, the most abundant lipid classes and subclasses included phosphatidylcholine, sphingomyelin, ceramides, fatty acids, and (mono-/di-/tri-) acylglycerols. The number of detected lipids here is roughly double the number of lipids detected in our previous work using single dimensional RP-LC-MS;[87] this improvement comes at the expense of analysis time. Previous work showed a linear increase in lipids detected vs peak capacity and approximate linearity with analysis time. The 2D data did not fit this trend, with much less lipids detected per peak capacity (Figure 3-10A&B). Further improvements in detection sensitivity or extraction protocols may improve the number of lipids detected and better agree with the 1D trend MS1 feature counts also showed linear trends with increased peak capacity and analysis time from the 1D RP work and again much less per peak capacity and time for the 2D analysis (Figure 3-10C&D). It should be noted that the Metabolomics Workbench database was also used in the 2D work where only LipidBlast was used in the 1D work. Similar improvements in lipid identification have been observed for multidimensional LC-MS lipidomics methods, likely due to decreased ionization suppression from higher peak capacity separations, cleaner mass spectra, and separation of isobaric and isomeric species.[116,128]

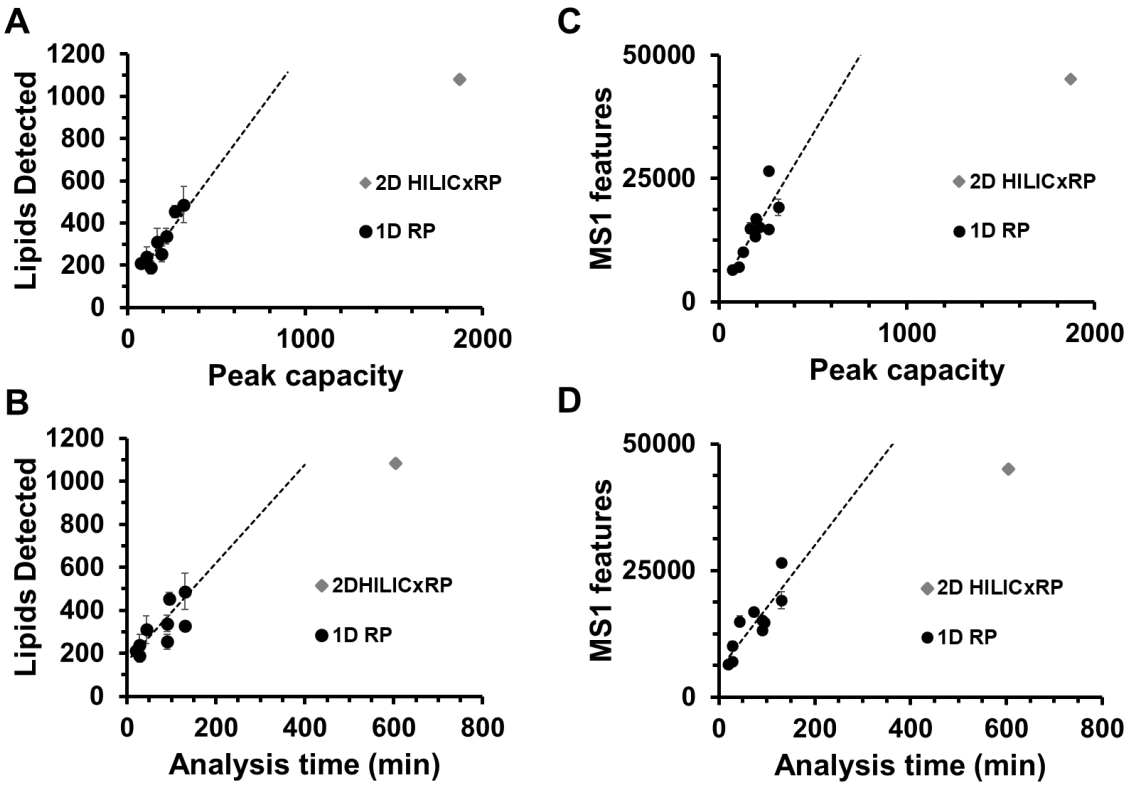

Figure 3-10. Number of lipids detected using library database matching as a function of chromatographic peak capacity (A) and analysis time (B). MS1 feature counts are plotted versus peak capacity (C) and analysis time (D). One dimensional RP-LC-MS data are reproduced from a previous report[87] and chapter 2 (black circles). A roughly linear increase in lipids detected was seen for one-dimensional peak capacities and analysis times and is compared with the two-dimensional work reported here (gray diamond).

The method developed here employed a 5 µL injection volume, requiring 2.5 µL of plasma; these small volume injections are advantageous for low input samples where sample collection is limited. It should be noted however that the actual volume of plasma used in the extraction was 50 µL, and using smaller volumes of plasma (e.g., < 5 µL) may require different sample preparation techniques as discussed in other reports.[130,141] Finally, the use of a microbore column (1 mm i.d.) in the first dimension and a capillary column (100 µm i.d.) in the second dimension provided relatively low solvent consumption – approximately 2.5 mL in the total 2D-LC method.

Further improvements in lipidome coverage could be achieved by using smaller inner diameter columns with lower flow rates, combining with ion mobility separations, or employing even higher resolution separations with smaller particles or longer columns. Additionally, lipidome

coverage could be increased with the current instrumentation by selectively adjusting the ^{2}D mobile phase composition depending on the fraction type. For example, ammonium fluoride buffer provides higher signal intensity for phosphatidylinositol species in negative ionization mode compared to ammonium formate or acetate buffers.[151] Lastly, additional metrics such as tandem mass, intensity, and internal standard data can be used to improve lipid identification confidence.

3.3.8. Comparisons with previous methods

Previous online 2D-LC lipidomics studies typically employed analysis times of 2 – 4 h, achieving peak capacities up to ~600. Using trapped ion mobility separations as the second dimension, a peak capacity of 991 was achieved in 190 min, however lipid identifications were less than 2D-LC.[114] Offline analysis times were typically > 5 h, with peak capacities estimated at ~ 500 – 1000.[89,113] High-resolution single dimension analyses of lipids have yielded peak capacities of 300 – 400 in 2 – 4 h using long (30 – 60 cm) columns.[85–87,138] Peak capacities are lower than what has been achieved with small molecules or peptides, likely due to the high viscosity of isopropanol which results in slower diffusion of lipids and limits particle size and column length. Peak capacities up to ~1800 can be achieved for peptides or small molecules with long columns and sub-2 μm particles.[65,144,152] Recent online 2D-LC work for peptide separations has shown peak capacities of 1500 in 30 min and 10,000 in 240 min.[153,154] Work shown here illustrates the advantages of offline 2D-LC and long microcolumns operated at 35 kpsi for relatively high resolving power of lipids compared to previously published work.

3.4. Conclusions

An offline, two-dimensional liquid chromatography-mass spectrometry method was developed for untargeted lipidomics analysis of human plasma. Hydrophilic interaction liquid chromatography using a 1 mm i.d. bare silica column was employed in the first dimension,

allowing separation of lipid classes. Second dimension reversed phase separations were performed on a custom-built UHPLC system at 35 kpsi using 50 cm x 100 µm i.d. columns packed with 1.7 µm C18 particles. High-resolution separations were achieved for each fraction, allowing separation by chain length and double bond characteristics of lipid species within a given class. Effect of resuspension volume, injection volume, and gradient steepness were investigated to improve signal intensity and chromatographic resolution. Lipids were detected based on library matching; approximately 1100 lipids were detected from a 5 µL injection of a human plasma extract. Overall, the method was orthogonal, provided a total peak capacity of about 1900, and used less than 3 mL of mobile phase.

Chapter 4. Capillary Ultrahigh Pressure Liquid Chromatography-Mass Spectrometry for Fast and High-Resolution Metabolomics Separations Using 1.1 µm Particles

Reproduced in part from Sorensen, M. J.; Kennedy, R. T. *Journal of Chromatography A* **2021**, 1635, 461706.

4.1. Introduction

Metabolomics utilizes measurements of a large number of metabolites from biological, environmental, or industrial sources.[11] Metabolomics has been applied in many areas, including food science, plant biology, biofuels, environmental studies, and biomarker and drug discovery for animal and human health.[1,3–5] Metabolites differ from lipids in that most compounds are much more polar and their molecular weights typically range from 50 – 400 Da, whereas lipids are typically quite nonpolar and range from 300 – 1200 Da. The current state of the art in liquid chromatography-mass spectrometry (LC-MS) based metabolomics utilizes 1.7 µm particle diameter (d_p) stationary phase particles packed into analytical scale columns (e.g., 1 – 2.1 mm inner diameter (i.d.)) of 5 to 15 cm length.[15,22,35,36] Such columns provide peak capacities of ~100 – 200 in 5 – 20 min gradients at flow rates amenable to electrospray ionization (ESI) for sensitive and information-rich analysis. The complexity and dynamic range of the metabolome however still exceeds the current state of the art, where typically thousands of compounds are present in a given sample. One single analytical technique is not yet sufficient to analyze an entire metabolome.[19] In this work, we evaluate use of both smaller d_p and longer capillary-scale columns for metabolomics.

Improvements in separation can often lead to better metabolomics data. For example, changing from columns packed with 3.5 µm to 1.7 µm stationary phase particles and utilizing a higher pressure system resulted in faster and more sensitive urine metabolomics analysis while doubling the separation peak capacity. These improvements provided cleaner mass spectra and more confident multivariate metabolic profiling.[25] Further work involving reduction of the column i.d. from 2.1 to 1 mm allowed for better sensitivity due to lower flow rates while maintaining high linear velocities, enabling confident discrimination between two dose groups with less than 5 min analysis times per assay.[155,156] Increasing pressure limits to ~20 kpsi and utilizing 200 cm long microcolumns packed with 3 µm particles, Shen et. al. demonstrated peak capacities around 1500 and detected 5000 metabolites from cell culture, with an analysis time of 2000 min.[65]

In principle, further improvements in separation efficiency or analysis time can be gained by employing even smaller (e.g., ~1 µm) stationary phase particles; these theoretical improvements were illustrated in Chapter 1. Widespread use of such particles has not been realized due to difficulties in synthesizing and efficiently packing small porous particles, the difficulty in maintaining separation efficiency while robustly interfacing to MS, and the increased pressure demand on instrument hardware.[137] Custom-built LC instrumentation capable of higher pressure (e.g. > 20 kpsi) has been developed by several research groups suggesting the potential to overcome the pressure limitations of working with smaller particles.[51] These systems have primarily been used with 30 – 200 cm long columns packed with 1.7 – 3 µm particles operated with long gradients of 400 – 2000 min. Such conditions yield high efficiency and peak capacity at the expense of analysis time. They have also mostly been demonstrated for peptide separations, and recently lipids and intact proteins.[50,51,65,67,87,157] Only a few reports have used ~1 µm porous particle packed columns, with mixed results compared with larger particles.[62,67] These applications

and demonstrations have again only been used for peptides.[67,158,159] Preparation and use of nonporous particle packed columns has been relatively successful; however, their relatively low loading capacity has limited their use for complex mixture analysis.[56,160–162]

Columns packed with micron-sized particles would benefit metabolomics assays where many complex samples must be analyzed and throughput is important. In this work, we used a custom-built gradient LC-MS system (Figure 1-5) capable of 35 kpsi operating pressure with 1.1 µm particles packed in to 20 cm long capillaries and 1.7 µm particles packed in to 50 cm long capillaries for relatively fast (analysis time 13 – 110 min) and high-resolution (peak capacity 200 – 500) separations. These experiments used capillary scale columns (75 – 150 µm i.d.) because of the ease of packing, compatibility with ultrahigh pressure systems, ease of making longer columns, and reduction of heating due to viscous friction.[49] Capillary LC columns can also provide better MS sensitivity with reduced ion suppression because of lower flow rates,[163] utility for sample-limited analysis, and economical use of mobile and stationary phases.[164] Capillary columns are routinely used in proteomics but have not yet been widely implemented in metabolomics.[165,166] Benzoyl chloride (BzCl) derivatization was used to improve retention of polar metabolites on reversed phase columns, as such labeling strategies have shown to be useful for both targeted and untargeted workflows.[167–169] Finally, the effect of different LC-MS variables on MS features was studied.

4.2. Materials and methods

4.2.1. Chemicals and materials

All chemicals and reagents were purchased from Sigma Aldrich (St. Louis, MO) unless specified otherwise. HPLC grade water, acetone, methanol, and acetonitrile were purchased from VWR (Radnor, PA). Potassium silicate (Kasil 2130) was purchased from PQ corporation (Valley

Forge, IA). 3,4-Dihydroxyphenylacetic acid (DOPAC) was purchased from Acros Organics (Geel, Belgium). Particle size characterization was done using a Zeiss LEO 1455VP Scanning Electron Microscope (SEM) (Jena, Germany) for imaging and ImageJ software (NIH; Bethesda, MD) for d_p measurements. Pneumatic amplifier pump (Haskel; Burbank, CA) DSHF-300 was used for column packing and DSXHF-903 was used for column flushing and LC operation.

4.2.2. Standards and benzoyl chloride derivatization

A standard amino acid test mixture consisting of 10 µM acetylcholine and BzCl labeled proline (Pro), valine (Val), tyrosine (Tyr), and tryptophan (Trp) was used for column evaluation. Each compound was dissolved in water and combined to make a 100 µM stock solution. For scan rate studies, a 26 compound mixture was used and prepared as previously described.[170] Derivatization was carried out by sequential addition of 100 mM sodium carbonate, 2% (v/v) BzCl in acetonitrile, and 1% (v/v) sulfuric acid in 20% (v/v) acetonitrile in water in a 2:1:1:1 ratio as previously described.[167] Selected compounds from the 26 compound mixture, namely Bz-phenylalanine (Bz-Phe), Bz-Tyr, and Bz-DOPAC were used for monitoring the effect of scan rate. The BzCl derivatized amino acid standard mixture was diluted to a final concentration of 10 µM using water.

4.2.3. Human plasma extraction

Metabolites were extracted from pooled human plasma using a mixture of ice-cold methanol/acetone/acetonitrile (v/v/v 1:1:1) as the extraction solvent. To 100 µL of plasma, 400 µL of extraction solvent was added, vortexed, and centrifuged at 12,100 x g at 4 °C for 10 min. The supernatant was removed to a glass HPLC vial, evaporated with nitrogen, and reconstituted with 100 µL of 90/10 (v/v) water/acetonitrile. The supernatant was then derivatized in the same manner described above.

4.2.4. Column packing

Polyimide-coated fused-silica capillaries with varying inner diameters and outer diameter of 360 µm were purchased from Polymicro Technologies, Inc. (Phoenix, AZ). Both the 1.7 µm and 1.1 µm particles were bridged ethyl hybrid (BEH) silica with C18 bonding (Waters Co; Milford, MA). Column frits were prepared by spotting an equal amount of potassium silicate and formamide on a glass microfiber filter paper (Reeve Angel; Clifton, NJ) and dabbing the end of the capillary ~ 5 times, and placed in a ~60 °C oven overnight.[93] For isocratic separations with MS detection, a pre-fritted, embedded spray tip (30 µm i.d.) (New Objective; Woburn, MA) was used instead of an outlet frit to limit post column dead volume. For isocratic separations with UV detection, a methacrylate-based monolithic frit was prepared upstream of the capillary end to make room for a flow cell immediately after the column bed.[171] Briefly, a monomer solution of 30/70 (v/v) glycidyl methacrylate/trimethylolpropane trimethacrylate with 1.5% (w/v) benzoin methyl ether was prepared in 30% toluene (v/v) in isooctane. Frits were loaded into the capillary via capillary action. Polymerization was achieved by exposure of a region of the capillary with a UV lamp (Spectronics; Westbury, NY) for 10 min. Acetone was used as the slurry solvent for all columns.[50,172] Slurry concentration for each particle size and the application of sonication while packing was chosen based on previous studies.[60–63] For 15 cm/1.7 µm columns representing commercial columns, packing was achieved using a 100 mg/mL slurry with a low-pressure packing apparatus at ~1000 psi and subsequently flushed at 15,000 psi in 50/50 (v/v) water/acetonitrile. For the 50 cm/1.7 µm columns and 20 cm/1.1 µm columns, slurry concentrations of 200 mg/mL and 30 mg/mL, respectively, were used. Low pressure (~1000 psi) was applied to form ~2 cm of packed bed, followed by immediate application of 30 kpsi while the

column was sonicated. The columns were subsequently flushed at 50 kpsi.[63] All columns were depressurized for 1 h, cut to the desired length, and an inlet frit was made as described above.

4.2.5. LC-MS operation

For isocratic separations, a split-flow injection system was employed as previously described with 50/50 (v/v) water/acetonitrile with 10 mM ammonium formate and 0.1 % formic acid.[55,173] For separations with UV detection, a Linear UVIS 200 (Thermo Scientific; Waltham, MA) variable wavelength spectrophotometer was used with a burned slot through the capillary post column for the flow cell. Data were sampled at 20 Hz with a 14-bit data acquisition card (National Instruments; Austin, TX) and acquired using an in-house LabView (National Instruments; Austin, TX) program. For separations with MS detection, a Thermo Finnigan LCQ Deca XP Plus (Thermo Fisher Scientific; San Jose, CA) using a nanospray ion source in positive ion mode was used for detection. A scheduled MRM method was employed using the following transitions: Acetylcholine (146-87), BzCl-Proline (220-174), BzCl-Valine (222-176), BzCl-Tryptophan (309-263), and BzCl-Tyrosine (390-240). The capillary voltage was 2 kV. Retention factors (k') were calculated using the following equation:

$$k' = \frac{t_R - t_0}{t_0} \qquad \text{eq. 4-1}$$

For all gradient separations, a modified UHPLC system capable of 35 kpsi operating pressure was used in the same manner as the previous chapters (Figure 1-5).[67,87] Average flow rates at 35 kpsi were 2.5 µL/min and 1.8 µL/min on the 20 cm x 150 µm, 1.1 µm d_p and 50 cm x 100 µm, 1.7 µm d_p columns, respectively. For the 15 cm columns representing commercial limits, a Waters NanoAcquity was used directly at 1 µL/min (~10 kpsi). Mobile phase A was water with 0.1 % formic acid. Mobile phase B was acetonitrile with 0.1% formic acid. All injections were performed in partial loop mode on the NanoAcquity. Peak capacity was calculated by dividing the

elution window by the average peak width (4σ – calculated by measuring FWHM and multiplying by 1.7) of metabolites and lipids eluting throughout the separation window. Column volumes were calculated assuming a total column porosity of 0.8. The column oven was 60 °C. The column outlet was connected to ~15 cm x 25 µm i.d. of empty capillary using a PicoClear union (New Objective; Woburn, MA). Effluent was connected to a Micromass Q-ToF Premier (Waters Co; Milford, MA) using a stainless-steel union and a fused silica spray needle with a 75 µm i.d. tapered to 30 µm tip (New Objective; Woburn, MA). The capillary voltage was 2.5 kV. The scan rate was set to 0.3 s unless otherwise specified and the inter-scan delay was 0.1 s. The MS was operated in full scan, positive ion mode with a mass window of 150-1000 m/z.

4.2.6. Feature detection

For the gradient separations with Q-TOF detection, mass spectra from 30 s (≤45 min analysis times) or 60 s (>45 min analysis times) windows of each chromatogram were extracted, baseline subtracted, and centered in Mass Lynx. A feature was defined as any signal with a unique m/z and retention time and above the average background signal from each separation.

4.3. Results and discussion

4.3.1. Benzoyl chloride derivatization for polar metabolites

Benzoyl chloride (BzCl) derivatization was employed in this work to improve retention of polar metabolites on the reversed phase C18 columns used here. The reaction scheme for BzCl labeling is shown in Figure 4-1. BzCl and other labeling techniques have been widely utilized in both targeted and untargeted LC-MS based metabolomic workflows. The advantages of these labeling strategies include not only increased retention in RP-LC, but also increased ionization

efficiency, improved stability, and better quantitation due to the use of ^{13}C-labeled reagents allowing a near-identical internal standard for every labeled compound.[167–169,174,175]

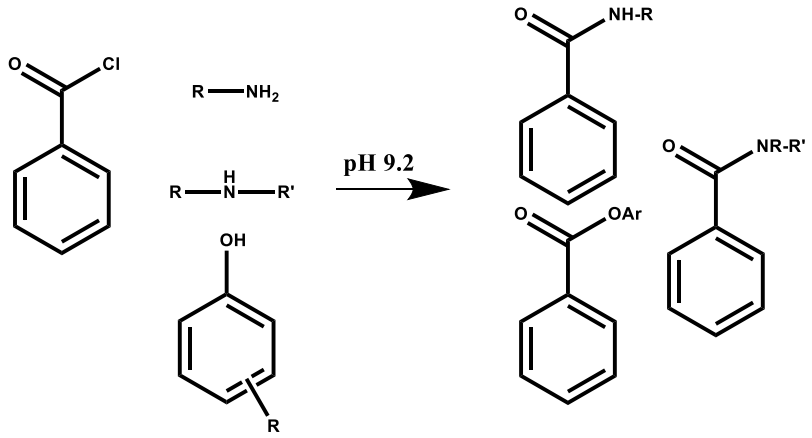

Figure 4-1. Benzoyl chloride derivatization reaction scheme. BzCl reacts at room temperature nearly instantaneously with compounds possessing primary amines, secondary amines, and phenols.

4.3.2. Particle size imaging

The limited reports on use of 1.1 µm porous particles is likely due to their low availability, high pressure requirement, and difficulties in packing.[51,62,67] We verified particle size and particle size distribution (PSD) of these particles using SEM (Figure 4-2A). The mean particle size was 1.3 µm, slightly larger than the 1.1 µm listing by the manufacturer. Similar discrepancies for 1.7 µm particles, which often appear as ~ 2 µm by SEM, have been shown.[63,86] (For consistency, we use the particle size listed by the manufacturer when referencing all particles.) The PSD for the 1.1 µm particles was 12% (120 particles counted), in good agreement with other porous particles indicating well-controlled sizing (Figure 4-2B).[176–178]

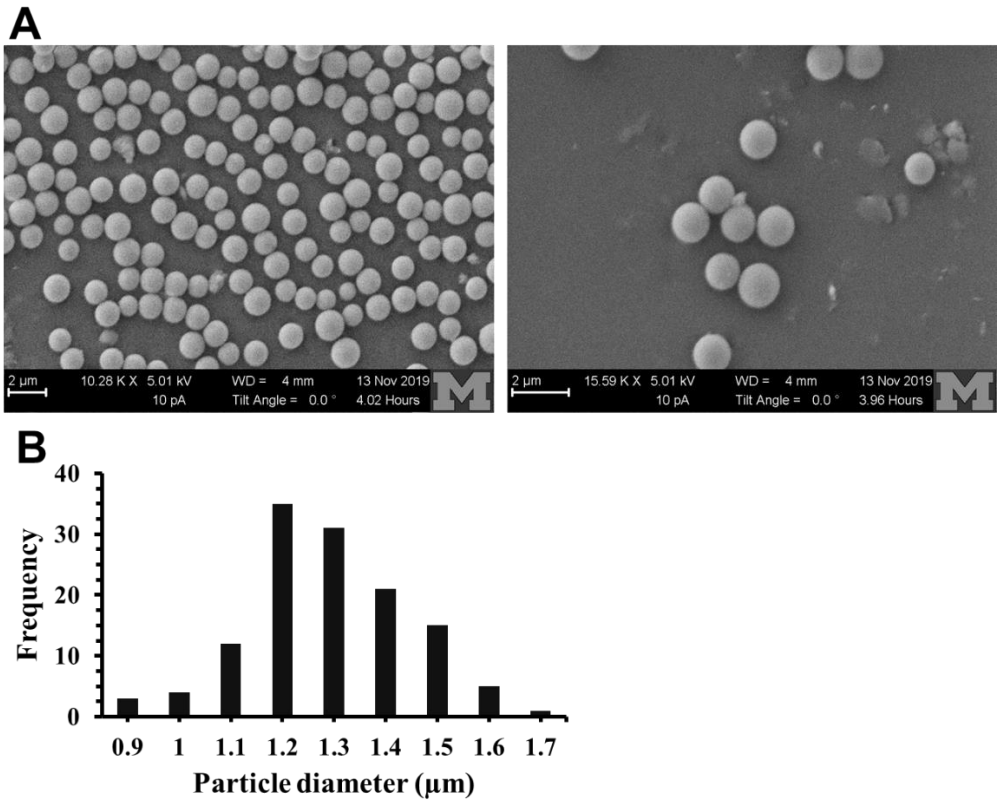

Figure 4-2. (A) SEM images of the 1.1 µm porous BEH particles used in this chapter. (B) Particle size distribution of the imaged particles (120 particles). Mean particle size was 1.3 µm with 12% PSD.

4.3.3. Kinetic plots for choice of particle size and column length

In this work, we investigated the potential of capillary LC-MS using 1.1 and 1.7 µm particles and ultrahigh pressure instrumentation for untargeted metabolomics separations. Kinetic plots (e.g., Figure 1-4) were used to find column lengths that could yield high efficiency while maintaining analysis times typical of metabolomics assays (e.g., ~5 – 30 min). For this kinetic analysis, particles sizes of 1.7 and 1.1 µm were considered due to particle availability and pressure limits of either 10 kpsi or 35 kpsi. Columns are assumed to be equally well-packed, with the following reduced van Deemter coefficients: a = 0.4, b = 1.9, c = 0.18.[50] As shown in Figure 4-3A, a 50 cm column with 1.7 µm particles at 35 kpsi should produce ~100,000 plates with a dead time just over 100 s. A 20 cm column with 1.1 µm particles should produce the same efficiency in

approximately half the time. In contrast, if using current commercial capillary LC systems with 10 kpsi and 15 cm column length, only ~ 30,000 plates is achieved in a dead time of 50 s.

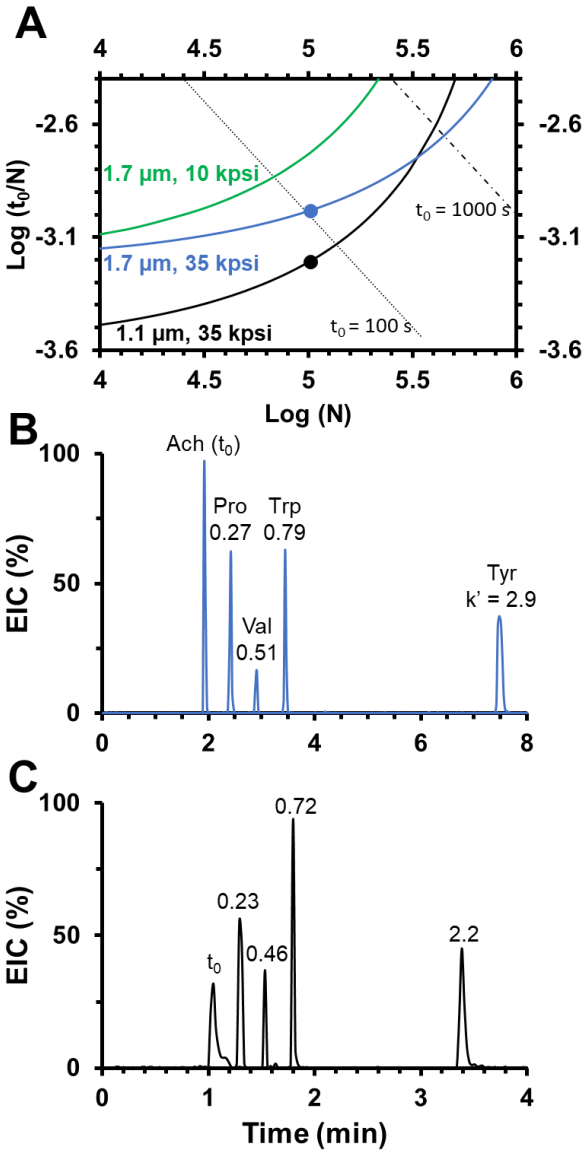

Figure 4-3. (A) Kinetic plot illustrating theoretical improvements when moving from 1.7 µm to 1.1 µm particles with 35 or 10 kpsi instrument pressure. The two dots represent the column length that would produce ~100,000 plates with each particle size and the set pressure limit of 35 kpsi. Diagonal dashed lines representing column dead times of 100 s and 1000 s are shown for clarity. EICs for the isocratic separations using (B) a ~40 cm x 75 µm i.d., 1.7 µm d_p column and (C) ~20 cm x 150 µm i.d., 1.1 µm d_p column of the standard amino acid mixture with acetylcholine (Ach) as a dead time marker. Faster separation with the 1.1 µm particle packed column shows approximate agreement with theoretical expectations. Similar peak shapes and retention factors (k') for BzCl labeled metabolites were obtained with both particle types. Mobile phase was 50/50 (v/v) water/acetonitrile with 10 mM ammonium formate and 0.1% formic acid.

4.3.4. Isocratic column evaluation using amino acid standards

Initial chromatographic experiments were directed towards determining if the packing conditions and UHPLC system used here resulted in good performance for capillary columns. Figure 4-3B & C shows results from isocratic separations of the BzCl labeled standard amino acid mixture, along with acetylcholine (Ach) as the dead time marker, for 1.7 µm particles packed into ~40 cm long x 75 µm i.d. and 1.1 µm particles packed into ~20 cm x 150 µm i.d. columns. (We found little difference in column performance with inner diameters of 75 – 150 µm for the isocratic conditions studied here, similar to recent studies using the same packing protocol employed here).[86,87] The shorter length of 40 cm compared to the expected 50 cm from the kinetic plot was due to the limited length of the embedded spray tip capillary at the time. The dead time for the 1.1 µm column was ~50% faster as expected from the kinetic plot, and similar retention factors were achieved between the two columns for each amino acid. The 20 cm column with 1.1 µm particles generated 80,000 plates and the 50 cm column with 1.7 µm particles generated 85,000 plates, measured for Bz-valine (k' ~ 0.5) Additionally, these results showed that coupling to MS while maintaining chromatographic performance is possible, whereas many reports have shown deteriorated performance when coupling with MS compared to UV detection.[179] Peak shape was, however, slightly affected by MS scan rate for these separations due to the slow acquisition speed of the MS used, which could marginally affect plate count measurements.[180,181] Future work for isocratic column evaluation is being done utilizing UV detection and near-on-column detection for faster acquisition speeds and limited post-column contribution to band broadening, respectively. Experimental data on ~ 40 cm microcolumns with an embedded spray tip with MS detection (Figure 4-4A) and with an upstream frit with near-on-column UV detection (Figure 4-4B) shows the difference in peak shape and number of sampling points per peak when using these two

different approaches. For the UV detection, analytes were ascorbic acid, hydroquinone, resorcinol, and catechol in order of elution. For MS detection, analytes were Ach, Bz-Pro, Bz-Val, and Bz-Trp in order of elution. Although different analytes and columns were used, there is a clear distinction between the UV and MS data.

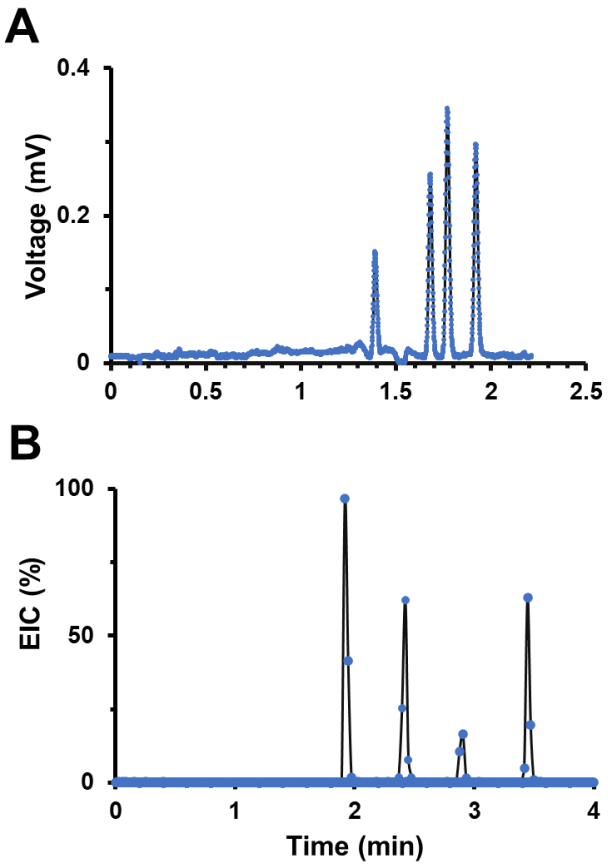

Figure 4-4. Effect of detector type on peak shape and sampling points per peak. In both cases, a ~40 cm column with 1.7 µm particles was used with either (A) upstream-fritted column with near-on-column UV detection or (B) embedded, packed spray tip with MS detection. Other conditions were the same as in Figure 4-3.

4.3.5. Gradient column evaluation using amino acid standards

The isocratic analysis confirmed relatively good packing conditions; however, automated gradient separations are of interest for metabolomics due to the need to analyze many samples and separate a large range of compounds. Figure 4-5A & B shows 35 kpsi gradient separations from a 0.2 µL injection of the standard amino acid mixture on a 20 cm x 150 µm i.d., 1.1 µm d_p

and a 50 cm x 100 µm i.d., 1.7 µm d_p column, achieving a peak capacity of 118 ± 5 (n = 3 injections) and 153 ± 4 (n = 3 injections) in 8 and 15 min, respectively. A gradient of 10X the column volume (8% ΔB/column volume) was used in both separations. These separations demonstrate that automated gradient formation with a commercial autosampler is possible while operating at 35 kpsi and maintaining the good performance of these columns. Importantly, the 1.1 µm particle packed column (20 cm x 150 µm i.d.) exhibited approximately similar peak capacity – 120 versus 150 – in about half the time compared to the 1.7 µm d_p column (50 cm x 100 µm i.d.). Interestingly, mixed results have previously been reported on the performance of such small particles (e.g., 0.8 – 1.3 µm) for peptide separations. In some instances, high peak capacities were achieved (~100 – 400) in 10 – 40 min. In other cases, longer columns packed with larger particles (e.g. 50 – 100 cm with 1.9 µm particles) provided higher peak capacity in the same amount of time than the shorter columns with smaller particles.[67,158,159] This disparity could be due to the difficulty in packing such small particles. Additionally, steeper gradients on longer columns could be more beneficial for peptides compared to shallower gradients on shorter columns due to the large solvent strength 'S' parameter of peptides.

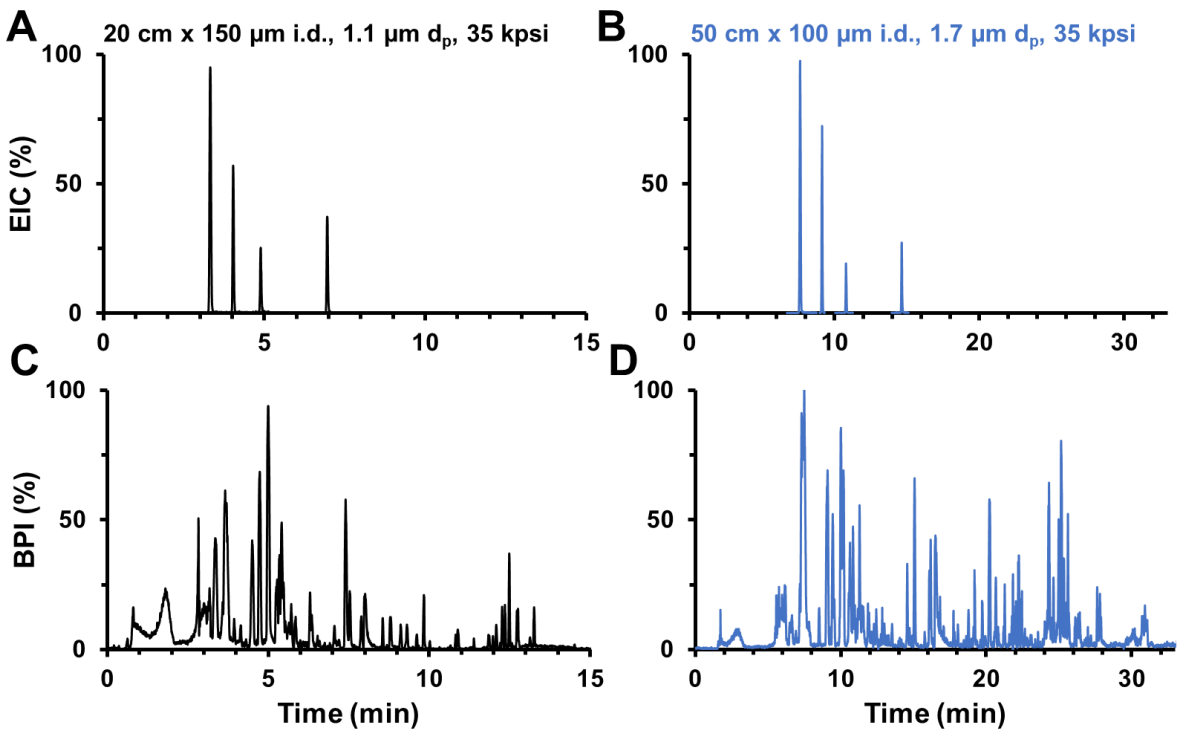

Figure 4-5. Gradient separations of (A and B) a 0.2 µL injection of the standard amino acid mixture and (C and D) a 1 µL injection of a complex plasma extract. Black traces (A and C) are separations on a 20 cm x 150 µm i.d., 1.1 µm d_p column and blue traces (B and D) are on a 50 cm x 100 µm i.d., 1.7 µm d_p column. Other conditions: 20 – 100% B gradient with a gradient volume of 10X column volume (8% ΔB/column volume); 35 kpsi operating pressure; 60 °C column oven. Mobile phase A was water with 0.1% formic acid and mobile phase B was acetonitrile with 0.1% formic acid.

Similar to the fast isocratic separations discussed above, the scan speed of the Q-ToF used for these gradient separations needs to be considered. According to the user manual, it is recommended that the fastest scan rate of Waters Q-ToF Premier is 0.3 s per scan (e.g., ~3 scans per second). Slower scan speeds can be used and offer higher signal intensity due to signal averaging, however the peak shape from lack of number of scans per peak and quantitation can be adversely affected for very narrow peaks.[180,181] The effect of 0.3 s and 0.6 s scan rates on peak shape and signal intensity was evaluated for a 13 min separation on a 20 cm x 150 µm, 1.1 µm d_p column at 35 kpsi (Figure 4-6). The signal intensity increased 20 – 39% for metabolite standards using 0.6 s scan speed compared to 0.3 s. The peak shape, however, suffered due to the fewer number of scans per peak and the 0.3 s scan rate was thus used for all future work.

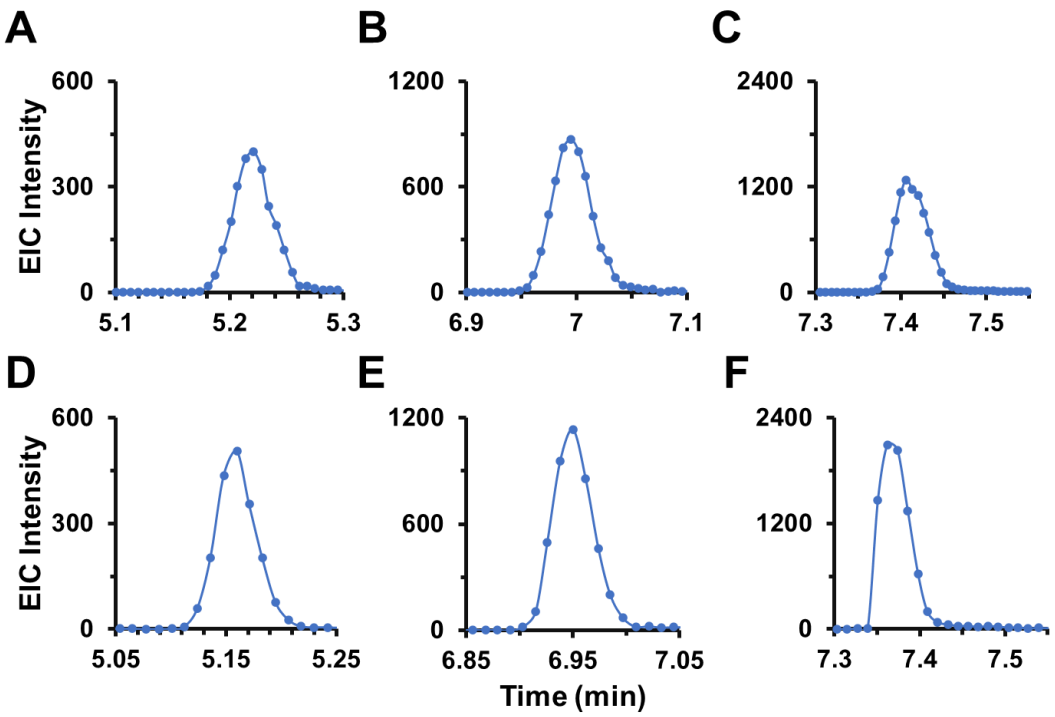

Figure 4-6. Effect of MS scan rate on peak shape and signal intensity for selected metabolite standards. In A, B, and C, a 0.3 s scan rate was used. D, E, and F, a 0.6 s scan rate was used. A 0.1 s inter-scan delay was used for both separations. Peak identifications are (A and D) Bz-Phe, (B and E) Bz-Tyr, and (C and F) Bz-DOPAC. Signal intensity increased 20 – 38% using a 0.6 s scan rate; however, peak shape was deteriorated due to the limited number of scans per peak.

4.3.6. Separations of complex plasma extract

4.3.6.1. Practical considerations for high efficiency capillary LC-MS metabolomics

Our studies with metabolite standards suggest agreement with the kinetic plots for both isocratic and gradient separations; however, practical constraints including injection volume and injection solvent can adversely affect separation performance and therefore negate the potential gains for practical metabolomics measurements. We chose to evaluate our columns with an extract of human plasma as an example of complex metabolomics samples.[5] We used BzCl derivatization to improve retention of polar metabolites on reversed phase columns; however, underivatized lipids and other metabolites were present and detected as well. Although an injection solvent of

100% mobile phase A provided the best peak shape and peak width for the standards (Figure 4-5A&B), this solvent was not practical with the complex plasma extract as precipitation and loss of signal of the more nonpolar metabolites was observed. An injection solvent of ~70/30 H_2O/ACN provided better signal intensity for late eluting peaks. Moreover, injecting larger volumes (e.g., 0.5 and 1 µL compared to 0.2 µL for standards) provided better signal for most metabolites and a higher number of features detected (see section 3.5). Example base peak intensity (BPI) chromatograms of a 1 µL injection of the plasma extract on a 20 cm x 150 µm i.d., 1.1 µm d_p and 50 cm x 100 µm i.d., 1.7 µm d_p column using a gradient volume of 10X column volume (8% ΔB/column volume) at 35 kpsi show good signal response across the separation space and similar peak shapes compared to the standards (Figure 4-5C&D). The changes in solvent and injection volume discussed above led to ~30%, ~12%, and ~0% increase in peak width for early, middle, and late eluting compounds, respectively, for a 13 min separation on the 20 cm x 150 µm i.d., 1.1 µm d_p column (Figure 4-7). It was thus important to consider peaks from compounds that eluted throughout the chromatogram when calculating peak capacity.

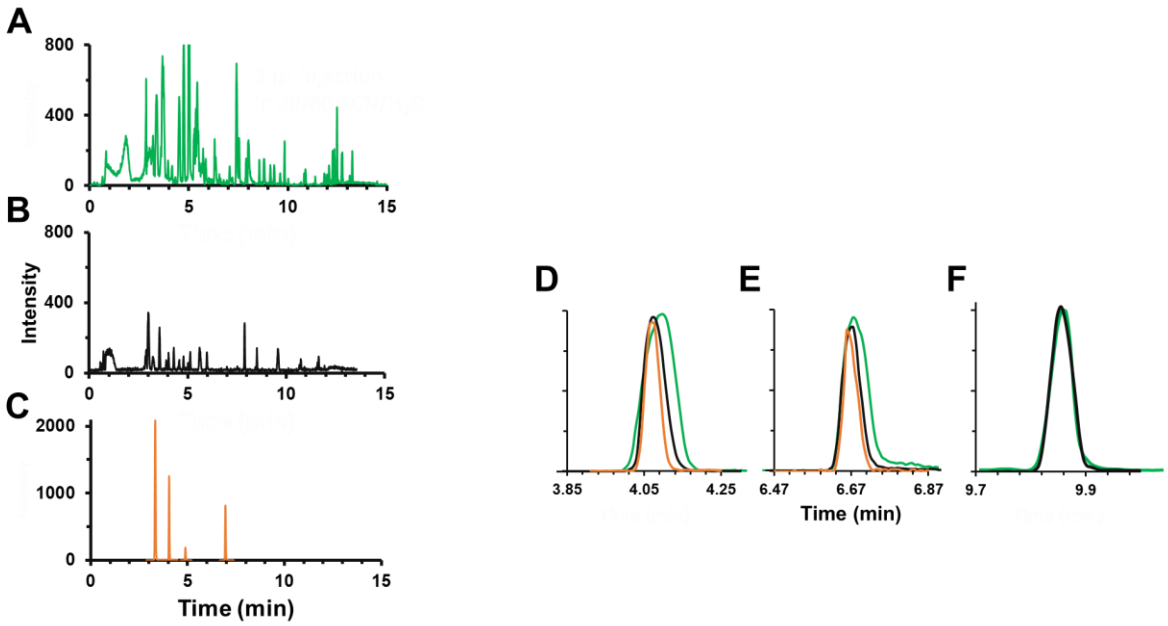

Figure 4-7. Influence of injection solvent and injection volume on peak widths and peak intensity for a 13 min separation on a 20 cm x 150 µm, 1.1 µm d_p column operated at 35 kpsi. Panels A and B show separation of a human plasma extract with an injection volume of 1 µL and 0.2 µL, respectively. The y-axis is kept constant to illustrate the increase in signal intensity across the separation space. Panel C is a 0.2 µL injection of the amino acid mixture dissolved in water. Panels D, E, and F show extracted ion chromatograms of early-, mid-, and late-eluting compounds, respectively, illustrating the magnitude in the increase in peak width due to injection solvent and volume. Peaks correspond to (D) Bz-Valine (m/z 222), (E) Bz-Tyrosine (m/z 390), and (F) LPC 16:0 (m/z 496). Retention times in D, E, and F were adjusted slightly to visually overlap the peaks.

4.3.6.2. Potential for fast separations using 1.1 µm particles

We evaluated the peak capacity from separations of the plasma extract at different analysis times and injection volumes for 1.7 µm d_p columns (15 and 50 cm long x 100 µm i.d.) and the 1.1 µm d_p column (20 cm x 150 µm i.d.) (Figure 4-8). The 15 cm column packed with 1.7 µm particles was operated at ~10 kpsi (constant 1 µL/min), representing current state-of-the-art capillary UHPLC. The 1.1 µm particle packed column consistently outperformed both the 50 cm and 15 cm x 100 µm i.d. columns with 1.7 µm particles in terms of peak capacity per analysis time for the conditions studied here.

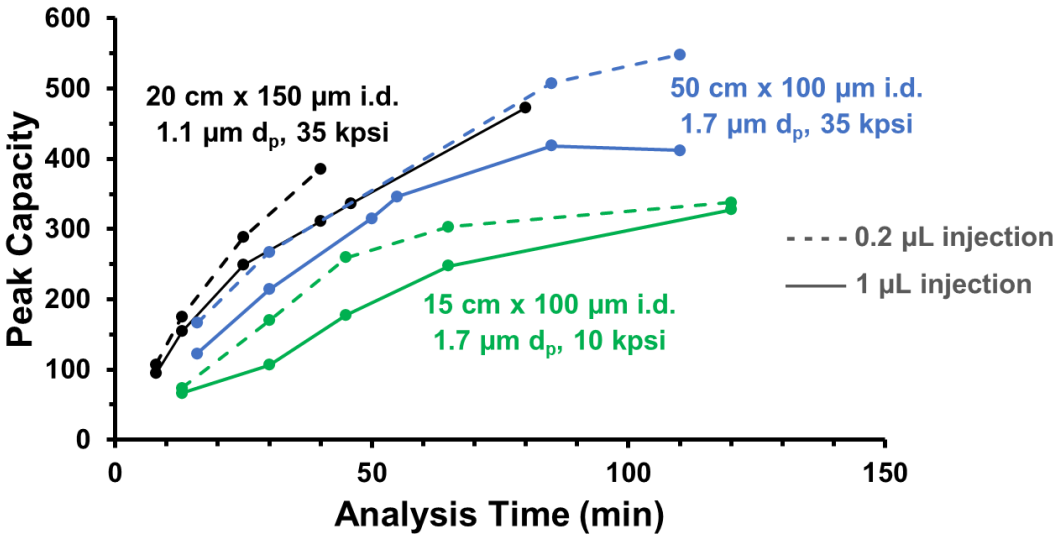

Figure 4-8. Peak capacity plotted as a function of analysis time for various columns investigated in this work. Dashed lines represent separations from a 0.2 µL injection and solid lines represent a 1 µL injection. The 20 cm and 50 cm columns were operated at 35 kpsi, and the 15 cm column operated at ~10 kpsi (1 µL/min), all with varying gradient times. Other conditions are the same as in figure 4-5.

We further examined the results from Figure 4-8 in two ways: potential for fast separations and potential for high-resolution separations. Choosing a relatively short analysis time of 13 min, we compared peak capacities of the shorter columns due to their smaller void times amenable for fast separations. The 1.1 µm d_p column (20 cm x 150 µm i.d.) generated a peak capacity of 153 ± 3 (n = 2 injections) and 183 ± 9 (n = 3 injections) for a 1 µL and 0.2 µL injection, respectively. These values were noticeably higher than the 1.7 µm d_p column (15 cm x 100 µm i.d. at 10 kpsi, representing commercial limits), which were 59 ± 5 (n = 3 injections) and 73 ± 6 (n = 3 injections) for a 1 µL and 0.2 µL injection, respectively. The good peak capacity in short times should be of benefit for metabolomics studies that require many samples to be analyzed. Our results for the larger particles appear to be reasonable as similar peak capacities, ~60 in 15 min, were recently reported with commercial capillary columns (15 cm with 1.7 µm particles) for small molecule separations with UV detection and comparable flow rates to those studied here.[182]

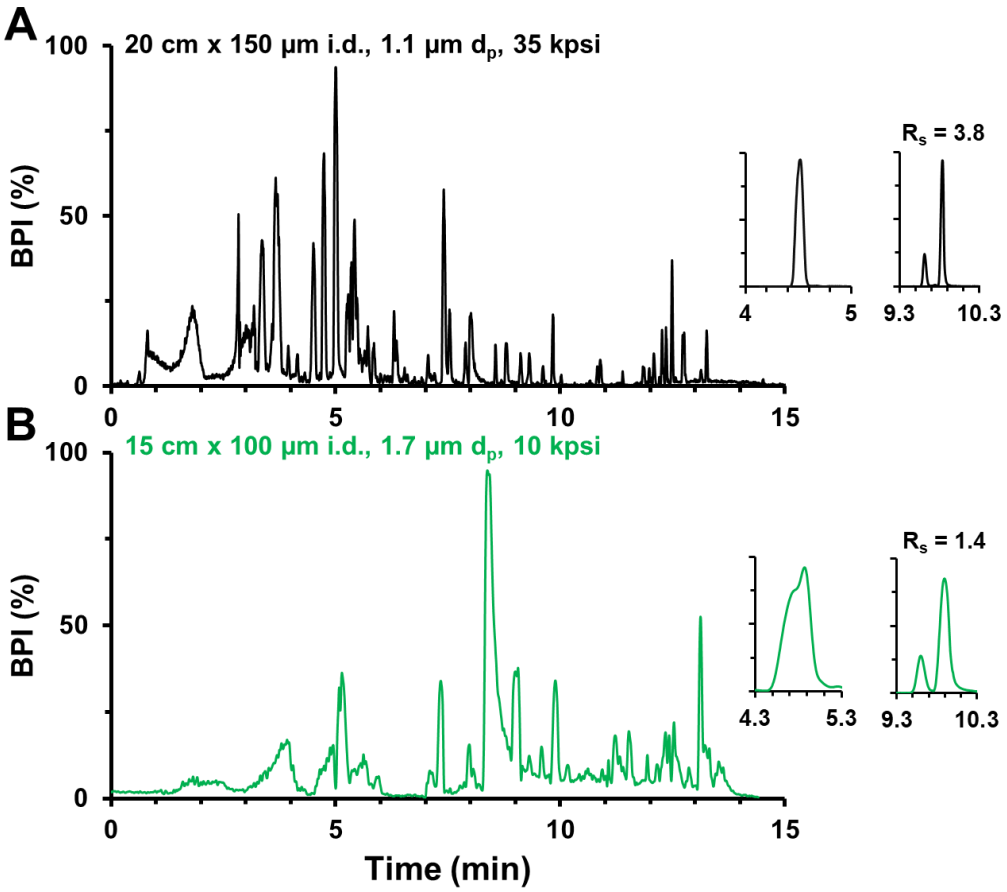

Figure 4-9. Comparison of (A) a 20 cm x 150 µm i.d., 1.1 µm d_p column at 35 kpsi and (B) a 15 cm x 100 µm i.d., 1.7 µm d_p at 10 kpsi (commercial limitations for capillary LC) for a relatively fast 13 min gradient. BPI chromatograms of BzCl labeled plasma extract for a 13 min gradient are shown for a 1 µL injection of a BzCl labeled metabolite extract. Representative EICs of an early eluting compound, Bz-valine (m/z 222), and a late eluting compound, lysophosphatidylcholine (LPC) 16:0 (m/z 496), are shown for comparison of peak shape and peak widths. The resolution (Rs) of LPC 16:0 sn-1 and sn-2 isomers is shown.

BPI chromatograms of a 1 µL injection for the 13 min gradient separation of the complex plasma extract on the 1.1 µm d_p (20 cm x 150 µm i.d.) and 1.7 µm d_p (15 cm x 100 µm i.d. at 10 kpsi) columns show the enhanced peak shape and peak capacity of the 1.1 µm column for relatively fast separations (Figure 4-9). Extracted ion chromatograms (EICs) of m/z 222 (Bz-valine) and m/z 496 (lysophosphatidylcholine (LPC) 16:0 (sn-1 and sn-2 isomer)) illustrate the improved peak width and resolution of the 1.1 µm d_p x 20 cm column (35 kpsi) compared to the 1.7 µm d_p x 15 cm column (10 kpsi). Early eluting peaks such as valine were particularly broad on the 15 cm x 100 µm i.d., 1.7 µm d_p column compared to the 20 cm x 150 µm, 1.1 µm d_p column for this 1 µL

injection. This disparity could be due to the larger column volume of the 20 cm x 150 µm i.d. (~2.8 µL) vs. the 15 cm x 100 µm i.d. (~0.94 µL); however, decreasing the injection volume to 0.2 µL resulted in little improvement on the 15 cm x 100 µm i.d., 1.7 µm d_p column at 13 min (dashed vs. solid green lines (square symbols) in Figure 3). We originally chose 150 µm i.d. for the short (20 cm) 1.1 µm particle packed column to approximately match the column volume of the 50 cm x 100 µm, 1.7 µm columns. To further investigate the column volume difference and better compare with the 15 cm x 100 µm i.d., 1.7 µm d_p column, we packed 20 cm x 100 µm i.d. capillaries with the 1.1 µm particles (column volume ~1.3 µL) and found only a slight decrease in peak capacity by ~18 % for a 0.2 µL injection relative to the 20 cm x 150 µm i.d., 1.1 µm d_p column (Figure 4-9). This change is a marginal decrease in peak capacity compared to the 60% lower peak capacity with the 15 cm x 100 µm i.d., 1.7 µm d_p column in Figures 4-8 and 4-9. The improvement in peak capacity with the smaller particles is therefore likely a combination of increased efficiency, larger column volume, higher packing pressure,[100] and higher operating pressure, as higher pressure has been shown to increase retention of small molecules.[55,183] Further studies should be focused on individually assessing the impact of these variables on injection volume for metabolite separations.

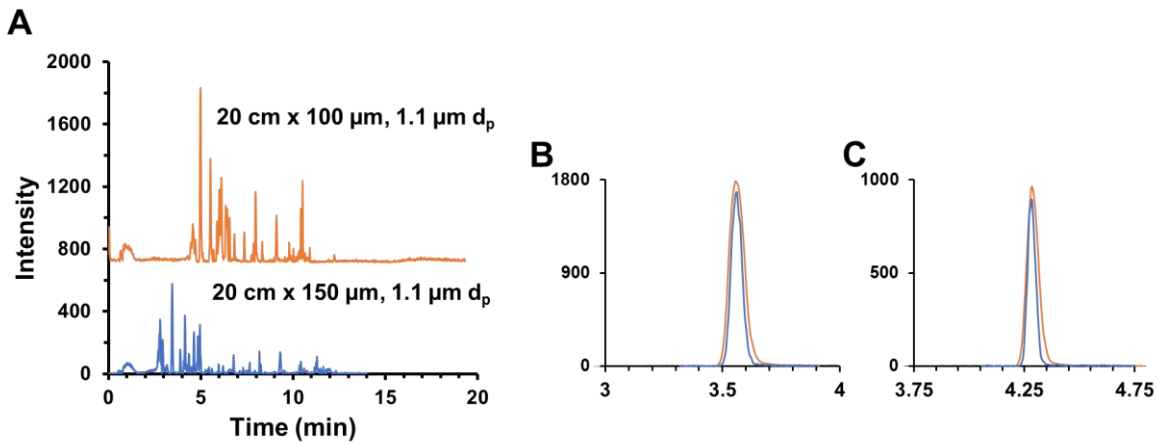

Figure 4-10. Influence of column inner diameter on peak widths for early eluting compounds on 20 cm long columns packed with 1.1 µm particles. Both columns were operated with the same mobile phase gradient of 8% ΔB/column volume and a 0.2 µL injection of a plasma extract. Extracted ion chromatograms for Bz-Pro and Bz-Val are shown in panels B and C, respectively, to illustrate the slight efficiency loss with the smaller diameter column. Retention times were adjusted slightly in B and C to overlap the peaks.

4.3.6.3. Potential for high-resolution separations

Our second examination of Figure 4-8 investigated the potential for achieving higher peak capacity using 1.1 µm particles. As shown in Figure 4-8, for a 1 µL injection, a target peak capacity of ~350 can be achieved in 45 min with the 1.1 µm d_p column (20 cm x 150 µm i.d.), compared to 60 min and 120 min for the 1.7 µm d_p columns (50 cm and 15 cm/10 kpsi x 100 µm i.d., respectively). BPI chromatograms of these three separations are shown in Figure 4-11, with EICs of m/z 496 (LPC 16:0) and m/z 391 displayed to compare peak shape and resolution between the three columns. The 1.1 µm particles can thus be used for relatively quick yet high peak capacity separations relative to the other columns if 35 kpsi is available.

Even higher resolution separations are of interest for isomers or isobaric compounds and for providing broader metabolome coverage. High-resolution separations of small molecules and metabolites have been demonstrated with peak capacities ranging from 1500 – 1800 using long (e.g., >100 cm) columns and ~33 h analysis times.[65,152] Such long separation times are useful in some conditions, but many metabolomics studies require numerous samples and such times can

become prohibitive. The potential for high-resolution separations in relatively short analysis times is an attractive feature of sub-2 µm columns operated at 35 kpsi. For a 0.2 µL injection, a peak capacity of ~400 is achieved with a 40 min separation on the 20 cm x 150 µm i.d., 1.1 µm d_p column, and a peak capacity of ~550 was achieved on the 50 cm x 100 µm i.d., 1.7 µm d_p column in 110 min (Figure 4-8). Smaller injection volumes than those studied here could lead to even higher peak capacities in the same time; however, MS sensitivity and identification of low level metabolites could suffer (discussed more in section 3.5). Furthermore, higher peak capacities or shorter analysis times could be attained with moving to even smaller particles and/or longer columns with higher instrument pressures.

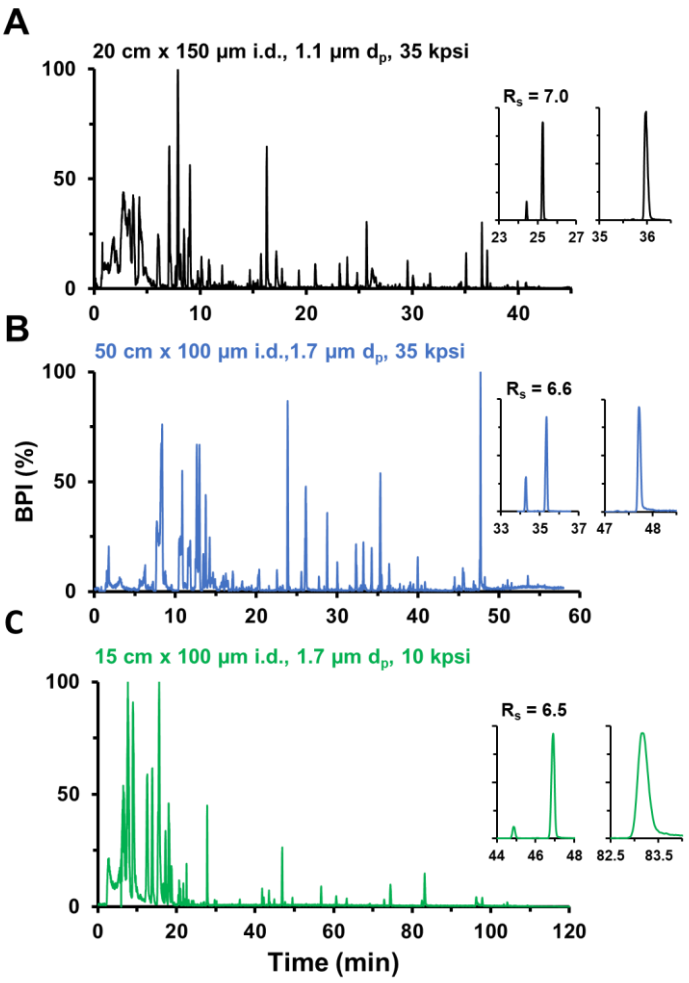

Figure 4-11. Example BPI chromatograms from a 1 µL injection of BzCl labeled plasma extract illustrating the time required to achieve a peak capacity of ~350 with the different columns, particle sizes, and pressure limits investigated in this work. EICs of m/z 496 (LPC 16:0) and 391 are displayed, with the resolution (Rs) of LPC 16:0 isomers shown.

4.3.7. Feature detection in human plasma

The previous sections discussed preparation and use of capillary columns that can provide higher separation efficiency and peak capacities than current commercially available particle sizes and column lengths in shorter analysis times. Real metabolomics assays however rely on confident and in-depth metabolome coverage and annotation. While higher peak capacity separations have shown broader metabolome and proteome coverage,[25,65,101] a number of LC-MS variables can affect MS response and metabolomics metrics. For example, steeper gradients have shown to provide higher MS signal due to the narrower peaks compared to shallower gradients.[184]

Furthermore, while higher flow rates have been shown to provide higher peak capacities for the same analysis time,[95,185] the ionization may suffer and hinder metabolite coverage. We therefore evaluated several variables using full-scan (MS1) feature detection as a proxy for the information content possible from the metabolomics assay (Figure 4-12). A feature was defined as any signal with a unique m/z and retention time and above the average background signal from each separation.

Increasing the injection volume from 0.2 to 1 µL consistently provided a much higher number of features detected from BzCl-labeled plasma extracts across the three column types investigated in this work (Figure 4-12A), despite the slight losses in peak capacity that were observed with these larger injection volumes (see Figure 4-7 and section 4.3.6). The effect of increasing peak capacity by varying the gradient time (e.g., Figure 4-8) on feature detection was also investigated (Figure 4-12B). For each column type, a general increase in the number of features detected was seen as the peak capacity increased. This trend is likely due to resolution of isobaric compounds and alleviation of ionization suppression compared with shorter and lower resolution separations.[101,186] Higher feature counts at longer analysis times could be over-inflated, however, as feature count is often biased compared to high confidence metabolite annotation and identification.[187] Interestingly, the lowest efficiency column – the 15 cm/1.7 µm at 10 kpsi – provided higher feature counts than the longer columns at higher pressure for the same peak capacity (albeit at longer analysis times to achieve the same peak capacity). This observation is likely due to the lower flow rate on the 15 cm x 100 µm i.d., 1.7 µm d_p column at 10 kpsi (1 µL/min versus ~1.8 – 2.5 µL/min on the columns run at 35 kpsi). Lower flow rates can provide increased ionization efficiency due to smaller initial droplet sizes and easier desolvation; this improvement in ionization can lead to less ionization suppression and interference from matrix effects.[90,163] To

further investigate this hypothesis and attempt to provide similar results with the higher efficiency columns, we operated the 20 cm x 150 µm i.d., 1.1 µm d_p column at lower flow rates (by operating the pneumatic pump at 10 and 15 kpsi) with the same gradient slope of 8% ΔB/column volume (Figure 4-12C). Reducing the flow rate down to 700 nL/min resulted in over double the number of features detected. Selected EICs of Bz-Trp and Bz-Tyr detected from the plasma extract showed higher peak intensities and larger peak areas with the lower flow rate separations (Figure 4-13). These data corroborate that lower flow rates indeed give higher MS response and thus more features detected for the conditions studied here.

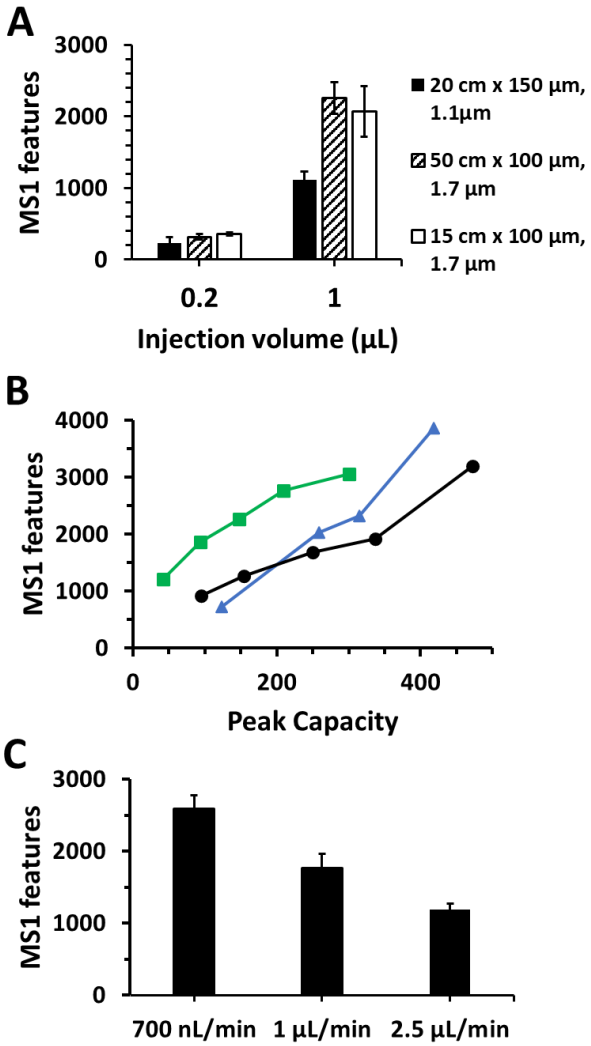

Figure 4-12. Effect of different LC-MS variables on MS1 feature detection from BzCl labeled plasma extract. (A) Effect of injection volume on feature count and peak capacity for the three columns shown in Figure 4-8. All separations used a gradient volume of 10X the column volume (8% ΔB/column volume). (B) Effect of increasing peak capacity through longer gradient times on feature count for a 1 µL injection on the same three columns. (C) Effect of flow rate (adjusted by changing inlet pressure) on feature count for a 1 µL injection on the 20 cm x 150 µm i.d., 1.1 µm d_p column using a gradient volume of 10X the column volume. Error bars represent standard error from duplicate injections.

Taken together, a higher injection volume combined with lower flow rates provided the highest number of features detected for a given analysis time. Increasing separation peak capacity through extending the gradient time also increased feature counts; however, this approach decreased analysis throughput. Further work involving reduction in column i.d. and flow rate to the low nL/min range may further increase metabolite coverage while maintaining the

chromatographic advantages of combining smaller particles with higher pressure. Reduction of column i.d. and use of nano-flow/capillary LC-MS has been heavily utilized in proteomics studies and has provided large increases in proteome coverage, and in some cases has been extended to metabolomics.[166,188–190] Use of trap columns may be needed to mitigate the gradient delay when going to such low flow rates and alleviate band broadening from injecting on such narrow columns. Thus, in order to combine the benefits of larger injection volumes and high-resolution separations for capillary LC-MS based metabolomics, pre-column focusing strategies likely need to be implemented.[191–193] Future studies should also employ a more rigorous evaluation of metabolite annotation and the effect of these variables on high confidence identification rather than features.[187,194,195]

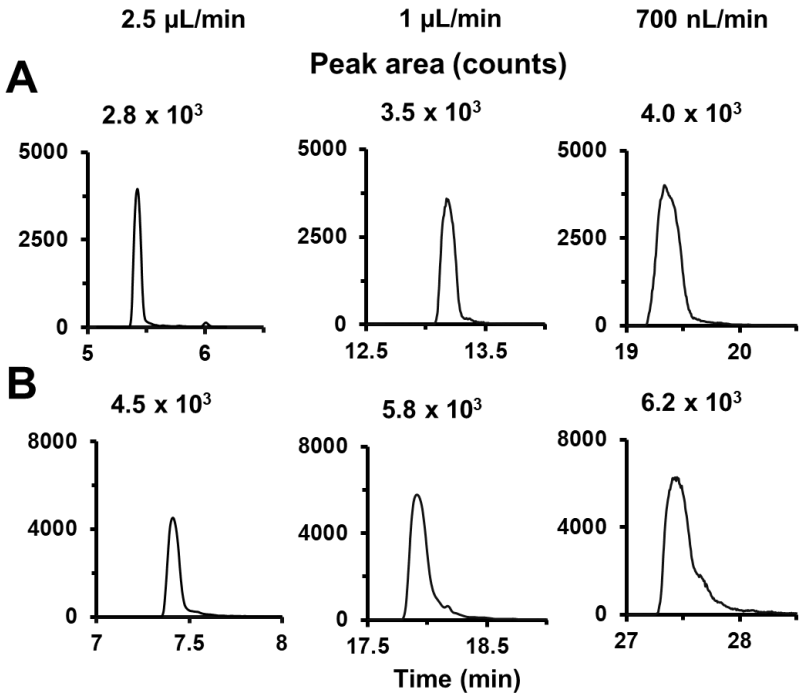

Figure 4-13. Extracted ion chromatograms and corresponding peak areas of Bz-Trp (A) and Bz-Tyr (B) detected in the plasma extract on the 20 cm x 150 µm i.d., 1.1 µm d_p column operated at 35 kpsi (~2.5 µL/min), 15 kpsi (~1 µL/min), and 10 kpsi (~700 nL/min). Peak areas increased as the flow rate was lowered. A constant gradient volume of 8% ΔB/column volume.

4.3.8. System robustness and repeatability

The repeatability of retention times and peak widths of the analytes are important for routine, long term metabolomics assays. We performed column repeatability tests for the 15 cm x 100 µm i.d., 1.7 µm d_p, 20 cm x 150 µm i.d., 1.1 µm d_p, and 50 cm x 100 µm i.d., 1.7 µm d_p columns discussed above. Average RSDs in retention time and peak width for the amino acid mixture for all columns were below 4% and 8%, respectively (Table 4-1). Additionally, the long-term use and repeatability of the 20 cm x 150 µm i.d., 1.1 µm d_p column was assessed over a 5 month period (Table 4-2). No signs of column degradation or clogging were observed, with average retention time and peak width RSDs of 6% and 11%, respectively, for the amino acid mixture. These deviations are similar to previously reported packed capillary C18 columns.[67,87,100]

Table 4-1. Repeatability of retention times and peak widths for columns in Figure 4-7 evaluated with the standard amino acid mixture.

	Ret time (min) Average ± SD (n = 3)					**Peak width (FWHM, s) Average ± SD (n = 3)**			
Column	**Bz-Pro**	**Bz-Val**	**Bz-Trp**	**Bz-Tyr**		**Bz-Pro**	**Bz-Val**	**Bz-Trp**	**Bz-Tyr**
20 cm x 150 µm, 1.1 µm	3.33 ± 0.03	4.03 ± 0.04	4.86 ± 0.05	6.64 ± 0.04		2.8 ± 0.2	2.2 ± 0.2	2.32 ± 0.06	2.2 ± 0.2
15 cm x 100 µm, 1.7 µm	3.7 ± 0.1	4.6 ± 0.2	5.5± 0.2	7.55 ± 0.2		13 ± 1	7.2 ± 0.5	4.8 ± 0.3	5.1 ± 0.5
50 cm x 100 µm, 1.7 µm	7.43 ± 0.07	8.93 ± 0.07	10.62 ± 0.06	14.78 ± 0.04		3.9 ± 0.2	3.1 ± 0.1	3.3 ± 0.2	3.5 ± 0.2

Table 4-2. Long term repeatability and durability demonstrated for a 20 cm x 150 µm i.d., 1.1 µm d_p column over a 5 month period. All separations were performed at 35 kpsi at 20 – 100% B with an 8% ΔB/column volume. Other conditions are the same as Figure 4-5.

	Ret time (min)					Peak width (FWHM, s)			
Date of analysis	**Bz-Pro**	**Bz-Val**	**Bz-Trp**	**Bz-Tyr**		**Bz-Pro**	**Bz-Val**	**Bz-Trp**	**Bz-Tyr**
11/14/2019	3.30	3.98	4.79	6.59		2.8	1.9	2.4	2.0
11/14/2019	3.37	4.08	4.90	6.67		2.6	2.4	2.3	2.3
11/15/2019	3.33	4.03	4.88	6.67		3.1	2.3	2.3	2.3
11/20/2019	3.43	4.21	5.12	6.96		3.6	2.8	2.4	2.5
12/3/2019	3.20	4.08	5.09	6.98		4.2	2.9	2.5	2.5
2/25/2020	3.83	4.53	5.37	7.23		2.8	2.7	2.8	2.5
2/26/2020	3.64	4.34	5.19	7.06		3.2	2.3	2.9	2.4
3/5/2020	3.85	4.67	5.64	7.72		3.5	3.1	2.6	2.3
3/13/2020	3.87	4.60	5.48	7.41		3.1	2.8	2.3	2.1
AVG	3.54	4.28	5.16	7.03		3.2	2.6	2.5	2.3
STD DEV	0.25	0.25	0.27	0.35		0.5	0.3	0.2	0.2
RSD (%)	7.0	5.8	5.3	5.0		15	13	8.2	7.5
Average RSD (%)				5.8					11

4.4. Conclusions

This study illustrates the feasibility and potential impact of using 1.1 µm particles in 20 cm long columns paired with a gradient capillary LC system capable of 35 kpsi for metabolomics assays. We have found packing conditions and instrumentation that allow approximate agreement with theory for using such columns with ultrahigh pressure instrumentation, while demonstrating routine use with practical considerations for metabolomics samples. The 1.1 µm particle packed columns enable higher peak capacity at relatively short, and practical, analysis times of 13 min compared to columns packed with larger particles as commonly used currently. The columns also allowed relatively high peak capacities (e.g., peak capacity 300 – 500) to be reached at a ~30% faster time compared to 50 cm x 100 µm i.d., 1.7 µm d_p columns, and nearly 3x faster time compared with 15 cm x 100 µm i.d., 1.7 µm d_p columns at 10 kpsi. For metabolomics assays, interplaying variables such as flow rate, peak capacity, and injection volume can all be manipulated to increase the number of features identified in the human plasma extract.

Chapter 5. Towards Peak Capacities Over 1000 and Gradient Separations at 50 kpsi

Introduction

The desire for comprehensive "omics" analyses continues to drive new developments in analytical instrumentation and technologies. Advancements in both liquid chromatography and mass spectrometry instrumentation have led to the full proteome analysis of yeast (~4000 proteins) in approximately one hour.[196] Further improvements including use of two-dimensional capillary LC-MS identified over 8,000 proteins from HeLa cells.[141] Clearly, advancements in separation prior to mass spectrometry have been invaluable towards expansion in the depth of information in omics workflows.[197] Specifically, separation peak capacity can increase compound coverage and identification confidence in untargeted methods.[25,65,101,125,157,198]

Advancements in chromatographic column formats have provided higher peak capacities than previously possible.[199,200] These advancements include the development of highly ordered pillar array columns (µPAC), long monolithic columns, small inner diameter open tubular columns, and columns packed with very small particles. Monolithic and pillar array columns have the advantages of very high permeability due to the design freedom in domain or pillar size and shape.[201,202] This low separation impedance offers the possibility to operate long columns (assuming a homogenous domain is formed across the entire column) without the need for extreme instrument pressure. Using a 3.5 m x 100 µm silica monolith column, a peak capacity of 1600 was achieved in a 2400 min separation window for peptide separations.[203] Similarly, over one million theoretical plates have been achieved using an 8 m long (4 x 2 m columns connected) pillar array column with dead times around 4 h.[152] Gradient separations of small molecules using this 8 m long

coupled column provided peak capacities of 1800 (including the dead time) in approximately 2050 min. For comparison to other work, when accounting for only the effective separation space, the peak capacity was 990 for a 2050 min gradient. Pillar array columns are perhaps beneficial over monolithic columns due to their high reproducibility in column preparation and the low eddy dispersion contribution attributable to the highly ordered nature of the stationary phase pillars. A disadvantage of µPACs is their relatively high resistance to mass transfer, limiting their performance at high linear velocities.

Open tubular (OT) columns also have the advantage of very low separation impedance and thus long columns can be employed. Capillary formats are again used because small inner diameters (<10 µm) are needed to decrease analyte diffusion distances.[204] Such small column inner diameters pose problems such as low sample loadability, low analyte retention, and poor repeatability of creating such small inner diameter capillaries.[205,206] Column clogging is also more likely with such small columns and coupling with mass spectrometry can be challenging due to the very low flow rates.[207] Despite these drawbacks, recent reports have shown impressive separations using open tubular columns. Approximately 700,000 plates were achieved for retained compounds on a 250 cm x 5 µm open tubular column with a dead time of 50 min. Recently, gradient separations of peptides with peak capacities of 2000 have been achieved in 3 – 5 h using 75 cm x 2 µm OT column.[208] By elevating the column temperature to 70 °C, a peak capacity of 2720 was achieved in 143 min.[209]

Packed columns have also provided large theoretical plate counts and peak capacities using long columns packed with small particles. Advantageous of using packed columns include high loading capacity of porous particles, wide availability of stationary phase chemistries and pore sizes, ease of coupling with MS, and relative (in comparison to microfabrication processes) ease

of preparing columns. The disadvantage of packed columns is the increase in operating pressure required to push mobile phase through such highly resistant columns.[49,51] Moreover, frictional heating and the increase in pressure from connection tubing requires capillary column formats to be employed, where flow rates are much lower.[49,137] Another disadvantage of packed columns is the difficulty in efficiently packing columns with such extreme dimensions, and packing conditions for one set of parameters is often not sufficient for another set. For example, a recent study demonstrated efficient packing (h_{min} = 1.5) of 1.3 µm particles in to ~34 cm long capillaries using a 20 mg/mL slurry packed at 30 kpsi.[64] The same conditions were used to pack a 100 cm column with the same particles, resulting in an h_{min} of 3.[60]

High peak capacities have been reported for capillary based ultrahigh pressure separations with packed columns. A peak capacity of 1500 was achieved for peptides in a 2000 min gradient using a 200 cm x 50 µm column with 3 µm C18 particles operated at 20 kpsi [65]. Using the same instrument, a peak capacity of 1200 was achieved in 900 min using a 90 cm column with 2 µm particles. More recently, peak capacities approaching 900 were achieved for peptides in 720 min using a 98 cm x 75 µm column packed with 1.9 µm particles and operated at 30 kpsi.[67] Lastly, work described in this thesis has demonstrated peak capacities of approximately 400 and 500 in 40 and 85 min, respectively, for small molecule separations at 35 kpsi.[210]

Despite the impressive results described in the previous paragraphs, there is still room to grow for improving peak capacities in one-dimensional separations, especially when coupled with mass spectrometry. In this chapter, potential for gradient separations using meter long columns and operation up to 50 kpsi is evaluated for small molecule separations with coupling to mass spectrometry.

5.2. Materials and methods

5.2.1. Chemicals and materials

All chemicals and reagents were purchased from Sigma Aldrich (St. Louis, MO) unless otherwise specified. HPLC grade acetonitrile and sulfuric acid were purchased from Fisher Scientific (Fairlawn, NJ). 3,4-Dihydroxyphenylacetic acid (DOPAC) was purchased from Acros Organics (Geel, Belgium). Stock solutions of 10 mM proline (Pro), valine (Val), tryptophan (Trp), tyrosine (Tyr), norepinephrine (NE), and DOPAC were prepared in water. A 25 mM stock solution of acetylcholine (Ach) was prepared in water. Pro, Val, Trp, and Tyr were combined and diluted to 100 µM. DOPAC and NE were diluted to 500 µM. Derivatization was completed by sequential addition of 100 mM sodium carbonate, 2% (v/v) benzoyl chloride in acetonitrile, and 1% (v/v) sulfuric acid in 20% (v/v) acetonitrile in water in a 2:1:1:1 ratio as previously described.[167] The mixture was diluted to 10 µM Pro, Trp, and Tyr, 20 µM DOPAC, and 50 µM NE.

5.2.2. Column packing

Columns were packing using an ultrahigh pressure packing apparatus. Polyimide-coated fused-silica capillary with varying inner diameters and outer diameter of 360 µm was purchased from Polymicro Technologies (Phoenix, AZ). All particles were bridged ethyl hybrid (BEH) silica with C18 bonding (Waters, Co; Milford, MA). Column frits were prepared by spotting an equal amount of potassium silicate and formamide on a glass microfiber filter paper (Reeve Angel; Clifton, NJ) and dabbing the end of the capillary ~5 times, and placed at 60 °C overnight.[93] Acetone was used as the slurry solvent for all columns. For columns with 1.7 µm particles, a slurry concentration of 200 mg/mL was used. For columns with 1.1 µm particles, a slurry concentration of 60 mg/mL was used. Packing was done at 30 kpsi. Low pressure (~1000 psi) was applied to

form ~2 cm of packed bed, followed by immediate application of 30 kpsi. Columns were placed in a sonication bath prior to packing. The packed columns were flushed at 50 kpsi with 50/50 (v/v) water/acetonitrile for 1 h. Columns were then depressurized for 1 h, cut to the desired length, and fritted at the inlet as described above.

5.2.3. LC-MS operation

Gradient separations were performed at ultrahigh pressures using the custom-built system described previously in chapters 2 – 4 and elsewhere.[67,87] Mobile phase A was 10 mM ammonium formate with 0.1% formic acid. Mobile phase B was acetonitrile. All injections were performed in partial loop mode on the NanoAcquity with a 0.2 µL injection volume. A 20-100% B gradient was used for all separations. Column volume was calculated assuming a total porosity of 0.8. For the 100 cm x 100 µm column, the volume was 6.3 µL. For the 70 cm x 100 µm column, the volume was 4.4 µL. Peak capacity was determined by measuring the full width at half maximum (FWHM) of metabolites eluting throughout the separation space. The 4σ peak width was calculated by multiplying FWHM by 1.7. The peak capacity was then calculated by dividing the separation window by the average 4σ peak width. The separation window was determined as the difference in elution time between the last eluting peak and the dead time. The end of the separation window was indicated by underivatized peaks corresponding to dioctyl phalate (DOP, $[M+H]^+$ 391) or didodecyl thiodipropionate (DDTDP, $[M+H]^+$ 515, $[M+NH_4]^+$ 532). The column oven was 60 °C. Effluent from the column was connected to either a Waters Xevo or Waters/Micromass Premier (Milford, MA) using a stainless-steel union and a fused silica spray needle of 75 µm i.d. tapered to 30 µm (New Objective; Woburn, MA). The capillary voltage was 2 – 2.5 kV, which was modified based on flow rate from different columns and pressures. The MS was operated in full scan, positive ion mode with a mass window of 100 – 1000 m/z.

5.3. Results and discussion

5.3.1. Column considerations

To realize the theoretical benefits of operating at such high pressures, columns that take advantage of these pressures must be efficiently packed. In other words, operating a 10 cm column with 1.7 µm particles at 35 kpsi would not improve separation performance relative to 10 kpsi; however, operating a 200 cm column packed with 1.7 µm particles at 50 kpsi would be beneficial (Figure 5-1B). These improvements are discussed in the introduction of this thesis and are well visualized using kinetic plots.[49,52,53] Figure 5-1 shows gradient kinetic plots illustrating peak capacity versus analysis time for different column lengths at 35 kpsi with 1.7 µm d_p (Figure 5-1A), different column lengths and pressure with 1.7 µm d_p (Figure 5-1B), and different particle sizes at 35 kpsi and 50 cm column length (Figure 5-1C). These plots clearly show the benefits of higher pressure for increasing peak capacity when column length and particle size is chosen carefully, but importantly also show when pushing these limits is not beneficial. Details on construction of these plots is described in Appendix 2.

Before engineering instrumentation to operate at such high pressures, we first evaluated whether such long columns can be efficiently packed with small particles that would benefit from increased operating pressures. Chapters 2 – 4 of this thesis describe relatively high-resolution separations of lipids and metabolites with separation times of typically 2 – 3 h, column lengths of 20 – 50 cm, and an instrument operating pressure of 35 kpsi. Higher peak capacities are expected with both longer columns and longer analysis times while still within this pressure regime. Thus, longer columns were first investigated for use while still at 35 kpsi operating pressure.

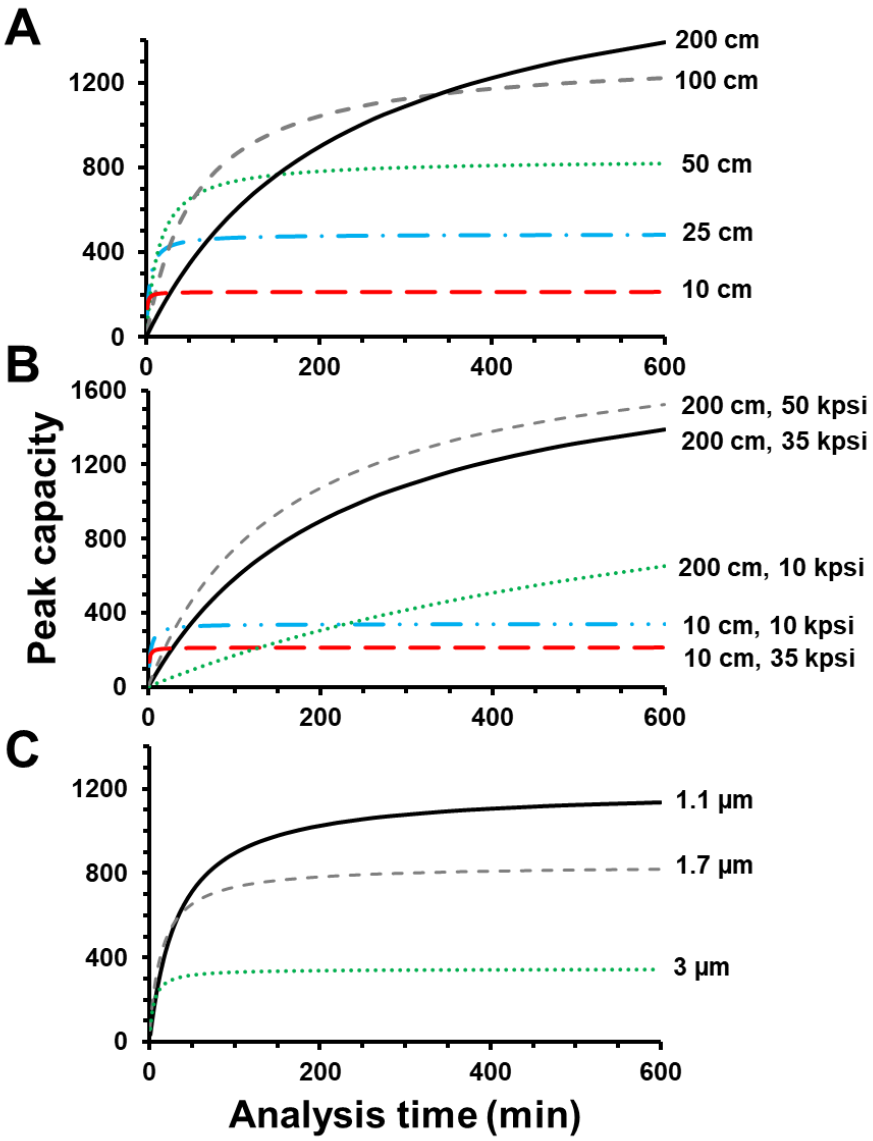

Figure 5-1. Effect of different column and instrument parameters on theoretical peak capacity using packed columns. (A) Effect of column length with 35 kpsi operating pressure and 1.7 µm particle size. (B) Effect of column length with different operating pressures all with 1.7 µm particle size. (C) Effect of particle size with 35 kpsi operating pressure and 50 cm column length. Other conditions: S = 12 (estimated for 300 Da molecule); 20-100% B gradient; column temp 60 °C. For further details on calculations see Appendix 2.

5.3.2. 100 cm x 100 µm, 1.7 µm column

Previously published work investigated column packing conditions for efficiently preparing 100 cm columns packed with 1.7 µm BEH C18 particles.[63,211] They found that packing at a low slurry concentration (1-20 mg/mL) led to axial heterogeneities and a poorly performing

column. Too high of a slurry concentration (180-200 mg/mL) also led to relatively poorly packed columns due to a high number of voids within the bed.[60–62,64] However, sonicating the column while packing at such high slurry concentrations (200 mg/mL) alleviated excessive void formation and provided, meter-long columns with efficient isocratic separations.[63]

In this work, gradient separations with 100 cm columns packed with 1.7 µm particles were performed using columns packed with sonication and high slurry concentrations as previously described.[63] Figure 5-2 shows example separations of a standard benzoyl chloride derivatized (Bz-) metabolite mixture at 35 kpsi on a 100 cm x 100 µm, 1.7 µm d_p column. Narrow, symmetrical peaks were achieved under different gradient lengths. Peak capacities were 990 and 1190 in 4 and 8 h separation times, respectively. Moreover, retention times were found to be repeatable with RSDs for all peaks 3.0% or less (Table 5-1).

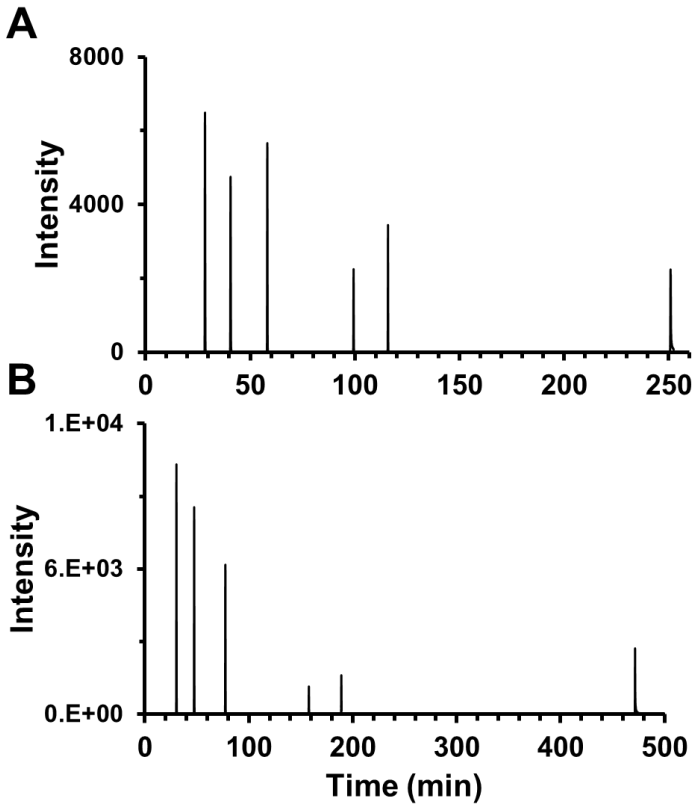

Figure 5-2. Example overlayed ion chromatograms of a standard BzCl labeled metabolite mixture on a 100 cm x 100 µm, 1.7 µm column operated at 35 kpsi. Gradient separations were performed with a 20 – 100% B gradient at varying gradient lengths. Mobile phase A was 10 mM ammonium formate; mobile phase B was acetonitrile; column temperature was 60 °C; injection volume was 0.2 µL.

Table 5-1. Retention time repeatability of BzCl labeled metabolite mixture on a 100 cm x 100 µm column packed with 1.7 µm particles and operated at 35 kpsi.

Analyte (*m/z*)	**Retention time (min)**								
	Run 1	**Run 2**	**Run 3**	**Run 4**	**Run 5**	**Run 6**	**Run 7**	**St Dev**	**%RSD**
Bz-Pro (220)	23.50	21.81	22.03	21.50	22.15	22.81	22.30	0.67	3.0
Bz-Val (222)	27.87	26.47	26.61	25.98	26.72	27.49	26.86	0.64	2.4
Bz-Trp (309)	32.11	30.56	30.69	29.91	30.80	31.68	30.96	0.73	2.4
Bz-Tyr (390)	41.46	40.32	40.34	39.23	40.36	41.35	40.51	0.75	1.8
Bz-DOPAC (394)	n/a	43.40	44.62	43.40	44.61	45.69	44.34	0.86	2.0
DOP (391)	66.03	66.77	66.56	64.67	65.72	67.96	66.29	1.01	1.5

Peak capacity of the 100 cm, 1.7 µm column operated at 35 kpsi was evaluated under different gradient times (Figure 5-3). As theory predicts, peak capacity increases on a logarithmic scale as gradient time is extended, eventually reaching a plateau. Gradient times up to ~8 h (480 min) were evaluated, corresponding to gradient slopes of 16% to 2% ΔB/column volume. For comparison, peak capacities are shown for a 50 cm x 100 µm, 1.7 µm d_p column at 35 kpsi and a 15 cm x 100 µm, 1.7 µm d_p column at 15 kpsi; most of this data is reproduced from chapter 4 and published elsewhere.[210] The 100 cm column provided much higher peak capacities than the shorter columns, especially at analysis times over 100 min. Importantly, use of 35 kpsi enabled implementation of long columns packed with 1.7 µm particles.

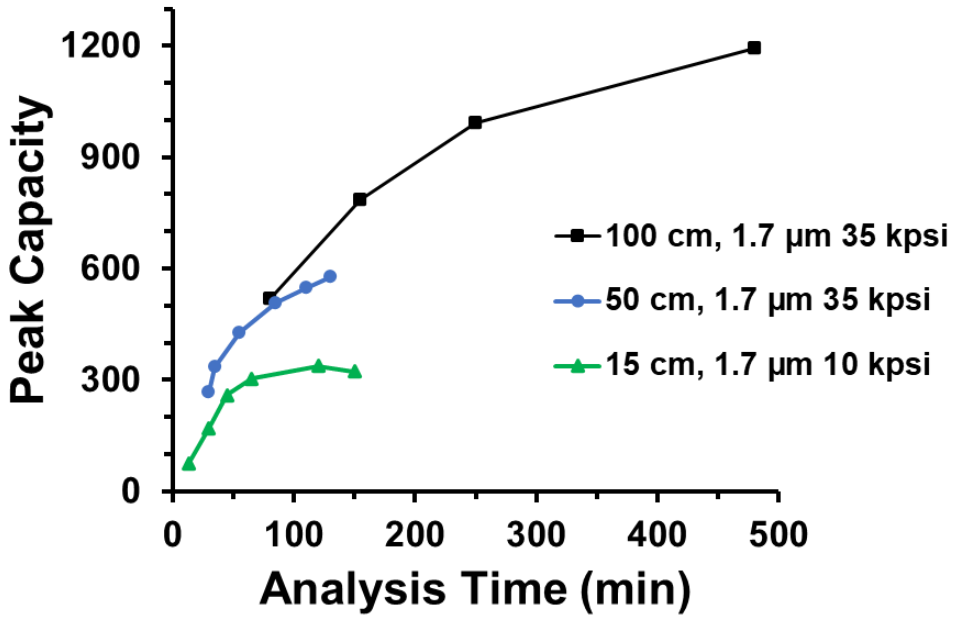

Figure 5-3. Comparison of column length and operating pressure on peak capacity. A 20 – 100% B gradient was used for all separations at varying gradient lengths. Other conditions were the same as Figure 5-2.

Although peak capacity has been well established over the years, there is still ambiguity in calculating peak capacity regarding the separation window and the average peak width – the two measurements needed to determine peak capacity. Although using the effective separation space (e.g., the time between the first and last eluting peak) is the most accurate approach, the entire

gradient time (e.g., including the dead time or time after the last peak is eluted when the gradient program is finishing) is often used which can overinflate peak capacity measurements. Additionally, it is common to only measure the peak width of the last eluting peak or a highly retained peak rather than the average of peaks eluting across the gradient. This approach may not represent the entire separation performance and can also change peak capacity measurements, especially if dead volume affects the peak width of early eluting peaks. To understand how these differences affect the data here, different peak capacity measurements were made on the same separation. Peak capacity for $t_{G,\ all}$ (entire gradient time and averaging peaks across the chromatogram), $t_{G,\ DOPAC}$ (entire gradient time and only peak width of Bz-DOPAC), and $t_{R,\ all}$ (separation window and averaging peak widths) were considered (Figure 5-4). Not surprising, when using the entire gradient time (t_G) rather than the effective separation window (t_R), a higher peak capacity is obtained. Similarly, when only using the peak width of a highly retained peak, in this case Bz-DOPAC, rather than average peak widths from the entire separation space, the peak capacity is higher. Lastly, using the effective separation space (t_R) and averaging peak widths gives the lowest and most conservative estimate of peak capacity. Up to a 20% difference in peak capacities were obtained when using these three methods. More drastic differences would be expected when using longer columns or lower pressures where the dead times are larger. Moving forward, a $t_{R,\ all}$ based peak capacity was used to calculate peak capacity.

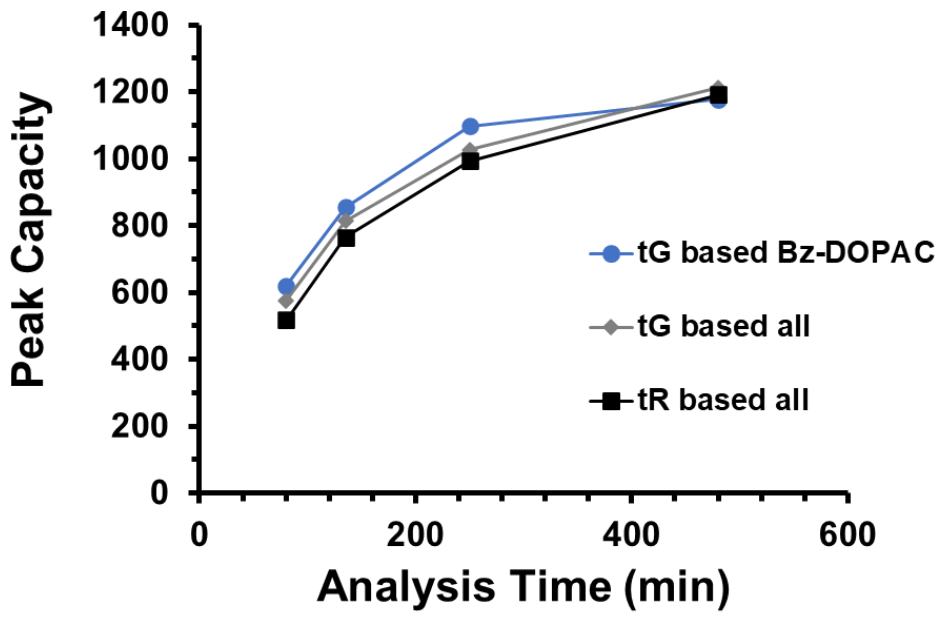

Figure 5-4. Impact of peak capacity calculation method on experimental peak capacity. Peak capacity was calculated based on tG and the peak width of Bz-DOPAC (blue circles), tG and the peak width of peaks throughout the separation space (grey diamonds), and tR-based separation space and the peak width of peaks throughout the separation space (black squares).

5.3.3. 100 cm x 100 µm, 1.7 µm column at 50 kpsi

Given that 100 cm columns packed with 1.7 µm particles provided high peak capacities for small molecule separations at 35 kpsi, separations at 50 kpsi were attempted with the same instrument (e.g., same valves and fittings). Leak-free operation was possible with the same instrument valves and fittings; however, repeatability and lifetime were poor. Nonetheless, a couple separations were achieved at 50 kpsi for the 100 cm, 1.7 µm column and are compared with separations at 35 kpsi; separations used a gradient slope of 16% and 8% ΔB/column volume (Figure 5-5). Notably, for the same gradient slope, separation time is shorter at 50 kpsi than 35 kpsi. Additionally, the dead time is shorter as expected, which benefits peak capacity when using a t_R-based calculation.

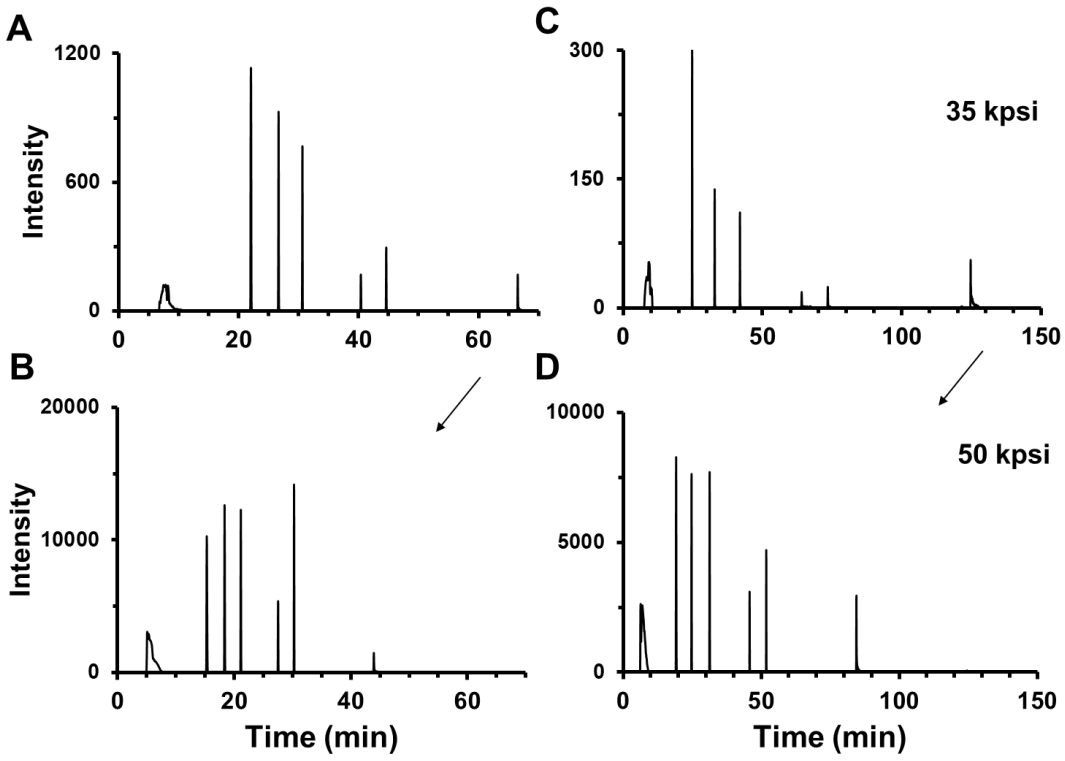

Figure 5-5. Separations of the standard mixture at 50 kpsi (B and D) and comparison to 35 kpsi (A and C). Separations were performed with a gradient slope of 16% (A and B) and 8% (C and D) ΔB/column volume. Dead time peaks are also shown for comparison between operating pressures. Other conditions are the same as Figure 5-2.

The peak capacities obtained at 50 kpsi under the two gradient lengths are plotted in Figure 5-6. Slight improvements in peak capacity per time were seen compared to separations at 35 kpsi. Separation times above 2 h were not able to be performed at 50 kpsi as the instrument hardware was not reliable, and so only a couple injections were completed. We also performed separations at 17 kpsi and saw further decreases in peak capacity relative to higher operating pressures. It should be noted that for a given analysis time at 17 kpsi, gradient slopes were half as steep as separations at 35 kpsi to achieve the same analysis time. For example, a 480 min separation at 35 kpsi employed a 2% ΔB/column volume, while 4% ΔB/column volume was required to generate a 480 min separation at 17 kpsi. Although peak capacities were lower at 17 kpsi, they were still relatively high, with a peak capacity of 1010 achieved in 8 h. Given the trend in peak capacity vs. operating pressure, it is likely that broadening due to longitudinal diffusion is smaller at higher

linear velocities (e.g., shift right on the van Deemter curve), improving peak widths and peak capacities at higher pressures. Previous reports have also showed that even deep in the C-term regime, peak capacities are higher at higher flow rates/linear velocities.[95,182,185]

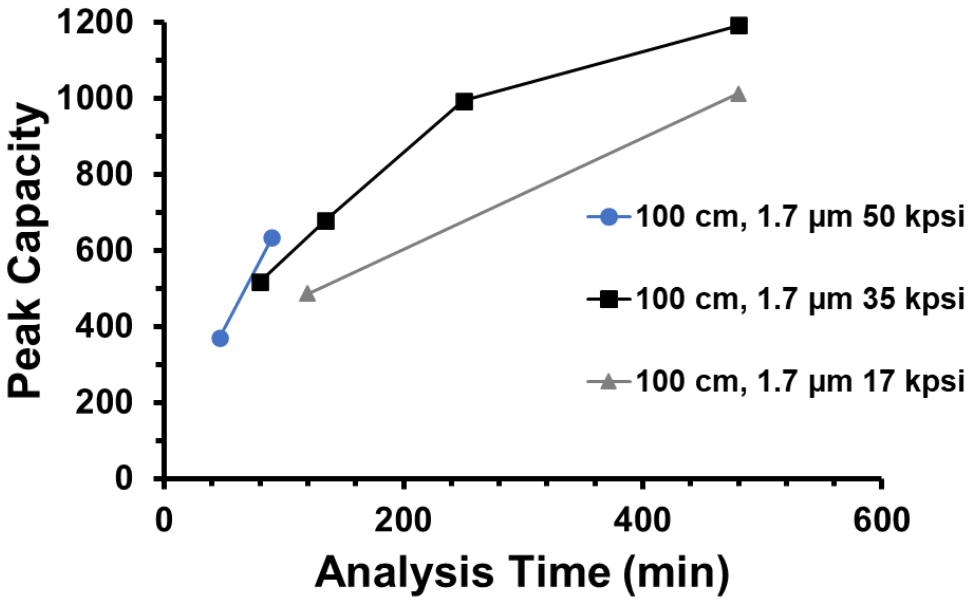

Figure 5-6. Effect of operating pressure and gradient length on peak capacity for small molecule standards on a 100 cm x 100 µm, 1.7 µm d_p column.

5.3.4. 70 cm x 100 µm, 1.1 µm column

Chapter 4 demonstrated relatively successful use of 1.1 µm particles packed in to 20 cm long columns for relatively high peak capacity separations at analysis times under 100 min and operated 35 kpsi. Higher resolution is possible with even longer columns with the 1.1 µm particles and operated at 35 kpsi and higher. A 70 cm x 100 µm column was packed with 1.1 µm particles and evaluated at different gradient lengths similar to the previous section. Peak capacities are plotted vs. analysis time for metabolite standards (Figure 5-7). While theory predicts higher plate counts on this column, peak capacities were lower than those obtained on the 100 cm column packed with 1.7 µm particles, indicating the column was not as well packed. Previous studies have shown axial heterogeneities and void formation as causes for poor performance in long columns

packed with such small particles. While sonication alleviated these packing voids with 1.7 µm particles, it did not appear to help with 1.1 µm particles in 70 cm columns under the conditions studied here. Quite different conditions were employed for the 1.1 µm vs. 1.7 µm particles; however, a similar approach was taken that seemed to work well for the 1.7 µm particles. Specifically, a slurry concentration of ~150 mg/mL was deemed "optimal" for 1.7 µm particles without sonication, and 200 mg/mL was "optimal" with sonication.[61,63] For ~1.3 µm particles, a ~20 mg/mL slurry was found to be optimal for ~30 cm column lengths but not for lengths of 100 cm.[64] Thus, for similar ~1.3 µm particles (labeled "1.1 µm") used here, we purposefully selected a high slurry concentration of 60 mg/mL for 70 cm columns. Despite this approach, the column did not appear to be as well packed as 1.7 µm particle packed columns. It is possible that different slurry concentrations and higher packing pressures could improve packing such small particles in to long columns. Given that shorter columns have been successfully packed with 1.3 µm particles, increasing the packing pressure may alleviate axial heterogeneities caused by a decrease in packing rate when using lower pressures.

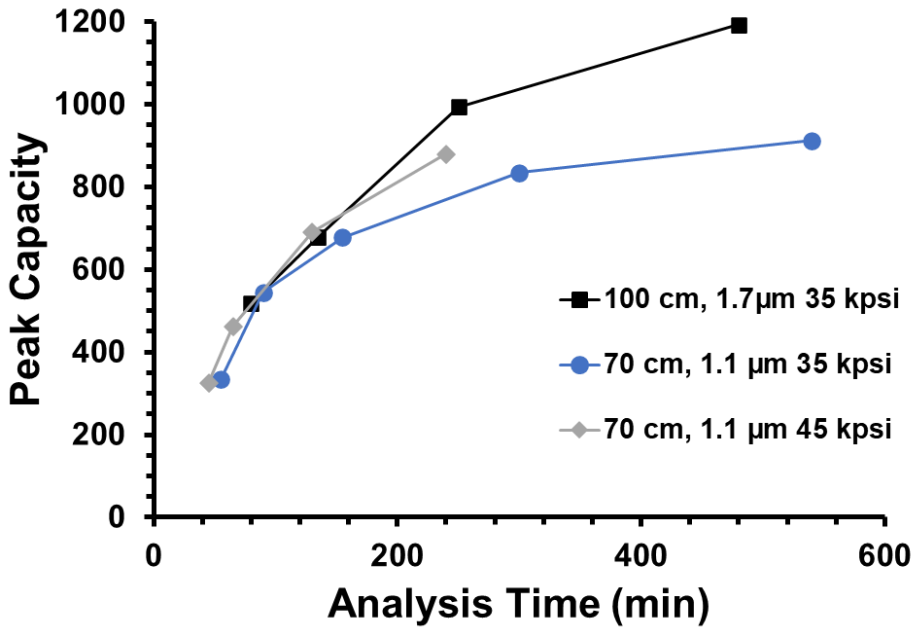

Figure 5-7. Peak capacity plotted versus analysis time on a 70 cm x 100 µm, 1.1 µm d_p column at 35 (blue circles) and 45 kpsi (gray diamonds). For reference, peak capacities of the 100 cm, 1.7 µm column are shown (black squares).

5.3.5. 70 cm x 100 µm, 1.1 µm column at 45 kpsi

Similar to the 100 cm, 1.7 µm d_p column, the 70 cm, 1.1 µm d_p column operated at 50 kpsi was attempted with the same instrument configuration. Leaks occurred at 50 kpsi, so 45 kpsi was used. Gradient separations of metabolite standards were again run at different gradient lengths (Figure 5-7). As before, the higher flow rates generated with higher operating pressure provided higher peak capacities than lower flow rates. Example chromatograms of the standard mixture on the 70 cm x 100 µm, 1.1 µm d_p column at 35 and 45 kpsi are shown in Figure 5-8.

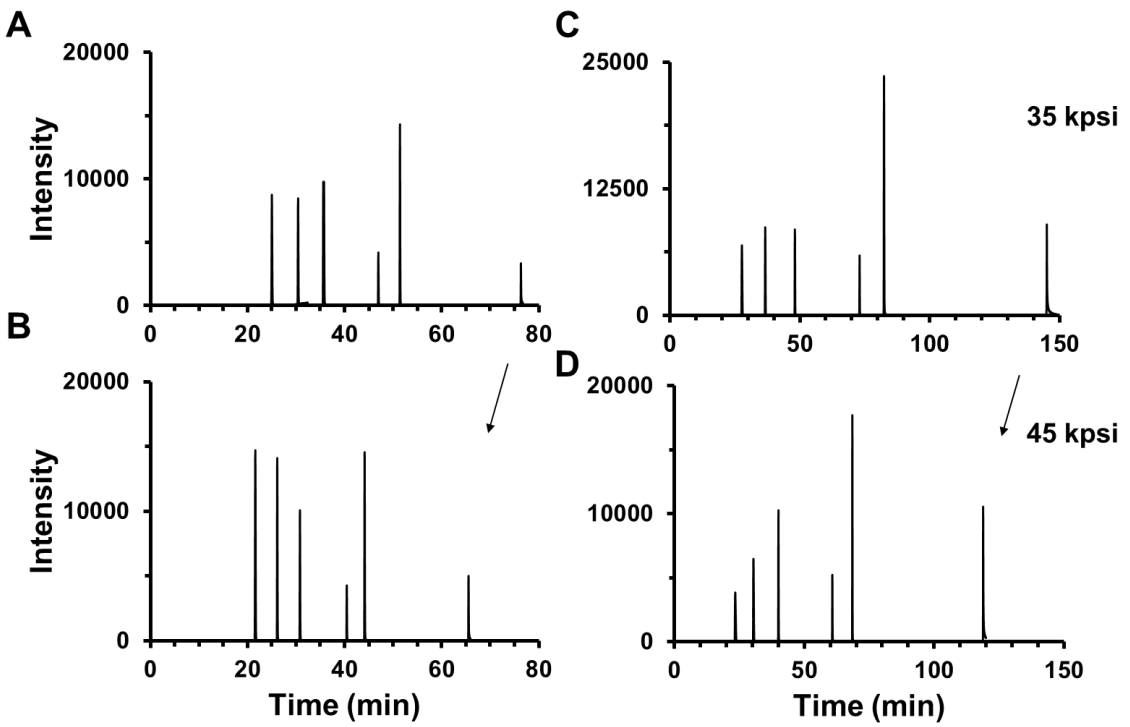

Figure 5-8. Example separations of Bz metabolites on a 70 cm x 100 µm, 1.1 µm d_p column at 35 (A & C) and 45 kpsi (B & D). Separations were performed with a gradient slope of 12 (A & B) or 6% ΔB/column volume.

5.3.6. Instrument considerations for routine use at 50 kpsi

It is clear from the previous sections that routine use of the current design of the custom-built UHPLC system at 50 kpsi is not feasible. The initial design of the custom-built gradient system shown in Figure 1-5 was tested to 45 kpsi;[67] however, much of the work was done at 30 kpsi as it was reported that the fittings often failed above 30 kpsi. Similarly, for most work described in the previous chapters of this dissertation, the operating pressure was 35 kpsi. The freeze/thaw valve has been tested up to ~ 60 kpsi,[212] although differences in solvent composition and capillary inner diameter may affect this limit. The HiP valves and tees used here are rated to 60 kpsi; these fittings are also available up to 150 kpsi but would require different fittings to be engineered to connect to capillary connections and capillary columns. Pneumatic amplifier pumps can also operate over 100 kpsi. Thus, the primary bottlenecks for routine operation at 50-60 kpsi are the microvolume tees that are used to connect capillary – i.e., connection to the pneumatic

pump, to the gradient storage loop, to the column, to the NanoAcquity, and to waste. These tees are from VICI/Valco and have either 1/32" or 1/16" fittings. In the current and previously published designs, fittings with 1/32" threads were used, with the main advantage of low dead volume providing linear gradients and minimum extra column band broadening.[67] While these tees were routinely reliable at 35 kpsi, inconsistent operation and frequent leaking occurred at higher pressures. Further tightening these connections with a small vise tool occasionally made a secure connection, however the metal threads would at times break inside the tee.

It was hypothesized that microvolume tees with 1/16" threads would allow for more grip strength and provide a better, more reliable connection at pressures around 50 kpsi or higher. A potential downside of moving to 1/16" tees is the potential increase in dead volume. While both tee geometries have a 150 µm bore within each arm and both are claimed to be "zero dead volume", it is possible that the larger tee cavities have bigger dead volumes. To estimate the dead volume of the system and compare the two tees, acetylcholine was injected on to a 100 cm x 100 µm, 1.7 µm column as a dead time marker. The peak width and number of theoretical plates were measured for both tee geometries using a 0.2 µL injection volume and 35 kpsi operating pressure. No significant differences were detected in terms of extra column volume, with the 1/16" and 1/32" tees obtaining 270 ± 15 (n = 3) and 279 ± 31 (n = 3) plates, respectively (Table 5-2).

While the larger tees seemed to provide a better fitting and did not break when tightening with a vise, there were still issues that prevented robust, routine use. Overtightening often lead to clogging of the tees, potentially due to the PEEK ferrule being crushed inside the tee and collapsing into the tee through-hole. Moreover, the capillary that butted up inside the tee would break when tightened. It is possible that different ferrules and use of a torque wrench would allow better use of these bigger fittings.

Table 5-2. Comparison in dead volume measured by theoretical plates for an unretained peak between 1/16" and 1/32" tees connecting the capillary column to the autosampler and the gradient storage loop.

Acetylcholine					
		t_R (min)	FWHM (min)	Plates	%RSD
1/32" tee	Run 1	11.91	1.70	272	11
	Run 2	13.10	1.97	245	
	Run 3	12.40	1.63	321	
1/16" tee	Run 1	12.20	1.77	263	5.5
	Run 2	12.88	1.78	290	
	Run 3	13.59	2.00	256	

5.3.7. Comparisons with literature

As discussed in the introduction, previous reports have demonstrated high peak capacity one-dimensional separations using long columns with different particle sizes (for packed beds) or domain structures (i.e., monolithic, µPAC). Figure 5-9 plots the peak capacity versus separation time from select publications in the past few years that have demonstrated high peak capacity compared to what is possible with commercially available pressure limits and column dimensions or column formats. Work described in this chapter typically outcompetes previous reports in terms of peak capacity per time. For example, a peak capacity of 580 and 1200 was achieved in 80 and 480 min, respectively, which correlates to 7.25 and 2.5 peaks per minute. In comparison, a peak capacity of 1800 was achieved in 2050 min with an 8 meter µPAC (orange circle), which correlates to 0.88 peaks per minute. We limited analysis time to below 1000 min, so other reports generated higher gross peak capacities at these very long analysis times. Additionally, recent reports utilizing open tubular columns greatly outperforms other packed bed and similar column formats in terms of both total peak capacity and peak capacity per time.[208,209]

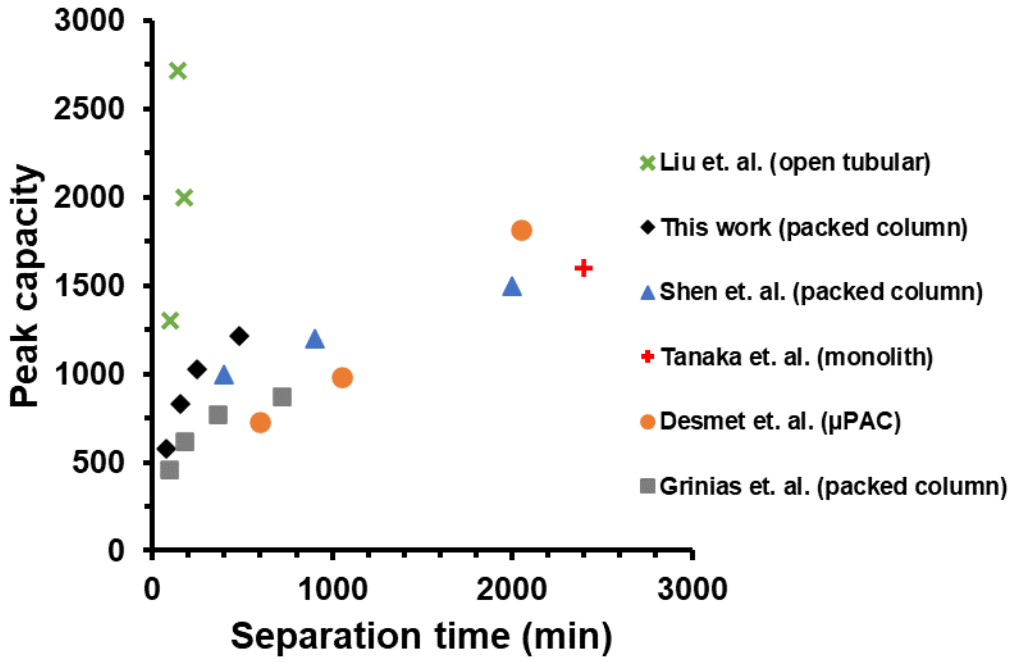

Figure 5-9. Peak capacity versus separation time for selected one-dimensional separations using long microcolumns with different particle sizes or column structures. All separations were done with either peptides or small molecules under reversed phase conditions with water-acetonitrile mobile phases at room temperature up to 70 °C.

6. Conclusions

This chapter describes column and instrument parameters that generated peak capacities over 1000 in a few hours for small molecule separations while coupled to mass spectrometry. Gradient kinetic plots were constructed that guided the choice of column length and particle size when using 35 – 50 kpsi operating pressure. Long columns (100 cm) packed with 1.7 µm particles outperformed columns packed with 1.1 µm particles (70 cm), suggesting packing improvements such as higher packing pressure are needed for micron-sized particles packed in long columns. Separations at 50 kpsi were achieved on 100 cm columns packed with 1.7 µm columns; however, improvements in instrument design are necessary for routine operation at these pressures. Larger microtees using 1/16” fittings were tested for use at 50 kpsi and the dead volume of the larger tees were evaluated. No significant difference was observed for plate counts of an unretained marker between the smaller and larger tees, indicating similar dead volumes.

While leaks were less frequent with the larger tees, clogging and broken capillary due to overtightening limited routine use at 50 kpsi. Use of a torque wrench to tighten the fittings more precisely could provide routine, leak-free operation at 50 kpsi.

Chapter 6. Conclusions and Future Directions

6.1. Conclusions

This thesis described applications of capillary liquid chromatography-mass spectrometry for metabolomics and lipidomics using custom-built instrumentation. A theoretical background on advantages of ultrahigh pressures at 35 – 50 kpsi were first introduced that provided guidance on different column parameters used in this thesis. Lipidomics methods were developed using one- and two-dimensional liquid chromatography at 35 kpsi coupled online with mass spectrometry. Column length, packing procedure, operating pressure, and gradient length were evaluated for separation of lipid isomers and complex lipid extracts from human plasma. Implementing a two-dimensional workflow utilizing HILIC in the first dimension to fractionate lipid classes from plasma followed by re-injection on 50 cm long reversed phase columns roughly doubled the peak capacity. Selective modification of gradient slope, resuspension volume, and injection volume for each fraction provided high orthogonality between the two dimensions with broad lipidome coverage. Lipid identification by MS1 data rather than tandem mass information limited the conclusions that could be drawn regarding how these columns improved MS/MS identification or improved identification confidence. Future widespread use of this technology may be limited by the custom-built nature of the instrumentation which generally requires more troubleshooting than current commercial instruments. Moreover, difficulty in creating low dead volume capillary connections by a routine user relative to wider bore formats and increased susceptibility of clogging with capillary LC-MS instrumentation may limit widespread use of this technology.

Finally, throughput must be balanced with the desired lipidome coverage, as both the longer 1D analysis times took 2 – 4 h and the 2D method was ~8 h. If throughput is of particular importance for the user, these methods may not be well suited.

Separation of metabolites were evaluated using the custom-built LC-MS at 35 – 50 kpsi. Use of 1.1 µm particles allowed relatively fast separations without compromising separation performance compared to larger particles. MS1 feature count was evaluated from separations of a plasma extract for practical metabolomics considerations. Feature count was influenced by interplaying variables including peak capacity, flow rate, and injection volume. Peak capacities over 1000 were achieved for metabolite standards on meter long columns packed with 1.7 µm particles, showing potential for greatly increasing the metabolome coverage in LC-MS based metabolomics. Finally, gradient separations at 50 kpsi were accomplished and discussed for routine use; these pressures should allow for unprecedented separation performance. Column packing procedures for columns to be used at these pressures, such as those with micron-sized particles and smaller, need to be investigated. Compared to other approaches for high-resolution separations such as using pillar array and monolithic columns, the packed columns and instrumentation used here provided higher peak capacities than previously published for analysis times under 600 min. The use of feature counts instead of database matching for identification limited the conclusions that could be drawn regarding applicability to metabolomics measurements. The large precolumn dead volumes relative to the peak volumes associated with capillary LC limit routine use of this technology for very polar metabolites that do not get well retained. Faster scanning mass spectrometers will be needed than those used here to keep up with the smaller peak widths obtained here relative to commercial columns.

Future work is discussed that includes implementing in-depth identification software using orthogonal data generated in LC-MS based metabolomics and lipidomics and potential for hybrid searching when using derivatization strategies; ultrahigh pressure separations using ion exchange and hydrophilic stationary phases; developing multi-omics methods to simultaneously separate and identify metabolites, peptides, and lipids; and investigating sub-micron particles for use in ultrahigh pressure separations.

6.2. Future directions

6.2.1. Improvements in metabolite and lipid identifications

In chapters 2-4, methods for efficiently separating metabolites and lipids from complex mixtures such as plasma were described using long columns packed with sub-2 µm particles and operated at ultrahigh pressures. Lipids for example were detected and preliminarily identified primarily using MS1 (or precursor ion) data and *in silico* libraries.[12] While this metric provided reasonable comparisons between the different columns investigated and the potential for each method to detect a certain number of lipids, the identification confidence was relatively low.[213] Future work should employ in-depth tandem MS data, retention time and equivalent carbon number data, and perhaps structural information provided by NMR. Additionally, identification software improvements should be studied and implemented to streamline data processing and provide user-friendly interfaces.

In chapter 4, benzoyl chloride derivatization was utilized to improve retention of polar metabolites on reversed phase columns. While this approach has been implemented heavily in targeted assays,[167,175] there has been limited use in untargeted metabolomics studies. A challenge in implementing this approach for untargeted methods is the difficulty in identifying unknowns following derivatization. In our work, we simply evaluated MS1 feature count, which is often an

overestimate of the number of actual real metabolites and is not a high confidence identification.[187] Hybrid searching is a potential solution to effectively identifying unknowns in an untargeted LC-MS based method following derivatization.[214] Future work should evaluate hybrid search strategies for use in assays such as BzCl derivatization. When isotopically labeled $^{13}C_6$-BzCl is used with standard $^{12}C_6$-BzCl, every peak with multiples of 6 m/z difference (e.g., 6 m/z for singly labeled, 12 m/z for doubly labeled, etc.) that elute at the same time should be a positive hit. Preliminary work suggests this approach is possible (Figure 6-1). Cerebrospinal fluid was collected from the nucleus accumbens in a rat brain using microdialysis at a flow rate of 0.5 µL/min. The collected dialysate volume was split in two, with one half derivatized with $^{12}C_6$-BzCl and the other half derivatized with $^{13}C_6$-BzCl, and then mixed back together (in collaboration with Dr. Youngsoo Kim and Brady Anderson). A 5 µL aliquot was injected onto a reversed phase column (15 cm x 2.1 mm, 1.8 µm HSS T3) coupled to a Q-ToF MS (Agilent 1290 UHPLC; Agilent 6546 Q-ToF) operated in full scan, positive ion mode. A total ion chromatogram shows many peaks eluting across the separation space (Figure 6-1A). A representative mass spectrum averaged from 9.6 – 9.8 min shows several feature pairs with the expected characteristic 6 m/z difference (Figure 6-1B). Evaluation of different hybrid search engines needs to be performed for accurate and facile identification of these compounds.

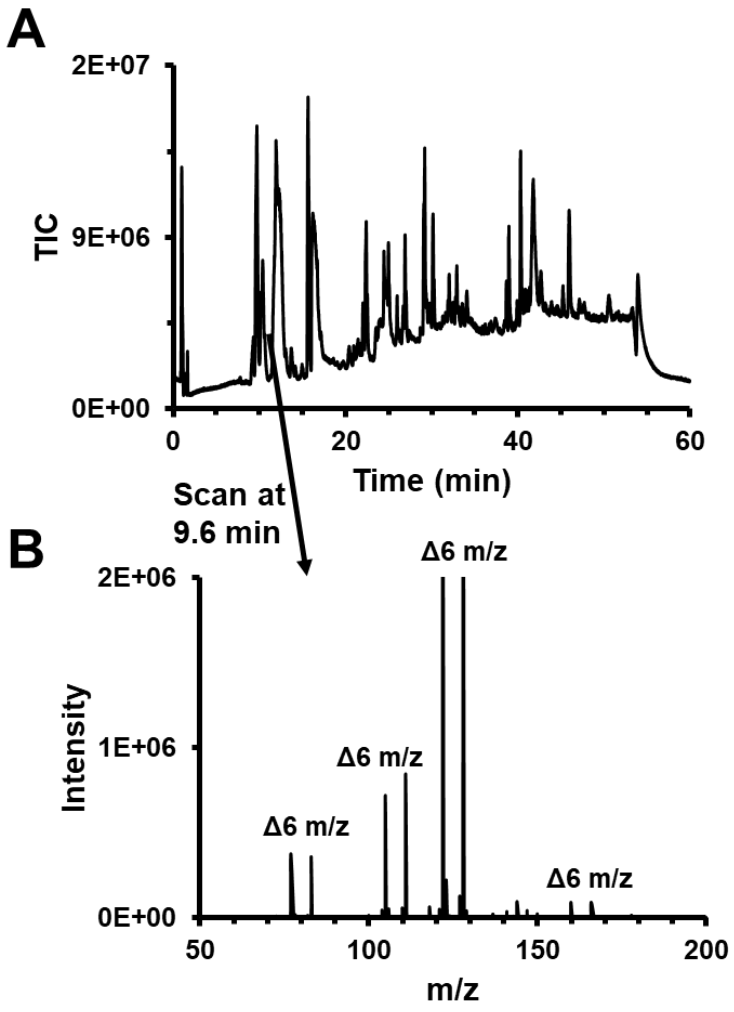

Figure 6-1. (A) Total ion chromatogram from a 5 µL injection of dialysate separately derivatized with $^{12}C_6$ and $^{13}C_6$-BzCl then mixed before injection. (B) Mass spectrum from scans at 9.6 – 9.8 min showing peaks with 6 m/z difference, indicative of a successful mixture of light/heavy BzCl derivatized compounds.

6.2.2. Ultrahigh pressure separations using HILIC and ion exchange particles

The bulk of this thesis described methods for packing and operating long microcolumns with sub-2 µm reversed phase (typically C18) particles. While reversed phase LC remains the dominant separation form in HPLC, alternative stationary phases can provide better selectivity and retention for certain compounds that are difficult to analyze. Hydrophilic interaction liquid chromatography (HILIC) and ion exchange chromatography are useful separation modes for separating polar and charged species; however, these stationary phases have not been packed in to

long columns or operated at pressures above 20 kpsi.[51] Recent work has illustrated the benefits of higher pressure and smaller particles for ion exchange particles in 10 – 15 cm commercial columns using 2.5 µm particles.[215] Current work in the lab is focused on procedures for efficiently packing long columns (~100 cm) with 1.7 µm BEH Amide particles (Waters) and 1.7 µm anion exchange particles (Agilent). Separation of polar compounds are shown in Figure 6-2A using a 50 cm x 75 µm column packed with the BEH Amide particles. A HILIC-type retention mechanism was observed with increasing retention as the percent of acetonitrile in the mobile phase was increased (Figure 6-2B). Further work has achieved over 100,000 theoretical plates at optimal linear velocities for polar compounds using a 100 cm microcolumn packed with 1.7 µm Amide particles (in collaboration with Brady Anderson). These advancements should open new avenues for generating in-depth metabolomics data with faster and higher resolution of polar and charged species than previously possible.

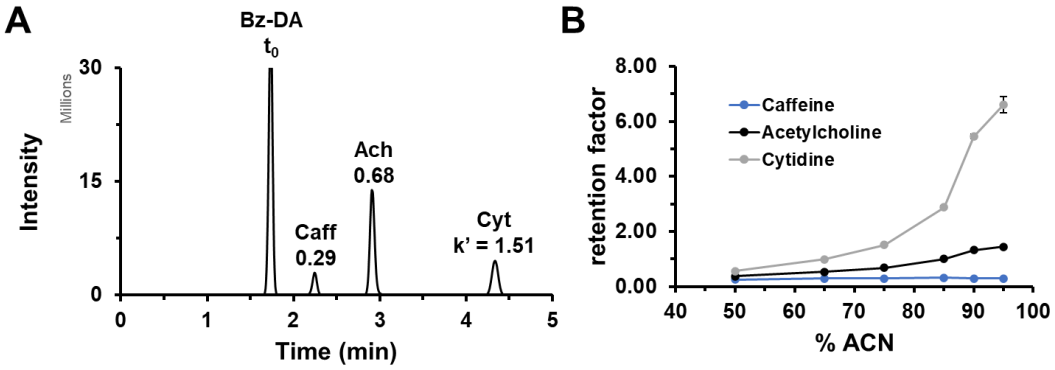

Figure 6-2. (A) Separation of polar compounds using a 50 cm x 75 µm column BEH Amide packed with 50 mg/mL in MeOH run at 25 kpsi at 75% ACN with 10 mM ammonium formate and 0.1% formic acid. MS detection was used with an integrated 30 µm spray tip. Abbreviations: Bz-DA, benzoyl-dopamine; Caff, caffeine; Ach, acetylcholine; Cyt, cytidine. (B) Retention factor as a function of percent acetonitrile in the mobile phase. This trend illustrates a HILIC-type of retention as expected using this stationary phase.

6.2.3. Multi-omics in a single shot technology using ultrahigh pressure capillary LC-MS

As discussed in the introductory sections of this thesis, thousands of biomolecules, including lipids, metabolites, nucleic acids, and proteins, are involved in cellular processes of

living organisms. The desire to understand these processes and the need to develop better drugs or understand diseases has led to the proliferation of various omics technologies such as metabolomics and proteomics. While these methods have provided valuable insight and discovery in systems biology, unresolved gaps remain, particularly when multiple biosynthesis pathways are involved for example in the same disease or same drug target. An integrated, multi-omics approach should overcome these challenges by providing metabolome, proteome, and lipidome data in a single chromatographic analysis. Simultaneous lipidome and proteome measurements have recently been successful in a single chromatographic analysis with a binary mobile phase pump using a 15 cm x 1 mm i.d. column with 2.1 µm BEH particles.[216] Future work will include metabolome measurements and use of a capillary based system. Additionally, future work should investigate extraction protocols and injection solvents amenable to metabolites, lipids, and peptides, as the previous work employed separate extraction protocols and injection from two separate vials. These modifications should lead to a more comprehensive analysis with decreased sample amounts while expanding the coverage and sensitivity. Use of 100% aqueous compatible particles (e.g., HSS T3 from Waters) will also allow better retention of polar metabolites compared to BEH particles. Preliminary work has been done using metabolite, peptide, and lipid standards injected from one vial onto a commercial 10 cm x 2.1 mm column with 1.8 µm HSS T3 particles (in collaboration with Devin Makey). A gradient of water, acetonitrile, and isopropanol was used to separate the compounds. Figure 6-3 shows an example separation of 5 metabolites, 3 lipids, and various tryptic peptides from enolase. Peptide signal intensities were low in this case due to the poor full-scanning capabilities of the triple quadrupole mass spectrometer used; in contrast, lipids and metabolites were detected using set MS/MS transitions. Use of the HSS T3 particles allowed starting the mobile phase gradient at 100% aqueous, allowing improved retention of polar

metabolites such as acetylcholine compared to columns such as BEH or other particle types that require small amounts (~3 – 5%) of organic content. Future work should investigate use of capillary scale columns packed with the HSS T3 particles on the custom-built UHPLC system. Coupling these separations with ion mobility spectrometry should also be explored to increase separation peak capacity, help separate isomers, and aid in identification. Ion mobility separations have the benefit of being fast (on the millisecond timescale), allowing online coupling with chromatographic separations.

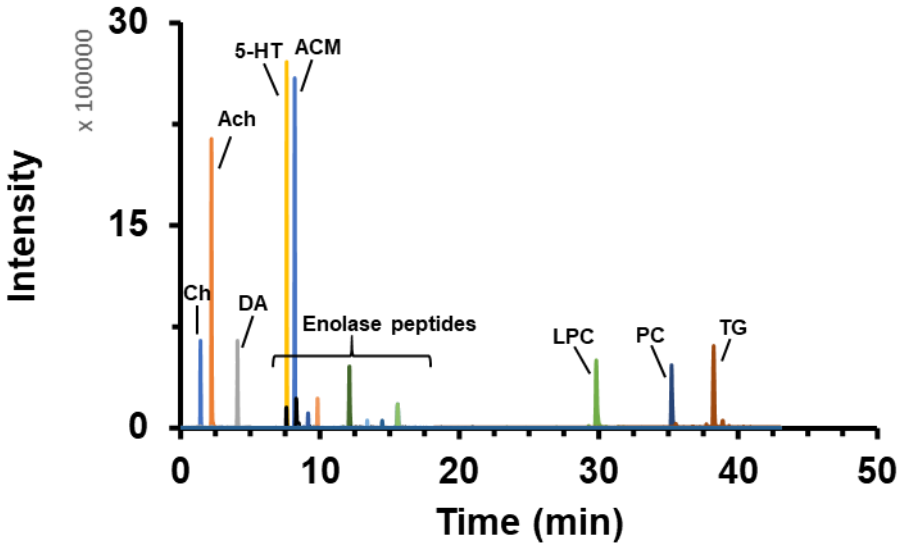

Figure 6-3. Separation of metabolite, lipid, and peptide standards in one chromatographic run with injection from a single vial. Abbreviations: Ch, choline; Ach, acetylcholine; 5-HT, serotonin; ACM: acetaminophen; LPC, lysophosphatidylcholine; PC, phosphatidylcholine; TG, triacylglycerol. Five µL was injected on to a 10 cm x 2.1 mm, 1.8 µm HSS T3 column.

6.2.4. Separations with sub-micron particles

In chapter 4, columns packed with 1.1 µm particles were used for fast and efficient separations of metabolites. These results were in good agreement with theory that faster separations can be achieved without compromising separation performance compared to larger particles. Use of even smaller particles below one micron should in theory provide even faster separations and in less time. A disadvantage of sub-micron particles is the large increase in

pressure requirements. With 35 – 50 kpsi available, column lengths of ~1 – 10 cm are beneficial (depending on the desired analysis time or plate count) over larger particle sizes.

Sub-micron particles are particularly advantageous for protein separations. The diffusion of proteins is much slower than that of peptides or small molecules, and so the impact of band broadening due to mass transfer is much higher than that of analytes with faster diffusion rates. Thus, the smaller diffusion distances afforded by sub-micron particles provides an even larger improvements in plate height for proteins. Moreover, excessive band broadening due to longitudinal diffusion will occur at much lower linear velocities for proteins relative to small molecules, meaning the pressure requirement is not as high for proteins. Theoretical van Deemter plots are illustrated for a small molecule with $D_m = 8 \times 10^{-6}$ cm^2/s (A) and for a 150 kDa protein with $D_m = 4.8 \times 10^{-7}$ cm^2/s (B) with 0.5, 1, and 2 µm particles (Figure 6-4). Clearly, plate height changes more drastically for proteins compared to small molecules. Additionally, the optimal linear velocity is lower for proteins, meaning less pressure is required to achieve this velocity. Reports of plate heights below 1 micron for protein separations have been reported using 300 – 500 nm diameter nonporous colloidal silica particles using commercial UHPLC instrumentation.[160,217,218]

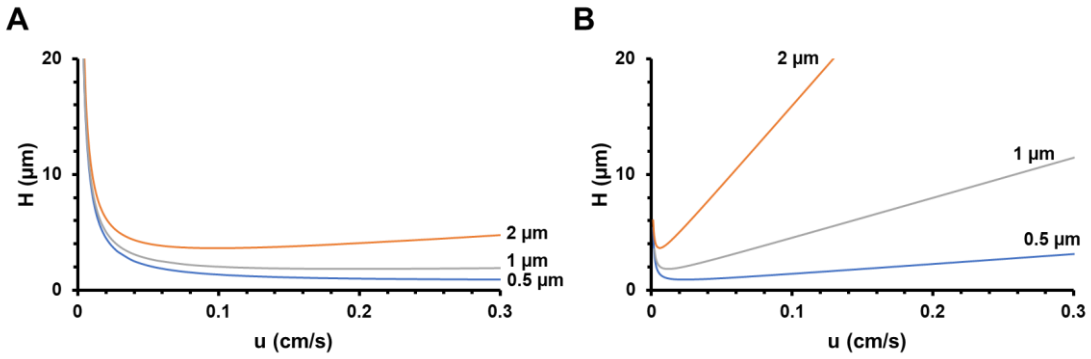

Figure 6-4. Theoretical van Deemter plots using 2, 1, and 0.5 µm fully porous particles with (A) a small molecule with $D_m = 8 \times 10^{-6}$ cm^2/s and for (B) a 150 kDa protein with $D_m = 4.8 \times 10^{-7}$ cm^2/s.

Slip flow has also been observed with sub-micron particles, providing enhanced flow rates compared to what is expected given Hagen-Poiseuille (no-slip) flow.[219] Slip flow occurs due to weak intermolecular interactions between a fluid and the surrounding walls, leading to enhanced flow rates of water or other polar solvents through hydrophobic nanoscale channels. Slip flow conditions also provide a narrower velocity profile compared to the conventional parabolic laminar flow profile, leading to plate heights lower than that expected from chromatographic theory. Separations of bovine serum albumin on a 2.1 cm long x 75 µm i.d. column filled with 470 nm nonporous colloidal silica particles provided plate heights as low as 15 nm using a pressure of only ~5000 psi.[220]

Most of these previous reports using slip flow with sub-micron particles used nonporous silica colloidal crystals.[160] Moreover, the separations have only been performed at commercial pressures. Future work can should be done to better understand slip flow using sub-micron porous particles compared to the nonporous colloidal particles. Theoretical work has shown differences between these two particle types in terms of both their flow rate enhancements and plate height improvements.[221] Work in our lab (in collaboration with Josh Jones) has been performed to experimentally study slip flow enhancements using 0.5 µm porous C18 silica particles at pressures up to 31 kpsi. Flow rate data was measured for 99% water, 50/50 water/acetonitrile, and 99% acetonitrile using a 6 cm x 100 µm capillary column packed with 0.5 µm particles. The fused silica capillary was used as is or was first coated with iododecane (C12) to ensure the walls were hydrophobic. It is expected that the flow rate of water (normalized for viscosity) is higher than that of acetonitrile due to greater immiscibility with the wall, and that the C12-coated column would provide higher flow rates for water than the uncoated. Figure 6-5 shows results from this study. In both the uncoated and C12-coated capillary columns with 0.5 µm columns, normalized flow rates

of water were higher than that of 50/50 water/acetonitrile or 99% acetonitrile, suggesting enhancements due to slip flow. Additionally, flow rates were 14 – 38% higher with the C12 coated capillary relative to the uncoated capillary, further indicating slip flow as a contributing factor to the enhanced flow rate (Figure 6-5B). More characterization needs to be done to fully understand the flow rate enhancements including column replicates, different alkyl chain length modifications, and different sub-micron particle sizes. Moreover, practical benefits of slip flow such as faster separations and lower than expected plate heights need to be investigated and compared with previous reports.

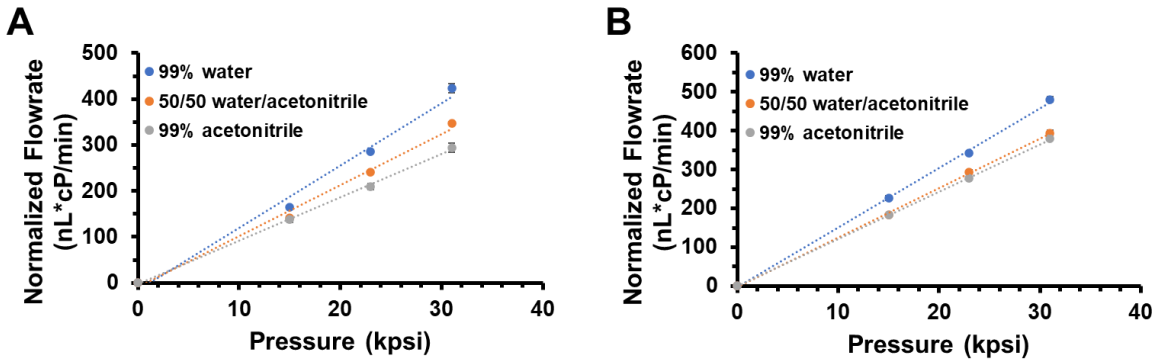

Figure 6-5. Normalized flow rate measured at different pressures and mobile phase compositions on a 6 cm x 100 µm capillary packed with 0.5 µm porous C18 silica particles. The fused silica capillary was uncoated (A) or coated with iododecane (C12).

Appendices

Appendix 1 – Targeted LC-MS/MS for Determination of Lipids and Neurochemicals with Applications to Diabetes, Obesity, Nanodisc Behavior, and *in vivo* Measurements

The bulk of this thesis described methods that were developed for untargeted metabolomics and lipidomics using full-scanning mass spectrometers with the goal of detecting all the metabolites or lipids in the samples of interest – typically plasma. As discussed in the introduction sections of this thesis, metabolomics is a valuable tool utilized in a wide range of applications including studying physiological mechanisms and understanding disease states. Targeted assays, where a set number of compounds are detected and quantified, are useful for certain applications such as hypothesis-driven studies where the compounds of interest are known beforehand and thought to be involved in the pathway or disease of interest in the study. Compared to untargeted approaches, targeted metabolomics typically offers better quantitation and can provide lower limits of detection due to fine-tuning of different LC and MS parameters for the specific metabolites of interest.

In this appendix, various targeted LC-MS/MS methods are described that were applied for different studies including diabetes, obesity, nanodisc formation, and *in vivo* neurochemical measurements. These methods were modified for different matrices including liver, plasma, cerebrospinal fluid, and adipose tissue cellular secretions. In most assays, limits of detection (LoDs) were sub-nM, which were often necessary to detect and quantify low-abundance species

within these complex matrices. For each application, method details are described, background and significance for each assay is briefly overviewed, and key results are summarized.

I. Determination of epinephrine and norepinephrine in plasma and liver

I.I. Background

Norepinephrine and epinephrine are important neurochemicals of the sympathetic nervous system (SNS) associated with various physiological roles including regulation of blood pressure, sugar levels, and heart rate. The release of these catecholamines is known as the "fight or flight" response and prepares the body for activity following a certain stimulus.[222] Determination of catecholamines from different biological tissues is difficult due to their relatively low abundance (e.g., ~pM – nM levels), necessitating sensitive methods, and the complexity of most tissues, necessitating selective techniques. In this work, an LC-MS/MS method was developed for selective and sensitive quantification of norepinephrine and epinephrine from mouse and rat liver and plasma to better understand the role of catecholamines in glucose regulation. This work was in collaboration with Dr. Jonathan Flak and Dr. Simon Evers in the labs of Professors Martin Myers and Darleen Sandoval, respectively. Specific contributions of Sorensen to this work include development of sample preparation protocols, development and use of LC-MS/MS method, and data workup.

I.II. Key findings

In this work, norepinephrine and epinephrine were determined from plasma and liver tissue of mice and rats. Chromatograms of 20 nM standards with corresponding deuterated internal standards are shown in Figure I-1. The first part of the work involved studying a subset of neurons

that were found to regulate blood glucose levels independently of insulin. Specifically, cholecystokinin receptor B (CCKBR)-expressing neurons in the ventromedial hypothalamic nucleus (VMN) were studied. It was found that activation of these VMN^{CCKBR} neurons increased blood glucose.[223] Norepinephrine and epinephrine levels were monitored following this activation in a controlled environment and food deprived environment. Circulating catecholamine levels suggested that the SNS may mediate blood glucose control following food deprivation compared to the control (Figure I-2).

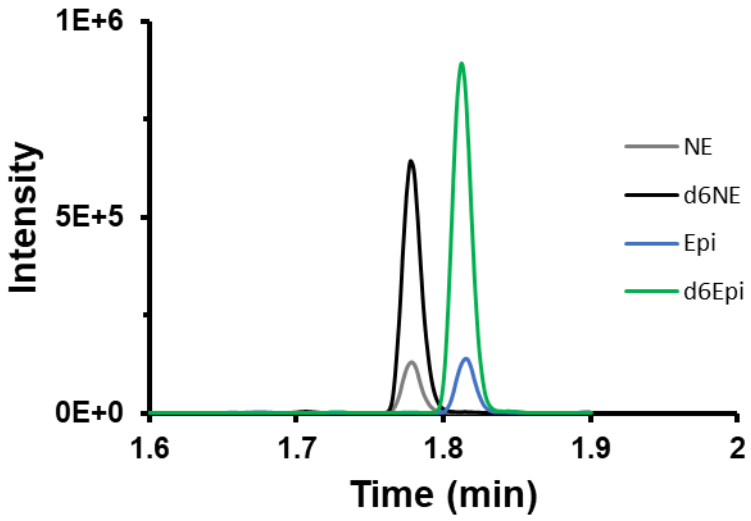

Appendix: Figure I-1. Chromatogram of benzoyl chloride labeled norepinephrine (NE) and epinephrine (Epi) and their deuterated internal standards. Five µL of 20 nM standards were injected on to a reversed phase column and detected using multiple reaction monitoring.

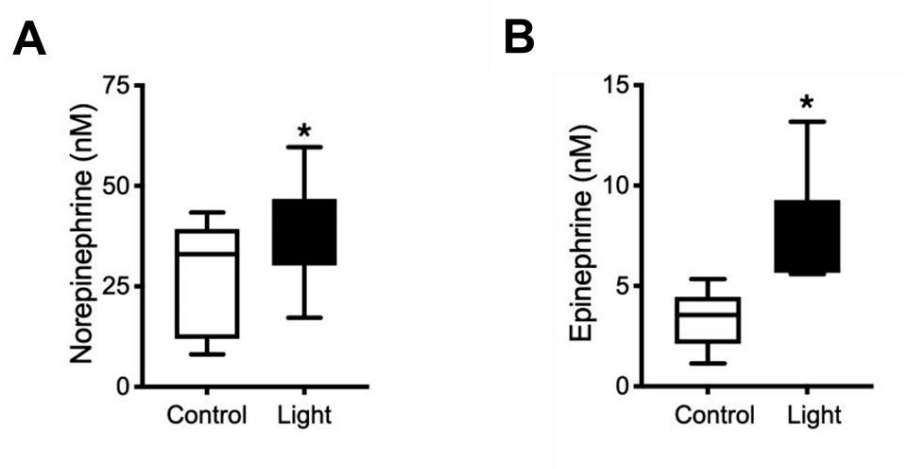

Appendix: Figure I-2. Circulating levels of norepinephrine (A) and epinephrine (B) in blood following activation of VMNCCKBR neurons in CCKBRChR2 mice. Animals were food deprived at the onset of the light cycle Data are plotted as box-and-whisker plots that show the spread from minimum to maximum, median, first quartile, and third quartile. *P < 0.05.

The second part of the work involved studying the effect of vertical sleeve gastrostomies on metabolism and health in rats. Vertical sleeve gastrectomy (VSG) is a procedure which removes part of the stomach as a means to help with weight loss. While often successful, VSG can cause complications, most notably hypoglycemia. The neuroendocrine response was monitored in VSG and sham (e.g., placebo surgery).[224] Additionally, the effect of 2-deoxyglucose (2DG), a non-metabolizable glucose agent that blocks glycolysis and thus imitates hypoglycemia, was studied. Epinephrine levels were found to be significantly higher when 2DG was administered after either VSG or sham surgery compared to if saline was administered (Figure I-3). This data indicates that hypoglycemia counterregulation is normal after VSG, and helps to understand the mechanisms underlying the glycemic variability observed after VSG.

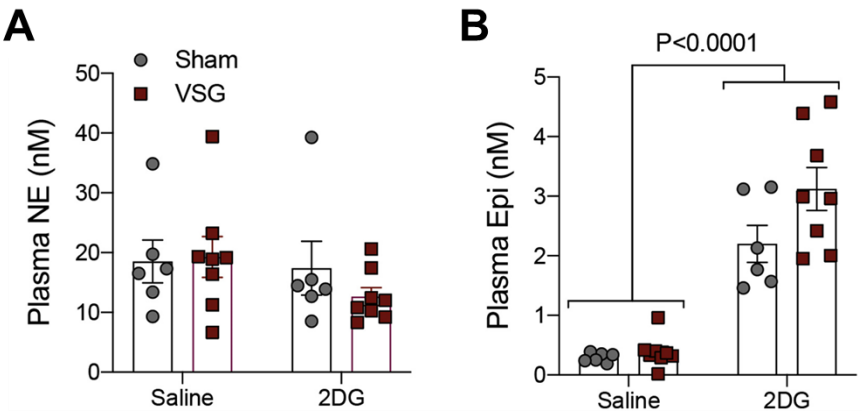

Appendix: Figure I-3 Circulating levels of norepinephrine (A) and epinephrine (B) in blood following vertical sleeve gastrectomy (VSG) or sham surgery and effect of 2-deoxyglucose (2DG) administration. Data are represented as mean ± SEM (n = 6 Sham-Sal and Sham-2DG; n = 8 VSG-Sal and VSG-2DG).

I.III. Methods

Unless otherwise specified, all chemicals were purchased from Sigma Aldrich (Saint Louis, MO). Limit of detection was determined by the following equation:[225]

$$LoD = LoB + 1.645(SD_{L1}) \quad \text{eq. A-1}$$

Where SD is standard deviation, L1 is the lowest concentration sample point, and LoB is limit of the blank, defined as $LoB = mean_{blank} + 1.645(SD_{blank})$.

For the determination of plasma epinephrine and norepinephrine concentrations, 9 µL of plasma was spiked with 1 µL of 12.5 mM ascorbic acid and 1 µL of a mixture containing 1 µM d_6-epinephrine and d_6-norepinephrine as internal standards to normalize for extraction efficiency and mass spectrometry ionization efficiency. For plasma samples, proteins were removed by the addition of 39 µL of ice-cold acetonitrile, followed by centrifugation for 10 min at 12,100 x *g*. For liver samples, an ice-cold mixture of 80/20 (v/v) acetonitrile/water was used as the extraction solvent. Approximately 10 – 15 mg of tissue was weighed in an Eppendorf tube. For each mg of tissue, 5 µL of extraction solvent and 0.1 µL of 1 µM internal standard were added, respectively. The tissue and solvent were vortexed and homogenized using a pestle grinder. A 20 µL aliquot of

the supernatant was removed and benzoylated by sequential addition of 10 μL of 100 mM sodium carbonate, 10 μL of benzoyl chloride (2% (v/v) in acetonitrile) and 10 μL of sulfuric acid (1% (v/v) in 20% (v/v) acetonitrile in water) as previously described.[167] Standard solutions of epinephrine and norepinephrine were prepared in aCSF, which is similar in salt composition to plasma without protein, to create a calibration range of 0.1–50 nM. Standards were spiked with the internal standard, diluted with acetonitrile and derivatized as described above. Calibration curves were prepared based on the peak area ratio of the standard to the internal standard by linear regression. All samples and standards were analyzed in triplicate using a Phenomenex Kinetex C18 chromatography column (100 x 2.1 mm, 1.7 μm, 100Å) on a Vanquish ultrahigh-pressure liquid chromatograph (Thermo Fisher Scientific, Gemering, Germany) interfaced to a TSQ Quantum Ultra triple quadrupole mass spectrometer (Thermo Fisher Scientific, San Jose, CA). Mobile phase A was 10 mM ammonium formate with 0.15% (v/v) formic acid in water. Mobile phase B was acetonitrile. The gradient used was as follows: initial, 5% B; 0.01 min, 19% B; 0.68 min, 26% B, 1.05 min, 75% B; 1.8 min, 100% B; 2.8 min, 100% B; 4 min, 5% B; 5.0 min, 5% B at 600 μL/min. Benzoylated norepinephrine eluted at 1.77 min and benzoylated epinephrine eluted at 1.81 min. The sample injection volume was 5 μL. The autosampler was kept at ambient temperature, and the column was held at 30 °C in still air mode. Electrospray ionization was used in positive mode at 4 kV. The capillary temperature was 400 °C, the vaporizer temperature was 350 °C, the sheath gas was 10, and the auxiliary gas was 5. Ions were detected in tandem mass spectrometry (MS/MS) mode. For epinephrine and d6-epinephrine, the precursor ions were m/z 478 and 484, respectively, with the tube lens set to 93 and collision energy of 26. For norepinephrine and d6-norepinephrine, the precursor ions were m/z 464 and 470, respectively, with a tube lens value of 81 and a collision energy of 19. The product ion was m/z 105 for all

analytes. Automated peak integration was performed using XCalibur 3.0 MS software. All peaks were visually inspected to ensure proper integration.

II. Determination of acetylcholine from adipose tissue cell secretions

Reproduced in part from Knights, A.J., Jun, H. et. al. (under review). Specific contributions from Sorensen to this work include development of LC-MS method, sample preparation and acetylcholine analysis, and data analysis.

II.I. Background

Acetylcholine is a small, organic compound that functions as a neurotransmitter in many animals as part of the cholinergic system.[226] Acetylcholine is involved in important roles such as muscle contractions, heart rate regulation, and bodily secretions. Specific to this work was the interest in the role of acetylcholine secretion to drive adaptive thermogenesis. Thermogenesis is the process of heat production in organisms and is primarily activated through sympathetic innervation of adipose tissue (e.g., fat cells). While adipose tissue has long been known to be a source of energy storage, it is now known to actively function in response to environmental and endogenous events to regulate metabolism and energy expenditure.[227] There is still much to be learned, however, about the signaling pathways involved in activating energy expenditure and mediating homeostasis. In this work, a population of cholinergic adipose macrophages that secrete acetylcholine to drive adaptive thermogenesis were identified in the stromal vascular fraction (SVF) of inguinal white adipose tissue (IWAT). Major findings of this work, specifically related to the separation and quantitation of acetylcholine using LC-MS and the monitoring of acetylcholine secretion from adipose tissue, will be discussed here. This work is in collaboration with Dr. Heejin Jun and Dr. Alexander Knights in Professor Jun Wu's lab. Specific contributions of Sorensen to this work include development of sample preparation protocols, development and use of LC-MS/MS method, and data workup.

II.II. Key findings

Because acetylcholine is a polar, positively charged compound, it typically has poor retention on reversed phase chromatography columns. While there have been reports of

acetylcholine analysis using cation exchange chromatography with mass spectrometry,[228] the high concentrations of salt in the mobile phase makes this approach challenging. We developed a RP-LC method using a shallow gradient that allowed slight retention of acetylcholine and baseline separation from iso-acetylcholine, an isomer with the same MS/MS transition as acetylcholine. Extracted ion chromatograms are shown in Figure II-1A and B for acetylcholine determined in selected samples. The method was applied to the monitoring of acetylcholine from adipose cell secretions, and similar retention times and peak shapes were observed for samples compared to standards.

It was recently shown that hematopoietic cells within subcutaneous fat express choline acetyltransferase (ChAT) and serve as a local source of acetylcholine.[229] Hematopoietic-specific deletion of *Chat* in *Chat$^{fl/fl}$;Vav-iCre* mice resulted in significantly reduced levels of acetylcholine secretion by IWAT SVF cells (Figure II-1C and D). Furthermore, acute cold exposure (e.g., exposing mice to a 4 °C environment for 4 h) caused an increase in acetylcholine secretion from *Chat$^{fl/fl}$* IWAT SVF cells. Acetylcholine levels showed no significant difference from cold exposure relative to a room temperature environment for *Chat$^{fl/fl}$;LysM-Cre* mice, which do not have acetylcholine-synthesizing macrophages. This data and other data from the paper (conducted by the first authors and not included in this appendix) suggest that cholinergic adipose macrophages respond to environmental stimuli and may be important for regulating thermogenic function in subcutaneous fat. Utilizing the cells investigated in this work and the molecular mechanisms that facilitate their function to activate energy expenditure may offer new opportunities for therapeutic developments in disorders such as obesity and diabetes.

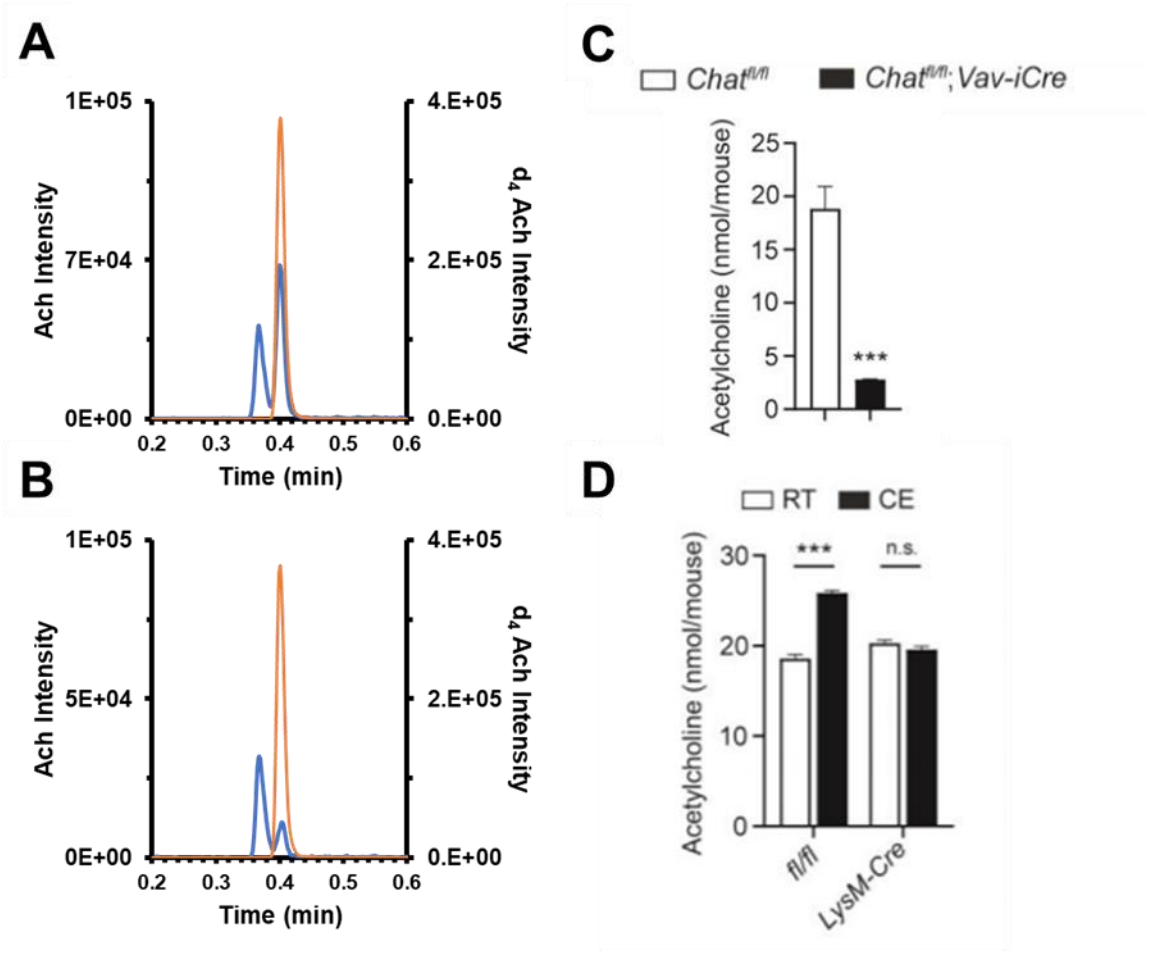

Appendix: Figure II-1. Extracted ion chromatograms from adipose cell secretion (A & B). The first peak is an isomer, iso-acetylcholine. The yellow trace is the internal standard, d4Ach. Acetylcholine levels for Chatfl/fl versus Chatfl/fl;Vav-iCre mice (C) and for Chatfl/fl versus Chatfl/fl;LysM-Cre following a cold environment (CE, 4 °C for 4 h) or room temperature. ***P < 0.001; n.s. = not significant.

II.III. Methods

Standard solutions of acetylcholine were prepared in 250 µM ascorbic acid in water to create a calibration range of 0.25–125 nM. Calibration curves were prepared based on the peak area ratio of the standard to the internal standard by linear regression. A deuterium labeled internal standard (d_4Ach (C/D/N isotopes, Pointe-Claire, Canada)) was added to samples and standards, diluted 1:3 (v/v) in water, and centrifuged for 10 min at 12,100 x *g*. The supernatant was transferred to an HPLC vial and analyzed as described below. All samples and standards were analyzed in triplicate using a Phenomenex Kinetex C18 chromatography column (100 x 2.1 mm, 1.7 µm, 100Å) on a

Vanquish ultrahigh-pressure liquid chromatograph (Thermo Fisher Scientific, Gemering, Germany) interfaced to a TSQ Quantum Ultra triple quadrupole mass spectrometer (Thermo Fisher Scientific, San Jose, CA). Mobile phase A was 10 mM ammonium formate with 0.15% (v/v) formic acid in water. Mobile phase B was acetonitrile. The gradient used was as follows: initial, 5% B; 0.60 min, 8% B; 0.68 min, 26% B, 1.05 min, 75% B; 1.8 min, 100% B; 2.2 min, 100% B; 2.2 min, 5% B; 3.0 min, 5% B at 600 μL/min. The sample injection volume was 5 μL. The autosampler was kept at ambient temperature, and the column was held at 30 ℃ in still air mode. Electrospray ionization was used in positive mode at 4 kV. The capillary temperature was 400 °C, the vaporizer temperature was 350 °C, the sheath gas was 10, and the auxiliary gas was 5. Ach ions were detected in MS/MS mode with the following transitions: (Ach) product: 87, precursor: 146; (d4-Ach) product: 91, precursor: 150. Tube lens and collision energy was 53 and 13, respectively. Automated peak integration was performed using XCalibur 3.0 MS software. All peaks were visually inspected to ensure proper integration.

III. Determination of neurochemicals from cerebrospinal fluid

III.I. Background

Measuring the concentration dynamics of neurochemicals in the brain *in vivo* is important for understanding brain function and remains a significant challenge. Studies of brain function can help in understanding and for potential treatment of mental and neurological diseases such as Alzheimer's, Parkinson's, depression, and addiction.[230] Challenges associated with *in vivo* neurochemical monitoring include the multitude of potential neurotransmitters and neurochemicals involved, the small size of neurons and neuronal networks, and the high speed of neuronal firing and neuronal fluctuations in response to various stimuli. A powerful approach for overcoming some of these challenges is the use of microfabricated push-pull sampling probes coupled to mass spectrometry.[231] The microfabricated probes are small (20 μm x 60 μm sampling area), providing 1000-fold smaller sampling areas compared to conventional sampling probes.[231,232] Use of MS and MS/MS allows for monitoring multiple analytes at once. Finally, use of oil to segment the flow following sampling allows for improved temporal resolution by limiting dispersion prior to analysis. In this work, an LC-MS/MS method was developed and used to evaluate various designs of microfabricated push-pull probes. These probes were tested *in vitro* (stirred vial of analytes in aCSF) and *in vivo* (mice and rats). This work is in collaboration with Thomas White in Professor Robert Kennedy's lab. Specific contributions of Sorensen to this work include development of sample preparation protocols, development and use of LC-MS/MS method, and data workup.

III.II. Key findings

A set of 26 neurotransmitters and other neurochemicals were determined and quantified using benzoyl chloride (BzCl) derivatization and reversed phase LC-MS/MS. Each analyte was

monitored via multiple reaction monitoring (MRM). Every analyte also had an isotopically labeled $^{13}C_6$-Bz internal standard which eluted at the same time as the standard analyte. Acetylcholine and choline do not get labeled and thus the internal standards were deuterated rather than $^{13}C_6$Bz-labeled. Figure III-1 shows an overlayed extracted ion chromatogram of 25 of the 26 targeted compounds detected from *in vivo* implantation of a probe in a rat's brain. For this experiment, ~1 µL of sample was collected with a recessed probe from rat striatum following anesthetization with 4% isoflurane. Sampling was done using a push and pull flow rate of 50 nL/min.

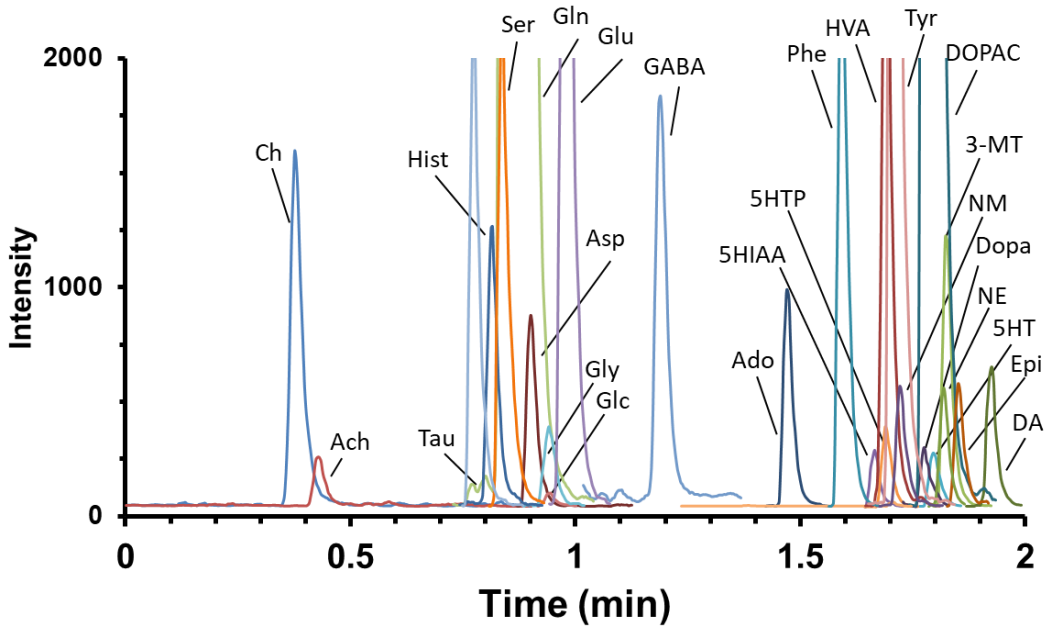

Appendix: Figure III-1. Overlayed ion chromatogram of 25 neurochemicals detected from an in vivo push-pull experiment. All compounds are BzCl labeled except choline and acetylcholine. All compounds were detected using multiple reaction monitoring.

The developed LC-MS/MS method allowed for evaluation of different microfabricated push-pull probes. Previous work demonstrated use of a flat-tip based geometry;[232] however, low recovery and clogging were common issues with this geometry for the conditions studied. Various

probe designs were tested including recessed, slanted, and v-shaped geometries in attempt to increase recovery and robustness. The effect of push and pull flow rates on analyte recovery *in vitro* were also studied. An example subset of data for *in vitro* studies is shown in Figure III-2. A clear trend is shown that with a higher push flow rate, a lower recovery is observed. Additionally, much higher recoveries were obtained for flat-tipped probes compared to the recessed probes. For dopamine, serotonin, and epinephrine, recoveries were 14 – 18% versus 0.4 – 1.9%, respectively.

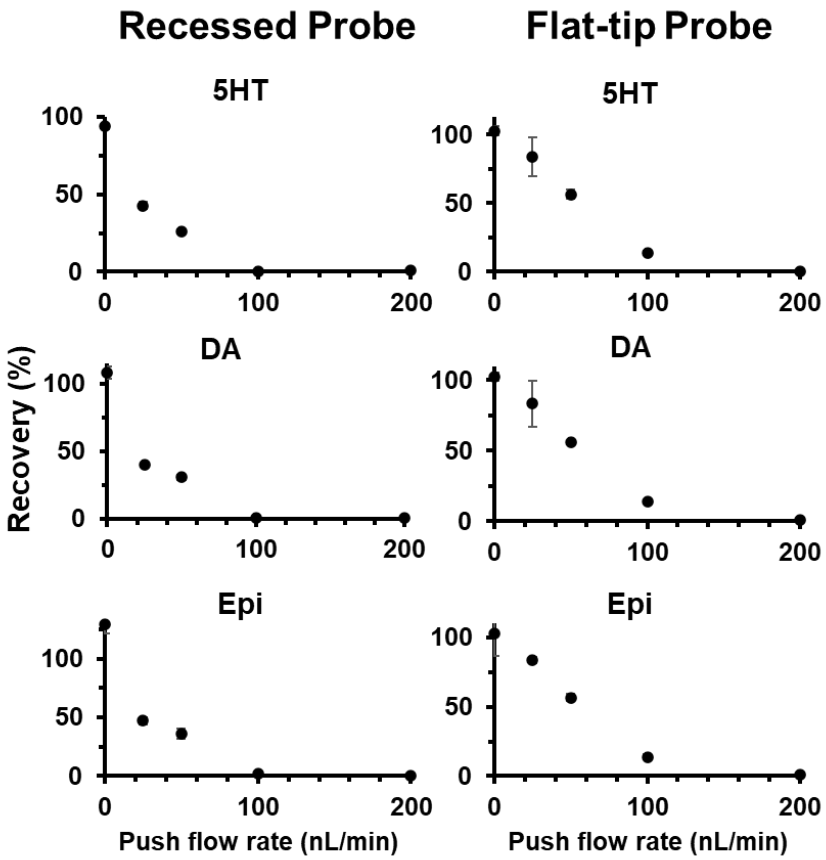

Appendix: Figure III-2. Effect of push flow rate on analyte recovery from an in vitro stirred vial experiment using two different probe designs. Pull flow was at 100 nL/min for all experiments. "Vial" refers to the sample taken directly from the stirred vail. Data plotted as mean ± SEM (n = 2). 5HT: serotonin; DA: dopamine; Epi: epinephrine.

Appendix: Table III-1. Method details for the targeted LC-MS/MS determination of 26 neurochemicals and their internal standards using benzoyl chloride derivatization. LoD was calculated according to equation A-1.

Analyte	Precursor (m/z)	Product (m/z)	Collision Energy (V)	Fragmentor (V)	Retention time (min)	LoD (nM)
Ch	104	60	20	120	0.38	8.14
Ach	146	87	10	120	0.43	3.95
Bz-3MT	376	105	25	120	1.80	0.06
Bz-5HIAA	313	146	25	120	1.65	2.12
Bz-5HT	385	264	25	140	1.80	0.24
Bz-5HTP	429	279	25	140	1.70	1.02
Bz-Ado	372	136	30	120	1.40	1.19
Bz-Asp	238	105	10	120	0.85	7.17
Bz-DA	466	105	22	140	1.90	0.03
Bz-DOPA	510	105	30	130	1.80	0.13
Bz-DOPAC	394	105	20	120	1.80	0.67
Bz-Epi	496	105	30	130	1.85	0.64
Bz-GABA	208	105	15	120	1.15	0.87
Bz-Glc	307	185	20	130	0.90	40
Bz-Gln	251	105	20	120	0.80	29
Bz-Glu	252	105	20	120	0.90	13
Bz-Gly	180	105	10	120	0.90	30
Bz-GSH	180	105	25	120	1.50	0.39
Bz-Hist	216	105	20	120	0.80	0.53
Bz-HVA	304	105	15	120	1.70	0.85
Bz-NE	482	105	30	130	1.80	0.01
Bz-NM	374	105	20	140	1.70	0.08
Bz-Phe	270	120	10	120	1.60	2.35
Bz-Ser	210	105	20	120	0.85	668
Bz-Tau	230	105	15	120	0.78	0.30
Bz-Tyr	390	105	30	140	1.70	14
d_4Ch	108	60	20	120	0.38	
d_4Ach	150	91	10	120	0.43	
$^{13}C_6$Bz-3MT	388	111	25	120	1.80	
^{13}C6Bz-5HIAA	319	146	25	120	1.65	
^{13}C6Bz-5HT	397	270	25	140	1.80	

^{13}C6Bz-5HTP	441	285	25	140	1.70	
^{13}C6Bz-Ado	378	136	30	120	1.40	
^{13}C6Bz-Asp	244	111	10	120	0.85	
^{13}C6Bz-DA	484	111	22	140	1.90	
^{13}C6Bz-DOPA	528	111	30	130	1.80	
^{13}C6Bz-DOPAC	406	111	20	120	1.80	
^{13}C6Bz-Epi	514	111	30	130	1.85	
^{13}C6Bz-GABA	214	111	15	120	1.15	
^{13}C6Bz-Glc	313	185	20	130	0.90	
^{13}C6Bz-Gln	257	111	20	120	0.80	
^{13}C6Bz-Glu	258	111	20	120	0.90	
^{13}C6Bz-Gly	186	111	10	120	0.90	
^{13}C6Bz-GSH	528	111	25	120	1.50	
^{13}C6Bz-Hist	222	111	20	120	0.80	
^{13}C6Bz-HVA	310	111	15	120	1.70	
^{13}C6Bz-NE	500	111	30	130	1.80	
^{13}C6Bz-NM	386	111	20	140	1.70	
^{13}C6Bz-Phe	276	120	10	120	1.60	
^{13}C6Bz-Ser	216	111	20	120	0.85	
^{13}C6Bz-Tau	236	111	15	120	0.78	
^{13}C6Bz-Tyr	402	111	30	140	1.70	

III.III. Methods

A method was developed for determination and quantitation of 26 neurochemicals from rat and mouse brain. Specifically, cerebrospinal fluid is collected from a microfabricated push-pull probe implanted inside the brain of the mouse or rat. Artificial cerebrospinal fluid (aCSF) was composed of 145 mM NaCl, 2.68 mM KCl, 1.4 mM CaCl2, 1.0 mM MgSO4, 1.55 mM Na2HPO4, and 0.45 mM NaH2PO4 adjusted to pH of 7.4 with 0.1 M NaOH. Stock solutions of 26 compounds were prepared similar to previously reported methods.[170,233] Calibration curves were prepared in aCSF with 250 μM ascorbic acid at various concentration ranges for each compound depending on the expected endogenous concentration for the given analyte. Push-pull perfusate (either *in*

vitro or *in vivo*) volume was typically around 1.5 μL and was collected in a PCR tube. A 1:1 dilution was done to increase the total volume for derivatization. Derivatization was employed by sequential addition of 100 mM sodium carbonate, benzoyl chloride (2% (v/v) in acetonitrile), and an internal standard solution containing ^{13}C-labeled compounds in 20% (v/v) acetonitrile in water with 1% (v/v) sulfuric acid in a 2:1 (v/v) ratio of perfusate:reagent. Standard solutions of were prepared in ACSF to create a calibration range. Calibration curves were prepared based on the peak area ratio of the standard to the internal standard by linear regression. All samples and standards were analyzed in triplicate using a Phenomenex Kinetex C18 chromatography column (100 x 2.1 mm, 1.7 μm, 100Å) on an Agilent 1290 ultrahigh-pressure liquid chromatograph interfaced to an Agilent 6410 triple quadrupole mass spectrometer. Mobile phase A was 10 mM ammonium formate with 0.15% (v/v) formic acid in water. Mobile phase B was acetonitrile. The gradient used was as follows: initial, 5% B; 0.01 min, 19% B; 0.68 min, 26% B, 1.05 min, 75% B; 1.8 min, 100% B; 2.8 min, 100% B; 4 min, 5% B; 5.0 min, 5% B at 600 μL/min. The sample injection volume was 5 μL. The autosampler was kept at ambient temperature, and the column was held at 30 °C. Electrospray ionization was used in positive mode at 3 kV. The gas temperature was 350 °C, gas flow was 11 L/min, and the nebulizer was at 55 psi. Ions were detected in tandem mass spectrometry (MS/MS) mode. Automated peak integration was performed using Mass Hunter software. All peaks were visually inspected to ensure proper integration.

IV. Determination of lipid levels in nanodisc environments

IV.I. Background

Lipid nanodiscs are disc-like lipid bilayers of 8 – 16 nm in diameter.[234] Similar to cellular membranes in living organisms, nanodiscs are typically composed of phospholipids and form in aqueous solutions with the polar head group on the perimeter and the hydrophobic tails interacting together in the middle. Nanodiscs are stabilized by amphipathic proteins, termed scaffold proteins, that encompass the hydrophobic tails and help to solubilize the nanodisc complex in aqueous solutions.[235]

Nanodiscs are valuable for studying membrane proteins and act as a surrogate cellular membrane. Membrane proteins are involved in numerous cellular functions, including cellular communication, energy transformations, and molecular transport in to and out of the cell or cellular organelles. Because of these critical roles, membrane proteins are the target of many therapeutics; however, membrane proteins are difficult to work with on their own due to their often amphipathic and/or hydrophobic nature and their altered or loss of function outside of the phospholipid bilayer. Nanodiscs are thus important for providing a surrogate native environment for studying membrane proteins. Despite their widespread use, there have not been many studies on the formation of nanodiscs with different phospholipid classes. In this work, a targeted LC-MS/MS method was developed to quantify different lipid species to better understand their incorporation in nanodiscs and how different ratios of lipids affects nanodisc formation and potentially membrane protein stability or function. This work is in collaboration with Marina Sarcinella in Professor Ryan Bailey's lab. Specific contributions of Sorensen to this work include development of sample preparation protocols, LC-MS/MS method, and data workup.

IV.II. Key findings

An example chromatogram of the 6 investigated lipids and the internal standard is shown in Figure IV-1. These lipids are commonly used in nanodisc studies.[234,235] Relatively good peak shape and resolution was seen for the lipids investigated. SM and PS co-eluted, and POPC, PE, and the internal standard (DOPC) co-eluted. Co-elution of these phospholipids is not surprising as all but DMPC had the same equivalent carbon number of 32, which is the dominant contribution of retention and selectivity in RPLC of lipids.[85] Figures of merit for the developed LC-MS method is shown in table IV-1. The linearity of all calibration curves was above 0.999 except for CL, which was 0.985. The linearity of CL could likely be improved by using an internal standard that is closer in structure to CL rather than the phospholipid used here. Additionally, only the precursor of CL was used; monitoring a product ion could improve linearity and improve the limit of detection.

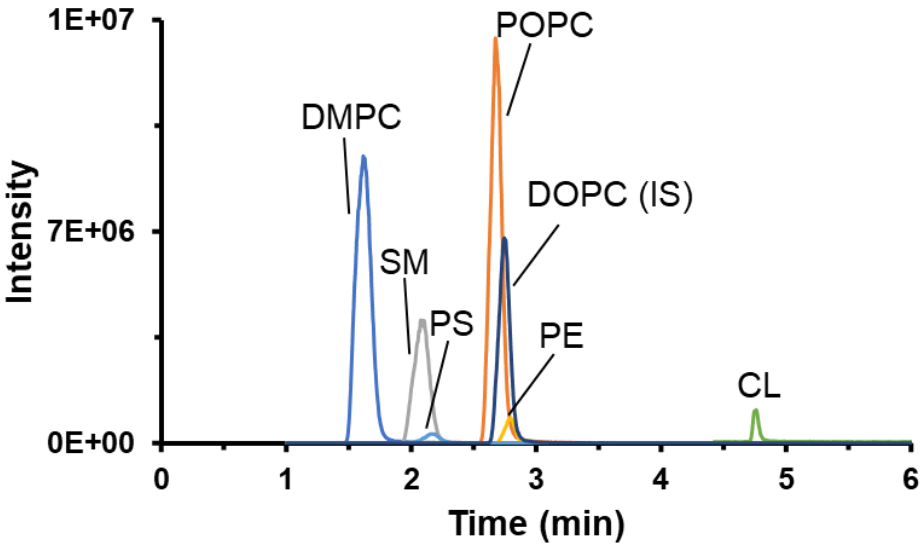

Appendix: Figure IV-1. Overlaid extracted ion chromatogram of the 6 lipids investigated here and the internal standard. A 5 µL injection volume was used and each lipid standard was 400 nM. The internal standard was 250 nM.

Appendix: Table IV-1. Figures of merit for determination of lipids from nanodisc environments.

Analyte	Limit of Detection (nM)	R^2	Calibration range (nM)	Precursor (m/z)	Product (m/z)	Collision energy (V)	Tube lens (V)
POPC	0.78	0.9995	1 - 1000	760.6	184	31	133
CL	2.7	0.9847	1 - 1000	603.6	603.6	0	130

PE	0.38	0.9997	1 - 1000	718.6	577	17	127
PS	0.70	0.9994	1 - 1000	762.6	577	16	133
SM	0.20	0.9993	1 - 1000	703.5	184	27	122
DMPC	0.39	0.9995	1 - 1000	678.6	184	28	130
DOPC (IS)	n/a	n/a	250	786.6	184	27	135

IV.III. Methods

All lipid standards were purchased from Avanti (Alabaster, AL). For extraction of lipids from different nanodisc environments, water, methanol, and chloroform were mixed well in a 4:8:4 (v/v/v) ratio relative to the nanodisc sample volume (e.g., 50 µL sample, 200 µL water and chloroform, 400 µL methanol). Next, water and chloroform were added in a 4:4 (v/v) ratio relative to the original nanodisc solution. Samples were vortexed briefly and centrifuged at 12,100 *x g* for 5 min at room temperature. The bottom organic layer was collected, evaporated with nitrogen, and resuspended in mobile phase B with internal standard.

Stock solutions of each compound were prepared in the mM range in chloroform. A mixture containing PC 14:0-14:0 ("DMPC"), PC 16:0-18:1 ("POPC"), PE 16:0-18:1 ("PE"), SM d18-1 16:0 ("SM"), PS 16:0-18:1 ("PS"), and cardiolipin 18:1 ("CL") were prepared each at 2 µM in mobile phase B. A calibration curve ranging from 1 to 1000 nM was prepared in mobile phase B. PC 18:1-18:1 ("DOPC") was used as an internal standard at a concentration of 250 nM. All samples and standards were analyzed using a Phenomenex Kinetex C18 chromatography column (100 x 2.1 mm, 1.7 µm, 100Å) on a Vanquish ultrahigh-pressure liquid chromatograph (Thermo Fisher Scientific; Gemering, Germany) interfaced to a TSQ Quantum Ultra triple quadrupole mass spectrometer (Thermo Fisher Scientific; San Jose, CA). Mobile phase A was 60/40 (v/v) water/acetonitrile with 10 mM ammonium formate and 0.1% (v/v) formic acid. Mobile phase B was 85/10/5 (v/v/v) isopropanol/acetonitrile/water with 10 mM ammonium formate and 0.1% (v/v)

formic acid. The gradient used was as follows: initial, 70% B; 4 min, 100% B; 5.5 min, 100% B, 5.8 min, 70% B; 7 min, 70% B at 400 μL/min. The sample injection volume was 5 μL. The autosampler was 30 °C, and the column was held at 60 °C in still air mode. Electrospray ionization was used in positive mode at 4 kV. The capillary temperature was 400 °C, the vaporizer temperature was 377 °C, the sheath gas was 60, and the auxiliary gas was 35. Ions were detected in MS/MS mode with the transitions listed in Table IV-1. Automated peak integration was performed using XCalibur 3.0 MS software. All peaks were visually inspected to ensure proper integration.

Appendix 2 – Calculations for Construction of Kinetic Plots

Kinetic plots are useful for understanding how different column and instrument parameters will affect the expected separation performance (theoretical plates or peak capacity). Below is a detailed description of the theory used to construct such plots used throughout this thesis.

First, columns were assumed to be equally well-packed. The plate height (H) was determined using equation A2-1, which is an approximate form of the van Deemter equation that is empirically found to be approximately accurate for packed capillary columns:[49]

$$H = d_p + \frac{2D_m}{u} + \frac{d_p^2 u}{5D_m} \qquad \text{eq. A2-1}$$

Where d_p is the particle diameter, D_m is the diffusion coefficient of the analyte in the mobile phase, and u is the mobile phase linear velocity. The mobile phase linear velocity was approximated by the following equation:[236]

$$u = \frac{P d_p^2 \varepsilon^2}{180 \eta L (1-\varepsilon^2)} \qquad \text{eq. A2-2}$$

Where ε is the column porosity and is 0.4 for randomly packed spheres of uniform size, L is column length, and η is the mobile phase viscosity. The mobile phase viscosity was calculated using the following equation:

$$\eta = \exp\left(\varphi\left(-3.476 + \frac{726}{T}\right) + (1-\varphi)\left(-1.762 + \frac{929}{T}\right)\right) \qquad \text{eq. A2-3}$$

Where T is temperature and φ is the percent acetonitrile in the mobile phase.

Theoretical plates were calculated by substituting equations A2-3 and A2-2 into A2-1, inputting the desired column length, and solving for N:

$$N = \frac{L}{H} \qquad \text{eq. A2-4}$$

Depending on the type of kinetic plot, variables that can be changed include column length, particle size, column porosity, pressure, and viscosity.

For peak capacity (n_c) estimates, the following equation was used:[99,203]

$$n_c = 1 + (\frac{\sqrt{N}}{4})(\frac{S\Delta c}{S\Delta c\frac{t_0}{t_G}+1}) \quad \text{eq. A2-5}$$

Where S is the solvent strength parameter from linear solvent strength theory,[237,238] Δc is the mobile phase gradient slope from the beginning to the end of the gradient, t_0 is the column dead time, and t_G is the gradient time. The value of S was estimated using the following equation:[239]

$$\ln S = 0.6915 \ln(MW) - 1.49 \quad \text{eq. A2-6}$$

Where MW is the molecular weight of the analyte. For calculations in chapter 5, Δc was 0.8, D_m was 1.2×10^{-5} cm^2/sec, T was 60 °C, φ was 0.2, and S was 12, which was estimated using equation A2-6 using a molecular weight of 300 Da. For isocratic kinetic plots, D_m was 8.0×10^{-6} cm^2/sec.

References

(1) Araújo, A. M.; Carvalho, M.; Carvalho, F.; Bastos, M. de L.; Guedes de Pinho, P. Metabolomic Approaches in the Discovery of Potential Urinary Biomarkers of Drug-Induced Liver Injury (DILI). *Critical Reviews in Toxicology* **2017**, *47* (8), 638–654. https://doi.org/10.1080/10408444.2017.1309638.

(2) Cajka, T.; Fiehn, O. Toward Merging Untargeted and Targeted Methods in Mass Spectrometry-Based Metabolomics and Lipidomics. *Anal. Chem.* **2016**, *88* (1), 524–545. https://doi.org/10.1021/acs.analchem.5b04491.

(3) Wishart, D. S. Emerging Applications of Metabolomics in Drug Discovery and Precision Medicine. *Nat Rev Drug Discov* **2016**, *15* (7), 473–484. https://doi.org/10.1038/nrd.2016.32.

(4) Houten, S. M. Metabolomics: Unraveling the Chemical Individuality of Common Human Diseases. *Ann Med* **2009**, *41* (6), 402–407. https://doi.org/10.1080/07853890902729794.

(5) Guo, L.; Milburn, M. V.; Ryals, J. A.; Lonergan, S. C.; Mitchell, M. W.; Wulff, J. E.; Alexander, D. C.; Evans, A. M.; Bridgewater, B.; Miller, L.; Gonzalez-Garay, M. L.; Caskey, C. T. Plasma Metabolomic Profiles Enhance Precision Medicine for Volunteers of Normal Health. *Proc Natl Acad Sci USA* **2015**, *112* (35), E4901–E4910. https://doi.org/10.1073/pnas.1508425112.

(6) Zhao, Y.-Y.; Cheng, X.; Lin, R.-C. Lipidomics Applications for Discovering Biomarkers of Diseases in Clinical Chemistry. In *International Review of Cell and Molecular Biology*; Elsevier, 2014; Vol. 313, pp 1–26. https://doi.org/10.1016/B978-0-12-800177-6.00001-3.

(7) Yadav, R. S.; Tiwari, N. K. Lipid Integration in Neurodegeneration: An Overview of Alzheimer's Disease. *Mol Neurobiol* **2014**, *50* (1), 168–176. https://doi.org/10.1007/s12035-014-8661-5.

(8) Fahy, E.; Subramaniam, S.; Murphy, R. C.; Nishijima, M.; Raetz, C. R. H.; Shimizu, T.; Spener, F.; van Meer, G.; Wakelam, M. J. O.; Dennis, E. A. Update of the LIPID MAPS Comprehensive Classification System for Lipids. *Journal of Lipid Research* **2009**, *50* (Supplement), S9–S14. https://doi.org/10.1194/jlr.R800095-JLR200.

(9) Sud, M.; Fahy, E.; Cotter, D.; Azam, K.; Vadivelu, I.; Burant, C.; Edison, A.; Fiehn, O.; Higashi, R.; Nair, K. S.; Sumner, S.; Subramaniam, S. Metabolomics Workbench: An International Repository for Metabolomics Data and Metadata, Metabolite Standards, Protocols, Tutorials and Training, and Analysis Tools. *Nucleic Acids Research* **2016**, *44* (D1), D463–D470. https://doi.org/10.1093/nar/gkv1042.

(10) Smith, C. A.; Maille, G. O.; Want, E. J.; Qin, C.; Trauger, S. A.; Brandon, T. R.; Custodio, D. E.; Abagyan, R.; Siuzdak, G. METLIN: A Metabolite Mass Spectral Database. *Therapeutic Drug Monitoring* **2005**, *27* (6), 747–751. https://doi.org/10.1097/01.ftd.0000179845.53213.39.

(11) Riekeberg, E.; Powers, R. New Frontiers in Metabolomics: From Measurement to Insight. *F1000Res* **2017**, *6*, 1148. https://doi.org/10.12688/f1000research.11495.1.
(12) Kind, T.; Liu, K.-H.; Lee, D. Y.; DeFelice, B.; Meissen, J. K.; Fiehn, O. LipidBlast in Silico Tandem Mass Spectrometry Database for Lipid Identification. *Nature Methods* **2013**, *10* (8), 755–758. https://doi.org/10.1038/nmeth.2551.
(13) Bowden, J. A.; Heckert, A.; Ulmer, C. Z.; Jones, C. M.; Koelmel, J. P.; Abdullah, L.; Ahonen, L.; Alnouti, Y.; Armando, A. M.; Asara, J. M.; Bamba, T.; Barr, J. R.; Bergquist, J.; Borchers, C. H.; Brandsma, J.; Breitkopf, S. B.; Cajka, T.; Cazenave-Gassiot, A.; Checa, A.; Cinel, M. A.; Colas, R. A.; Cremers, S.; Dennis, E. A.; Evans, J. E.; Fauland, A.; Fiehn, O.; Gardner, M. S.; Garrett, T. J.; Gotlinger, K. H.; Han, J.; Huang, Y.; Neo, A. H.; Hyötyläinen, T.; Izumi, Y.; Jiang, H.; Jiang, H.; Jiang, J.; Kachman, M.; Kiyonami, R.; Klavins, K.; Klose, C.; Köfeler, H. C.; Kolmert, J.; Koal, T.; Koster, G.; Kuklenyik, Z.; Kurland, I. J.; Leadley, M.; Lin, K.; Maddipati, K. R.; McDougall, D.; Meikle, P. J.; Mellett, N. A.; Monnin, C.; Moseley, M. A.; Nandakumar, R.; Oresic, M.; Patterson, R.; Peake, D.; Pierce, J. S.; Post, M.; Postle, A. D.; Pugh, R.; Qiu, Y.; Quehenberger, O.; Ramrup, P.; Rees, J.; Rembiesa, B.; Reynaud, D.; Roth, M. R.; Sales, S.; Schuhmann, K.; Schwartzman, M. L.; Serhan, C. N.; Shevchenko, A.; Somerville, S. E.; St. John-Williams, L.; Surma, M. A.; Takeda, H.; Thakare, R.; Thompson, J. W.; Torta, F.; Triebl, A.; Trötzmüller, M.; Ubhayasekera, S. J. K.; Vuckovic, D.; Weir, J. M.; Welti, R.; Wenk, M. R.; Wheelock, C. E.; Yao, L.; Yuan, M.; Zhao, X. H.; Zhou, S. Harmonizing Lipidomics: NIST Interlaboratory Comparison Exercise for Lipidomics Using SRM 1950–Metabolites in Frozen Human Plasma. *Journal of Lipid Research* **2017**, *58* (12), 2275–2288. https://doi.org/10.1194/jlr.M079012.
(14) Wishart, D. S.; Knox, C.; Guo, A. C.; Eisner, R.; Young, N.; Gautam, B.; Hau, D. D.; Psychogios, N.; Dong, E.; Bouatra, S.; Mandal, R.; Sinelnikov, I.; Xia, J.; Jia, L.; Cruz, J. A.; Lim, E.; Sobsey, C. A.; Shrivastava, S.; Huang, P.; Liu, P.; Fang, L.; Peng, J.; Fradette, R.; Cheng, D.; Tzur, D.; Clements, M.; Lewis, A.; De Souza, A.; Zuniga, A.; Dawe, M.; Xiong, Y.; Clive, D.; Greiner, R.; Nazyrova, A.; Shaykhutdinov, R.; Li, L.; Vogel, H. J.; Forsythe, I. HMDB: A Knowledgebase for the Human Metabolome. *Nucleic Acids Research* **2009**, *37* (suppl_1), D603–D610. https://doi.org/10.1093/nar/gkn810.
(15) Dettmer, K.; Aronov, P. A.; Hammock, B. D. Mass Spectrometry-Based Metabolomics. *Mass Spectrometry Reviews* **2007**, *26* (1), 51–78. https://doi.org/10.1002/mas.20108.
(16) Lenz, E. M.; Wilson, I. D. Analytical Strategies in Metabonomics. *Journal of Proteome Research* **2007**, *6* (2), 443–458. https://doi.org/10.1021/pr0605217.
(17) Segers, K.; Declerck, S.; Mangelings, D.; Heyden, Y. V.; Eeckhaut, A. V. Analytical Techniques for Metabolomic Studies: A Review. *Bioanalysis* **2019**, *11* (24), 2297–2318. https://doi.org/10.4155/bio-2019-0014.
(18) Emwas, A.-H.; Roy, R.; McKay, R. T.; Tenori, L.; Saccenti, E.; Gowda, G. A. N.; Raftery, D.; Alahmari, F.; Jaremko, L.; Jaremko, M.; Wishart, D. S. NMR Spectroscopy for Metabolomics Research. *Metabolites* **2019**, *9* (7). https://doi.org/10.3390/metabo9070123.
(19) Aretz, I.; Meierhofer, D. Advantages and Pitfalls of Mass Spectrometry Based Metabolome Profiling in Systems Biology. *Int J Mol Sci* **2016**, *17* (5). https://doi.org/10.3390/ijms17050632.

(20) Brügger, B. Lipidomics: Analysis of the Lipid Composition of Cells and Subcellular Organelles by Electrospray Ionization Mass Spectrometry. *Annual Review of Biochemistry* **2014**, *83* (1), 79–98. https://doi.org/10.1146/annurev-biochem-060713-035324.

(21) Rampler, E.; Abiead, Y. E.; Schoeny, H.; Rusz, M.; Hildebrand, F.; Fitz, V.; Koellensperger, G. Recurrent Topics in Mass Spectrometry-Based Metabolomics and Lipidomics—Standardization, Coverage, and Throughput. *Anal. Chem.* **2021**, *93* (1), 519–545. https://doi.org/10.1021/acs.analchem.0c04698.

(22) Wang, Y.; Liu, S.; Hu, Y.; Li, P.; Wan, J.-B. Current State of the Art of Mass Spectrometry-Based Metabolomics Studies – a Review Focusing on Wide Coverage, High Throughput and Easy Identification. *RSC Adv.* **2015**, *5* (96), 78728–78737. https://doi.org/10.1039/C5RA14058G.

(23) Khoury, S.; El Banna, N.; Tfaili, S.; Chaminade, P. A Study of Inter-Species Ion Suppression in Electrospray Ionization-Mass Spectrometry of Some Phospholipid Classes. *Analytical and Bioanalytical Chemistry* **2016**, *408* (5), 1453–1465. https://doi.org/10.1007/s00216-015-9245-6.

(24) Hancock, S. E.; Poad, B. L. J.; Batarseh, A.; Abbott, S. K.; Mitchell, T. W. Advances and Unresolved Challenges in the Structural Characterization of Isomeric Lipids. *Analytical Biochemistry* **2017**, *524*, 45–55. https://doi.org/10.1016/j.ab.2016.09.014.

(25) Wilson, I. D.; Nicholson, J. K.; Castro-Perez, J.; Granger, J. H.; Johnson, K. A.; Smith, B. W.; Plumb, R. S. High Resolution "Ultra Performance" Liquid Chromatography Coupled to Oa-TOF Mass Spectrometry as a Tool for Differential Metabolic Pathway Profiling in Functional Genomic Studies. *Journal of Proteome Research* **2005**, *4* (2), 591–598. https://doi.org/10.1021/pr049769r.

(26) Annesley, T. M. Ion Suppression in Mass Spectrometry. *Clinical Chemistry* **2003**, *49* (7), 1041–1044. https://doi.org/10.1373/49.7.1041.

(27) Dunn, W. B.; Broadhurst, D.; Begley, P.; Zelena, E.; Francis-McIntyre, S.; Anderson, N.; Brown, M.; Knowles, J. D.; Halsall, A.; Haselden, J. N.; Nicholls, A. W.; Wilson, I. D.; Kell, D. B.; Goodacre, R. Procedures for Large-Scale Metabolic Profiling of Serum and Plasma Using Gas Chromatography and Liquid Chromatography Coupled to Mass Spectrometry. *Nature Protocols* **2011**, *6* (7), 1060–1083. https://doi.org/10.1038/nprot.2011.335.

(28) Lisec, J.; Schauer, N.; Kopka, J.; Willmitzer, L.; Fernie, A. R. Gas Chromatography Mass Spectrometry–Based Metabolite Profiling in Plants. *Nature Protocols* **2006**, *1* (1), 387–396. https://doi.org/10.1038/nprot.2006.59.

(29) Ramautar, R.; Demirci, A.; Jong, G. J. de. Capillary Electrophoresis in Metabolomics. *TrAC Trends in Analytical Chemistry* **2006**, *25* (5), 455–466. https://doi.org/10.1016/j.trac.2006.02.004.

(30) Zhang, W.; Hankemeier, T.; Ramautar, R. Next-Generation Capillary Electrophoresis–Mass Spectrometry Approaches in Metabolomics. *Current Opinion in Biotechnology* **2017**, *43*, 1–7. https://doi.org/10.1016/j.copbio.2016.07.002.

(31) Ramautar, R.; Somsen, G. W.; de Jong, G. J. CE-MS for Metabolomics: Developments and Applications in the Period 2014-2016: CE and CEC. *ELECTROPHORESIS* **2017**, *38* (1), 190–202. https://doi.org/10.1002/elps.201600370.

(32) Laboureur, L.; Ollero, M.; Touboul, D. Lipidomics by Supercritical Fluid Chromatography. *International Journal of Molecular Sciences* **2015**, *16* (12), 13868–13884. https://doi.org/10.3390/ijms160613868.
(33) Shulaev, V.; Isaac, G. Supercritical Fluid Chromatography Coupled to Mass Spectrometry – A Metabolomics Perspective. *Journal of Chromatography B* **2018**, *1092*, 499–505. https://doi.org/10.1016/j.jchromb.2018.06.021.
(34) Desfontaine, V.; Losacco, G. L.; Gagnebin, Y.; Pezzatti, J.; Farrell, W. P.; González-Ruiz, V.; Rudaz, S.; Veuthey, J.-L.; Guillarme, D. Applicability of Supercritical Fluid Chromatography – Mass Spectrometry to Metabolomics. I – Optimization of Separation Conditions for the Simultaneous Analysis of Hydrophilic and Lipophilic Substances. *Journal of Chromatography A* **2018**, *1562*, 96–107. https://doi.org/10.1016/j.chroma.2018.05.055.
(35) Zhou, B.; Xiao, J. F.; Tuli, L.; Ressom, H. W. LC-MS-Based Metabolomics. *Mol. BioSyst.* **2012**, *8* (2), 470–481. https://doi.org/10.1039/C1MB05350G.
(36) Nassar, A. F.; Wu, T.; Nassar, S. F.; Wisnewski, A. V. UPLC–MS for Metabolomics: A Giant Step Forward in Support of Pharmaceutical Research. *Drug Discovery Today* **2017**, *22* (2), 463–470. https://doi.org/10.1016/j.drudis.2016.11.020.
(37) Giddings, J. C. *Unified Separation Science*; Wiley: New York, 1991.
(38) Snyder, L. R.; Kirkland, J. J.; Dolan, J. W. *Introduction to Modern Liquid Chromatography*, 3rd ed.; Wiley: Hoboken, N.J, 2010.
(39) Davis, J. M.; Giddings, J. Calvin. Statistical Theory of Component Overlap in Multicomponent Chromatograms. *Analytical Chemistry* **1983**, *55* (3), 418–424. https://doi.org/10.1021/ac00254a003.
(40) Danne-Rasche, N.; Coman, C.; Ahrends, R. Nano-LC/NSI MS Refines Lipidomics by Enhancing Lipid Coverage, Measurement Sensitivity, and Linear Dynamic Range. *Analytical Chemistry* **2018**, *90* (13), 8093–8101. https://doi.org/10.1021/acs.analchem.8b01275.
(41) Tetko, I. V.; Gasteiger, J.; Todeschini, R.; Mauri, A.; Livingstone, D.; Ertl, P.; Palyulin, V. A.; Radchenko, E. V.; Zefirov, N. S.; Makarenko, A. S.; Tanchuk, V. Yu.; Prokopenko, V. V. Virtual Computational Chemistry Laboratory – Design and Description. *J Comput Aided Mol Des* **2005**, *19* (6), 453–463. https://doi.org/10.1007/s10822-005-8694-y.
(42) Grushka, Elimelech. Chromatographic Peak Capacity and the Factors Influencing It. *Analytical Chemistry* **1970**, *42* (11), 1142–1147. https://doi.org/10.1021/ac60293a001.
(43) van Deemter, J. J.; Zuiderweg, F. J.; Klinkenberg, A. Longitudinal Diffusion and Resistance to Mass Transfer as Causes of Nonideality in Chromatography. *Chemical Engineering Science* **1956**, *5* (6), 271–289. https://doi.org/10.1016/0009-2509(56)80003-1.
(44) J. Calvin, G. *Dynamics of Chromatography Principles and Theory*, 1st ed.; Marcel Dekker Inc., 1965. https://doi.org/10.1201/9781315275871.
(45) Kennedy, G. J.; Knox, J. H. The Performance of Packings in High Performance Liquid Chromatography (HPLC) I. Porous and Surface Layered Supports. *Journal of Chromatographic Science* **1972**, *10* (9), 549–556. https://doi.org/10.1093/chromsci/10.9.549.

(46) Horvath, C.; Lin, H.-J. Movement and Band Spreading of Unsorbed Solutes in Liquid Chromatography. *Journal of Chromatography A* **1976**, *126*, 401–420. https://doi.org/10.1016/S0021-9673(01)84088-7.
(47) Gritti, F.; Guiochon, G. Perspectives on the Evolution of the Column Efficiency in Liquid Chromatography. *Analytical Chemistry* **2013**, *85* (6), 3017–3035. https://doi.org/10.1021/ac3033307.
(48) Gritti, F.; Guiochon, G. The Current Revolution in Column Technology: How It Began, Where Is It Going? *Journal of Chromatography A* **2012**, *1228*, 2–19. https://doi.org/10.1016/j.chroma.2011.07.014.
(49) Jorgenson, J. W. Capillary Liquid Chromatography at Ultrahigh Pressures. *Annual Review of Analytical Chemistry* **2010**, *3* (1), 129–150. https://doi.org/10.1146/annurev.anchem.1.031207.113014.
(50) Blue, L. E.; Franklin, E. G.; Godinho, J. M.; Grinias, J. P.; Grinias, K. M.; Lunn, D. B.; Moore, S. M. Recent Advances in Capillary Ultrahigh Pressure Liquid Chromatography. *Journal of Chromatography A* **2017**, *1523*, 17–39. https://doi.org/10.1016/j.chroma.2017.05.039.
(51) Sorensen, M. J.; Anderson, B. G.; Kennedy, R. T. Liquid Chromatography above 20,000 PSI. *TrAC Trends in Analytical Chemistry* **2020**, *124*, 115810. https://doi.org/10.1016/j.trac.2020.115810.
(52) Desmet, G.; Clicq, D.; Gzil, P. Geometry-Independent Plate Height Representation Methods for the Direct Comparison of the Kinetic Performance of LC Supports with a Different Size or Morphology. *Analytical Chemistry* **2005**, *77* (13), 4058–4070. https://doi.org/10.1021/ac050160z.
(53) Poppe, H. Some Reflections on Speed and Efficiency of Modern Chromatographic Methods. *Journal of Chromatography A* **1997**, *778* (1–2), 3–21. https://doi.org/10.1016/S0021-9673(97)00376-2.
(54) Carr, P. W.; Wang, X.; Stoll, D. R. Effect of Pressure, Particle Size, and Time on Optimizing Performance in Liquid Chromatography. *Analytical Chemistry* **2009**, *81* (13), 5342–5353. https://doi.org/10.1021/ac9001244.
(55) MacNair, J. E.; Lewis, K. C.; Jorgenson, J. W. Ultrahigh-Pressure Reversed-Phase Liquid Chromatography in Packed Capillary Columns. *Analytical Chemistry* **1997**, *69* (6), 983–989. https://doi.org/10.1021/ac961094r.
(56) MacNair, J. E.; Patel, K. D.; Jorgenson, J. W. Ultrahigh-Pressure Reversed-Phase Capillary Liquid Chromatography: Isocratic and Gradient Elution Using Columns Packed with 1.0-Mm Particles. *Analytical Chemistry* **1999**, *71* (3), 700–708. https://doi.org/10.1021/ac9807013.
(57) Wu, N.; Liu, Y.; Lee, M. L. Sub-2μm Porous and Nonporous Particles for Fast Separation in Reversed-Phase High Performance Liquid Chromatography. *Journal of Chromatography A* **2006**, *1131* (1–2), 142–150. https://doi.org/10.1016/j.chroma.2006.07.042.
(58) Mellors, J. S.; Jorgenson, J. W. Use of 1.5-Mm Porous Ethyl-Bridged Hybrid Particles as a Stationary-Phase Support for Reversed-Phase Ultrahigh-Pressure Liquid Chromatography. *Anal. Chem.* **2004**, *76* (18), 5441–5450. https://doi.org/10.1021/ac049643d.
(59) Ismail, O. H.; Catani, M.; Pasti, L.; Cavazzini, A.; Ciogli, A.; Villani, C.; Kotoni, D.; Gasparrini, F.; Bell, D. S. Experimental Evidence of the Kinetic Performance Achievable

with Columns Packed with New 1.9μm Fully Porous Particles of Narrow Particle Size Distribution. *Journal of Chromatography A* **2016**, *1454*, 86–92. https://doi.org/10.1016/j.chroma.2016.05.038.
(60) Reising, A. E.; Godinho, J. M.; Bernzen, J.; Jorgenson, J. W.; Tallarek, U. Axial Heterogeneities in Capillary Ultrahigh Pressure Liquid Chromatography Columns: Chromatographic and Bed Morphological Characterization. *Journal of Chromatography A* **2018**, *1569*, 44–52. https://doi.org/10.1016/j.chroma.2018.07.037.
(61) Reising, A. E.; Godinho, J. M.; Jorgenson, J. W.; Tallarek, U. Bed Morphological Features Associated with an Optimal Slurry Concentration for Reproducible Preparation of Efficient Capillary Ultrahigh Pressure Liquid Chromatography Columns. *Journal of Chromatography A* **2017**, *1504*, 71–82. https://doi.org/10.1016/j.chroma.2017.05.007.
(62) Bruns, S.; Franklin, E. G.; Grinias, J. P.; Godinho, J. M.; Jorgenson, J. W.; Tallarek, U. Slurry Concentration Effects on the Bed Morphology and Separation Efficiency of Capillaries Packed with Sub-2 Mm Particles. *J Chromatogr A* **2013**, *1318*, 189–197.
(63) Godinho, J. M.; Reising, A. E.; Tallarek, U.; Jorgenson, J. W. Implementation of High Slurry Concentration and Sonication to Pack High-Efficiency, Meter-Long Capillary Ultrahigh Pressure Liquid Chromatography Columns. *Journal of Chromatography A* **2016**, *1462*, 165–169. https://doi.org/10.1016/j.chroma.2016.08.002.
(64) Reising, A. E.; Godinho, J. M.; Hormann, K.; Jorgenson, J. W.; Tallarek, U. Larger Voids in Mechanically Stable, Loose Packings of 1.3 Mm Frictional, Cohesive Particles: Their Reconstruction, Statistical Analysis, and Impact on Separation Efficiency. *Journal of Chromatography A* **2016**, *1436*, 118–132. https://doi.org/10.1016/j.chroma.2016.01.068.
(65) Shen, Y.; Zhang, R.; Moore, R. J.; Kim, J.; Metz, T. O.; Hixson, K. K.; Zhao, R.; Livesay, E. A.; Udseth, H. R.; Smith, R. D. Automated 20 Kpsi RPLC-MS and MS/MS with Chromatographic Peak Capacities of 1000−1500 and Capabilities in Proteomics and Metabolomics. *Analytical Chemistry* **2005**, *77* (10), 3090–3100. https://doi.org/10.1021/ac0483062.
(66) Xiang, Y.; Liu, Y.; Stearns, S. D.; Plistil, A.; Brisbin, M. P.; Lee, M. L. Pseudolinear Gradient Ultrahigh-Pressure Liquid Chromatography Using an Injection Valve Assembly. *Analytical Chemistry* **2006**, *78* (3), 858–864. https://doi.org/10.1021/ac058024h.
(67) Grinias, K. M.; Godinho, J. M.; Franklin, E. G.; Stobaugh, J. T.; Jorgenson, J. W. Development of a 45kpsi Ultrahigh Pressure Liquid Chromatography Instrument for Gradient Separations of Peptides Using Long Microcapillary Columns and Sub-2μm Particles. *Journal of Chromatography A* **2016**, *1469*, 60–67. https://doi.org/10.1016/j.chroma.2016.09.053.
(68) De Pauw, R.; Swier, T.; Degreef, B.; Desmet, G.; Broeckhoven, K. On the Feasibility to Conduct Gradient Liquid Chromatography Separations in Narrow-Bore Columns at Pressures up to 2000 Bar. *Journal of Chromatography A* **2016**, *1473*, 48–55. https://doi.org/10.1016/j.chroma.2016.10.008.
(69) Motoyama, A.; Venable, J. D.; Ruse, C. I.; Yates, J. R. Automated Ultra-High-Pressure Multidimensional Protein Identification Technology (UHP-MudPIT) for Improved Peptide Identification of Proteomic Samples. *Analytical Chemistry* **2006**, *78* (14), 5109–5118. https://doi.org/10.1021/ac060354u.

(70) Gritti, F.; Stankovich, J. J.; Guiochon, G. Potential Advantage of Constant Pressure versus Constant Flow Gradient Chromatography for the Analysis of Small Molecules. *Journal of Chromatography A* **2012**, *1263*, 51–60. https://doi.org/10.1016/j.chroma.2012.09.004.
(71) Subramaniam, S.; Fahy, E.; Gupta, S.; Sud, M.; Byrnes, R. W.; Cotter, D.; Dinasarapu, A. R.; Maurya, M. R. Bioinformatics and Systems Biology of the Lipidome. *Chemical Reviews* **2011**, *111* (10), 6452–6490. https://doi.org/10.1021/cr200295k.
(72) Ummarino, D. Lipidomics Refines CVD Risk Prediction: Diabetes. *Nature Reviews Cardiology* **2016**, *13* (12), 697–697. https://doi.org/10.1038/nrcardio.2016.180.
(73) Noh, S. A.; Kim, S.-M.; Park, S. H.; Kim, D.-J.; Lee, J. W.; Kim, Y. G.; Moon, J.-Y.; Lim, S.-J.; Lee, S.-H.; Kim, K. P. Alterations in Lipid Profile of the Aging Kidney Identified by MALDI Imaging Mass Spectrometry. *J. Proteome Res.* **2019**, *18* (7), 2803–2812. https://doi.org/10.1021/acs.jproteome.9b00108.
(74) Rob, N. M. W. Lipid Composition of Cell Membranes and Its Relevance in Type 2 Diabetes Mellitus. *Current Diabetes Reviews* **2012**, *8* (5), 390–400.
(75) Fahy, E.; Subramaniam, S.; Murphy, R. C.; Nishijima, M.; Raetz, C. R. H.; Shimizu, T.; Spener, F.; van Meer, G.; Wakelam, M. J. O.; Dennis, E. A. Update of the LIPID MAPS Comprehensive Classification System for Lipids. *J. Lipid Res.* **2009**, *50 Suppl*, S9-14. https://doi.org/10.1194/jlr.R800095-JLR200.
(76) Jurowski, K.; Kochan, K.; Walczak, J.; Barańska, M.; Piekoszewski, W.; Buszewski, B. Analytical Techniques in Lipidomics: State of the Art. *Critical Reviews in Analytical Chemistry* **2017**, *47* (5), 418–437. https://doi.org/10.1080/10408347.2017.1310613.
(77) Rustam, Y. H.; Reid, G. E. Analytical Challenges and Recent Advances in Mass Spectrometry Based Lipidomics. *Analytical Chemistry* **2018**, *90* (1), 374–397. https://doi.org/10.1021/acs.analchem.7b04836.
(78) Otieno, A. C.; Mwongela, S. M. Capillary Electrophoresis-Based Methods for the Determination of Lipids—A Review. *Analytica Chimica Acta* **2008**, *624* (2), 163–174. https://doi.org/10.1016/j.aca.2008.06.026.
(79) Lísa, M.; Cífková, E.; Khalikova, M.; Ovčačíková, M.; Holčapek, M. Lipidomic Analysis of Biological Samples: Comparison of Liquid Chromatography, Supercritical Fluid Chromatography and Direct Infusion Mass Spectrometry Methods. *Journal of Chromatography A* **2017**, *1525*, 96–108. https://doi.org/10.1016/j.chroma.2017.10.022.
(80) Fuchs, B.; Süß, R.; Teuber, K.; Eibisch, M.; Schiller, J. Lipid Analysis by Thin-Layer Chromatography—A Review of the Current State. *Journal of Chromatography A* **2011**, *1218* (19), 2754–2774. https://doi.org/10.1016/j.chroma.2010.11.066.
(81) t'Kindt, R.; Sandra, P.; Sandra, K. Reversed-Phase Liquid Chromatography Mass Spectrometry (RP-LC-MS) in Lipidomics. In *Encyclopedia of Lipidomics*; Wenk, M. R., Ed.; Springer Netherlands: Dordrecht, 2016; pp 1–16. https://doi.org/10.1007/978-94-007-7864-1_61-1.
(82) Sokol, E.; Almeida, R.; Hannibal-Bach, H. K.; Kotowska, D.; Vogt, J.; Baumgart, J.; Kristiansen, K.; Nitsch, R.; Knudsen, J.; Ejsing, C. S. Profiling of Lipid Species by Normal-Phase Liquid Chromatography, Nanoelectrospray Ionization, and Ion Trap–Orbitrap Mass Spectrometry. *Analytical Biochemistry* **2013**, *443* (1), 88–96. https://doi.org/10.1016/j.ab.2013.08.020.
(83) Schwalbe-Herrmann, M.; Willmann, J.; Leibfritz, D. Separation of Phospholipid Classes by Hydrophilic Interaction Chromatography Detected by Electrospray Ionization Mass

Spectrometry. *Journal of Chromatography A* **2010**, *1217* (32), 5179–5183. https://doi.org/10.1016/j.chroma.2010.05.014.
(84) Cífková, E.; Hájek, R.; Lísa, M.; HolĽapek, M. Hydrophilic Interaction Liquid Chromatography□mass Spectrometry of (Lyso)Phosphatidic Acids, (Lyso)Phosphatidylserines and Other Lipid Classes. *Journal of Chromatography A* **2016**, *1439*, 65–73. https://doi.org/10.1016/j.chroma.2016.01.064.
(85) Ovčačíková, M.; Lísa, M.; Cífková, E.; Holčapek, M. Retention Behavior of Lipids in Reversed-Phase Ultrahigh-Performance Liquid Chromatography–Electrospray Ionization Mass Spectrometry. *Journal of Chromatography A* **2016**, *1450*, 76–85. https://doi.org/10.1016/j.chroma.2016.04.082.
(86) Miller, K. E.; Jorgenson, J. W. Comparison of Microcapillary Column Length and Inner Diameter Investigated with Gradient Analysis of Lipids by Ultrahigh-pressure Liquid Chromatography-mass Spectrometry. *J. Sep. Sci.* **2020**, jssc.202000545. https://doi.org/10.1002/jssc.202000545.
(87) Sorensen, M. J.; Miller, K. E.; Jorgenson, J. W.; Kennedy, R. T. Ultrahigh-Performance Capillary Liquid Chromatography-Mass Spectrometry at 35 Kpsi for Separation of Lipids. *Journal of Chromatography A* **2020**, *1611*, 460575. https://doi.org/10.1016/j.chroma.2019.460575.
(88) Blaženović, I.; Shen, T.; Mehta, S. S.; Kind, T.; Ji, J.; Piparo, M.; Cacciola, F.; Mondello, L.; Fiehn, O. Increasing Compound Identification Rates in Untargeted Lipidomics Research with Liquid Chromatography Drift Time–Ion Mobility Mass Spectrometry. *Analytical Chemistry* **2018**, *90* (18), 10758–10764. https://doi.org/10.1021/acs.analchem.8b01527.
(89) Narváez-Rivas, M.; Vu, N.; Chen, G.-Y.; Zhang, Q. Off-Line Mixed-Mode Liquid Chromatography Coupled with Reversed Phase High Performance Liquid Chromatography-High Resolution Mass Spectrometry to Improve Coverage in Lipidomics Analysis. *Analytica Chimica Acta* **2017**, *954*, 140–150. https://doi.org/10.1016/j.aca.2016.12.003.
(90) Schmidt, A.; Karas, M.; Dulcks, T. Effect of Different Solution Flow Rates on Analyte Ion Signals in Nano-ESI MS, or: When Does ESI Turn into Nano-ESI? *J Am Soc Mass Spectrom* **2003**, *14* (5), 492–500. https://doi.org/10.1016/S1044-0305(03)00128-4.
(91) Liebisch, G.; Vizcaíno, J. A.; Köfeler, H.; Trötzmüller, M.; Griffiths, W. J.; Schmitz, G.; Spener, F.; Wakelam, M. J. O. Shorthand Notation for Lipid Structures Derived from Mass Spectrometry. *Journal of Lipid Research* **2013**, *54* (6), 1523–1530. https://doi.org/10.1194/jlr.M033506.
(92) Bligh, E. G.; Dyer, W. J. A RAPID METHOD OF TOTAL LIPID EXTRACTION AND PURIFICATION. *Canadian Journal of Biochemistry and Physiology* **1959**, *37* (8), 911–917. https://doi.org/10.1139/o59-099.
(93) Maiolica, A.; Borsotti, D.; Rappsilber, J. Self-Made Frits for Nanoscale Columns in Proteomics. *PROTEOMICS* **2005**, *5* (15), 3847–3850. https://doi.org/10.1002/pmic.200402010.
(94) Cajka, T.; Fiehn, O. LC–MS-Based Lipidomics and Automated Identification of Lipids Using the LipidBlast In-Silico MS/MS Library. In *Lipidomics*; Bhattacharya, S. K., Ed.; Springer New York: New York, NY, 2017; Vol. 1609, pp 149–170. https://doi.org/10.1007/978-1-4939-6996-8_14.

(95) Wang, X.; Stoll, D. R.; Schellinger, A. P.; Carr, P. W. Peak Capacity Optimization of Peptide Separations in Reversed-Phase Gradient Elution Chromatography: Fixed Column Format. *Analytical Chemistry* **2006**, *78* (10), 3406–3416. https://doi.org/10.1021/ac0600149.
(96) McGuffin, V. L.; Evans, C. E. Influence of Pressure on Solute Retention in Liquid Chromatography. *Journal of Microcolumn Separations* **1991**, *3* (6), 513–520. https://doi.org/10.1002/mcs.1220030606.
(97) Sandra, K.; Pereira, A. dos S.; Vanhoenacker, G.; David, F.; Sandra, P. Comprehensive Blood Plasma Lipidomics by Liquid Chromatography/Quadrupole Time-of-Flight Mass Spectrometry. *Journal of Chromatography A* **2010**, *1217* (25), 4087–4099. https://doi.org/10.1016/j.chroma.2010.02.039.
(98) Eghbali, H.; Sandra, K.; Detobel, F.; Lynen, F.; Nakanishi, K.; Sandra, P.; Desmet, G. Performance Evaluation of Long Monolithic Silica Capillary Columns in Gradient Liquid Chromatography Using Peptide Mixtures. *Journal of Chromatography A* **2011**, *1218* (21), 3360–3366. https://doi.org/10.1016/j.chroma.2010.10.045.
(99) Neue, U. D. Theory of Peak Capacity in Gradient Elution. *Journal of Chromatography A* **2005**, *1079* (1–2), 153–161. https://doi.org/10.1016/j.chroma.2005.03.008.
(100) Shishkova, E.; Hebert, A. S.; Westphall, M. S.; Coon, J. J. Ultra-High Pressure (>30,000 Psi) Packing of Capillary Columns Enhancing Depth of Shotgun Proteomic Analyses. *Analytical Chemistry* **2018**, *90* (19), 11503–11508. https://doi.org/10.1021/acs.analchem.8b02766.
(101) Köcher, T.; Swart, R.; Mechtler, K. Ultra-High-Pressure RPLC Hyphenated to an LTQ-Orbitrap Velos Reveals a Linear Relation between Peak Capacity and Number of Identified Peptides. *Analytical Chemistry* **2011**, *83* (7), 2699–2704. https://doi.org/10.1021/ac103243t.
(102) Poad, B. L. J.; Zheng, X.; Mitchell, T. W.; Smith, R. D.; Baker, E. S.; Blanksby, S. J. Online Ozonolysis Combined with Ion Mobility-Mass Spectrometry Provides a New Platform for Lipid Isomer Analyses. *Analytical Chemistry* **2018**, *90* (2), 1292–1300. https://doi.org/10.1021/acs.analchem.7b04091.
(103) Bird, S. S.; Marur, V. R.; Stavrovskaya, I. G.; Kristal, B. S. Separation of Cis–Trans Phospholipid Isomers Using Reversed Phase LC with High Resolution MS Detection. *Analytical Chemistry* **2012**, *84* (13), 5509–5517. https://doi.org/10.1021/ac300953j.
(104) Ståhlman, M.; Pham, H. T.; Adiels, M.; Mitchell, T. W.; Blanksby, S. J.; Fagerberg, B.; Ekroos, K.; Borén, J. Clinical Dyslipidaemia Is Associated with Changes in the Lipid Composition and Inflammatory Properties of Apolipoprotein-B-Containing Lipoproteins from Women with Type 2 Diabetes. *Diabetologia* **2012**, *55* (4), 1156–1166. https://doi.org/10.1007/s00125-011-2444-6.
(105) Baba, T.; Campbell, J. L.; Le Blanc, J. C. Y.; Baker, P. R. S. Structural Identification of Triacylglycerol Isomers Using Electron Impact Excitation of Ions from Organics (EIEIO). *J Lipid Res* **2016**, *57* (11), 2015–2027. https://doi.org/10.1194/jlr.M070177.
(106) Avela, H. F.; Sirén, H. Advances in Lipidomics. *Clinica Chimica Acta* **2020**, *510*, 123–141. https://doi.org/10.1016/j.cca.2020.06.049.
(107) Lee, H.-C.; Yokomizo, T. Applications of Mass Spectrometry-Based Targeted and Non-Targeted Lipidomics. *Biochemical and Biophysical Research Communications* **2018**, *504* (3), 576–581. https://doi.org/10.1016/j.bbrc.2018.03.081.

(108) Kruve, A. Strategies for Drawing Quantitative Conclusions from Nontargeted Liquid Chromatography–High-Resolution Mass Spectrometry Analysis. *Anal. Chem.* **2020**, *92* (7), 4691–4699. https://doi.org/10.1021/acs.analchem.9b03481.
(109) Tumanov, S.; Kamphorst, J. J. Recent Advances in Expanding the Coverage of the Lipidome. *Current Opinion in Biotechnology* **2017**, *43*, 127–133. https://doi.org/10.1016/j.copbio.2016.11.008.
(110) Rustam, Y. H.; Reid, G. E. Analytical Challenges and Recent Advances in Mass Spectrometry Based Lipidomics. *Analytical Chemistry* **2018**, *90* (1), 374–397. https://doi.org/10.1021/acs.analchem.7b04836.
(111) Giddings, J. C. Concepts and Comparisons in Multidimensional Separation. *J. High Resol. Chromatogr.* **1987**, *10* (5), 319–323. https://doi.org/10.1002/jhrc.1240100517.
(112) Giddings, J. C. Two-Dimensional Separations: Concept and Promise. *Anal. Chem.* **1984**, *56* (12), 1258A-1270A. https://doi.org/10.1021/ac00276a003.
(113) Lísa, M.; Cífková, E.; Holčapek, M. Lipidomic Profiling of Biological Tissues Using Off-Line Two-Dimensional High-Performance Liquid Chromatography–Mass Spectrometry. *Journal of Chromatography A* **2011**, *1218* (31), 5146–5156. https://doi.org/10.1016/j.chroma.2011.05.081.
(114) Baglai, A.; Gargano, A. F. G.; Jordens, J.; Mengerink, Y.; Honing, M.; van der Wal, S.; Schoenmakers, P. J. Comprehensive Lipidomic Analysis of Human Plasma Using Multidimensional Liquid- and Gas-Phase Separations: Two-Dimensional Liquid Chromatography–Mass Spectrometry vs . Liquid Chromatography–Trapped-Ion-Mobility–Mass Spectrometry. *Journal of Chromatography A* **2017**, *1530*, 90–103. https://doi.org/10.1016/j.chroma.2017.11.014.
(115) Dugo, P.; Fawzy, N.; Cichello, F.; Cacciola, F.; Donato, P.; Mondello, L. Stop-Flow Comprehensive Two-Dimensional Liquid Chromatography Combined with Mass Spectrometric Detection for Phospholipid Analysis. *Journal of Chromatography A* **2013**, *1278*, 46–53. https://doi.org/10.1016/j.chroma.2012.12.042.
(116) Bang, D. Y.; Moon, M. H. On-Line Two-Dimensional Capillary Strong Anion Exchange/Reversed Phase Liquid Chromatography–Tandem Mass Spectrometry for Comprehensive Lipid Analysis. *Journal of Chromatography A* **2013**, *1310*, 82–90. https://doi.org/10.1016/j.chroma.2013.08.069.
(117) Lv, W.; Shi, X.; Wang, S.; Xu, G. Multidimensional Liquid Chromatography-Mass Spectrometry for Metabolomic and Lipidomic Analyses. *TrAC Trends in Analytical Chemistry* **2019**, *120*, 115302. https://doi.org/10.1016/j.trac.2018.11.001.
(118) Kalili, K. M.; de Villiers, A. Systematic Optimisation and Evaluation of On-Line, off-Line and Stop-Flow Comprehensive Hydrophilic Interaction Chromatography×reversed Phase Liquid Chromatographic Analysis of Procyanidins, Part I: Theoretical Considerations. *Journal of Chromatography A* **2013**, *1289*, 58–68. https://doi.org/10.1016/j.chroma.2013.03.008.
(119) Guiochon, G.; Marchetti, N.; Mriziq, K.; Shalliker, R. A. Implementations of Two-Dimensional Liquid Chromatography. *Journal of Chromatography A* **2008**, *1189* (1–2), 109–168. https://doi.org/10.1016/j.chroma.2008.01.086.
(120) Stoll, D. R.; Carr, P. W. Two-Dimensional Liquid Chromatography: A State of the Art Tutorial. *Anal. Chem.* **2017**, *89* (1), 519–531. https://doi.org/10.1021/acs.analchem.6b03506.

(121) Pirok, B. W. J.; Stoll, D. R.; Schoenmakers, P. J. Recent Developments in Two-Dimensional Liquid Chromatography: Fundamental Improvements for Practical Applications. *Anal. Chem.* **2019**, *91* (1), 240–263. https://doi.org/10.1021/acs.analchem.8b04841.
(122) Schoenmakers, P. J.; Pirok, B. W. J. Practical Approaches to Overcome the Challenges of Comprehensive Two-Dimensional Liquid Chromatography. *LCGC Eurpoe* **2018**, *31* (5), 242–249.
(123) Holčapek, M.; Ovčačíková, M.; Lísa, M.; Cífková, E.; Hájek, T. Continuous Comprehensive Two-Dimensional Liquid Chromatography–Electrospray Ionization Mass Spectrometry of Complex Lipidomic Samples. *Analytical and Bioanalytical Chemistry* **2015**, *407* (17), 5033–5043. https://doi.org/10.1007/s00216-015-8528-2.
(124) Navarro-Reig, M.; Jaumot, J.; Tauler, R. An Untargeted Lipidomic Strategy Combining Comprehensive Two-Dimensional Liquid Chromatography and Chemometric Analysis. *Journal of Chromatography A* **2018**, *1568*, 80–90. https://doi.org/10.1016/j.chroma.2018.07.017.
(125) Li, M.; Tong, X.; Lv, P.; Feng, B.; Yang, L.; Wu, Z.; Cui, X.; Bai, Y.; Huang, Y.; Liu, H. A Not-Stop-Flow Online Normal-/Reversed-Phase Two-Dimensional Liquid Chromatography–Quadrupole Time-of-Flight Mass Spectrometry Method for Comprehensive Lipid Profiling of Human Plasma from Atherosclerosis Patients. *Journal of Chromatography A* **2014**, *1372*, 110–119. https://doi.org/10.1016/j.chroma.2014.10.094.
(126) Nie, H.; Liu, R.; Yang, Y.; Bai, Y.; Guan, Y.; Qian, D.; Wang, T.; Liu, H. Lipid Profiling of Rat Peritoneal Surface Layers by Online Normal- and Reversed-Phase 2D LC QToF-MS[S]. *Journal of Lipid Research* **2010**, *51* (9), 2833–2844. https://doi.org/10.1194/jlr.D007567.
(127) Wolters, D. A.; Washburn, M. P.; Yates, J. R. An Automated Multidimensional Protein Identification Technology for Shotgun Proteomics. *Anal. Chem.* **2001**, *73* (23), 5683–5690. https://doi.org/10.1021/ac010617e.
(128) Wang, S.; Li, J.; Shi, X.; Qiao, L.; Lu, X.; Xu, G. A Novel Stop-Flow Two-Dimensional Liquid Chromatography–Mass Spectrometry Method for Lipid Analysis. *Journal of Chromatography A* **2013**, *1321*, 65–72. https://doi.org/10.1016/j.chroma.2013.10.069.
(129) Danne-Rasche, N.; Rubenzucker, S.; Ahrends, R. Uncovering the Complexity of the Yeast Lipidome by Means of NLC/NSI-MS/MS. *Analytica Chimica Acta* **2020**, *1140*, 199–209. https://doi.org/10.1016/j.aca.2020.10.012.
(130) Zardini Buzatto, A.; Kwon, B. K.; Li, L. Development of a NanoLC-MS Workflow for High-Sensitivity Global Lipidomic Analysis. *Analytica Chimica Acta* **2020**, *1139*, 88–99. https://doi.org/10.1016/j.aca.2020.09.001.
(131) Byeon, S. K.; Lee, J. Y.; Moon, M. H. Optimized Extraction of Phospholipids and Lysophospholipids for Nanoflow Liquid Chromatography-Electrospray Ionization-Tandem Mass Spectrometry. *Analyst* **2012**, *137* (2), 451–458. https://doi.org/10.1039/c1an15920h.
(132) Sanders, K. L.; Edwards, J. L. Nano-Liquid Chromatography-Mass Spectrometry and Recent Applications in Omics Investigations. *Anal. Methods* **2020**, *12* (36), 4404–4417. https://doi.org/10.1039/D0AY01194K.

(133) Duncan, K. D.; Fyrestam, J.; Lanekoff, I. Advances in Mass Spectrometry Based Single-Cell Metabolomics. *Analyst* **2019**, *144* (3), 782–793. https://doi.org/10.1039/C8AN01581C.
(134) Stadlmann, J.; Hudecz, O.; Krššáková, G.; Ctortecka, C.; Van Raemdonck, G.; Op De Beeck, J.; Desmet, G.; Penninger, J. M.; Jacobs, P.; Mechtler, K. Improved Sensitivity in Low-Input Proteomics Using Micropillar Array-Based Chromatography. *Anal. Chem.* **2019**, *91* (22), 14203–14207. https://doi.org/10.1021/acs.analchem.9b02899.
(135) Cong, Y.; Motamedchaboki, K.; Misal, S. A.; Liang, Y.; Guise, A. J.; Truong, T.; Huguet, R.; Plowey, E. D.; Zhu, Y.; Lopez-Ferrer, D.; Kelly, R. T. Ultrasensitive Single-Cell Proteomics Workflow Identifies >1000 Protein Groups per Mammalian Cell. *Chem. Sci.* **2021**, 10.1039.D0SC03636F. https://doi.org/10.1039/D0SC03636F.
(136) Kelly, R. T. Single-Cell Proteomics: Progress and Prospects. *Mol Cell Proteomics* **2020**, *19* (11), 1739–1748. https://doi.org/10.1074/mcp.R120.002234.
(137) Broeckhoven, K.; Desmet, G. Advances and Challenges in Extremely High-Pressure Liquid Chromatography in Current and Future Analytical Scale Column Formats. *Anal. Chem.* **2020**, *92* (1), 554–560. https://doi.org/10.1021/acs.analchem.9b04278.
(138) Sandra, K.; Vandenbussche, J.; t'Kindt, R.; Claerebout, B.; Op de Beeck, J.; De Malsche, W.; Desmet, G.; Sandra, P. Evaluation of Micro-Pillar Array Columns (MPAC) Combined with High Resolution Mass Spectrometry for Lipidomics. *LCGC* **2017**, *30* (6), 6–13.
(139) Wang, Z.; Yu, D.; Cupp-Sutton, K. A.; Liu, X.; Smith, K.; Wu, S. Development of an Online 2D Ultrahigh-Pressure Nano-LC System for High-PH and Low-PH Reversed Phase Separation in Top-Down Proteomics. *Anal. Chem.* **2020**, *92* (19), 12774–12777. https://doi.org/10.1021/acs.analchem.0c03395.
(140) Yu, D.; Wang, Z.; Cupp-Sutton, K. A.; Liu, X.; Wu, S. Deep Intact Proteoform Characterization in Human Cell Lysate Using High-PH and Low-PH Reversed-Phase Liquid Chromatography. *J. Am. Soc. Mass Spectrom.* **2019**, *30* (12), 2502–2513. https://doi.org/10.1007/s13361-019-02315-2.
(141) Dou, M.; Tsai, C.-F.; Piehowski, P. D.; Wang, Y.; Fillmore, T. L.; Zhao, R.; Moore, R. J.; Zhang, P.; Qian, W.-J.; Smith, R. D.; Liu, T.; Kelly, R. T.; Shi, T.; Zhu, Y. Automated Nanoflow Two-Dimensional Reversed-Phase Liquid Chromatography System Enables In-Depth Proteome and Phosphoproteome Profiling of Nanoscale Samples. *Anal. Chem.* **2019**, *91* (15), 9707–9715. https://doi.org/10.1021/acs.analchem.9b01248.
(142) Cífková, E.; Holčapek, M.; Lísa, M.; Ovčačíková, M.; Lyčka, A.; Lynen, F.; Sandra, P. Nontargeted Quantitation of Lipid Classes Using Hydrophilic Interaction Liquid Chromatography–Electrospray Ionization Mass Spectrometry with Single Internal Standard and Response Factor Approach. *Analytical Chemistry* **2012**, *84* (22), 10064–10070. https://doi.org/10.1021/ac3024476.
(143) Godinho, J. M.; Reising, A. E.; Tallarek, U.; Jorgenson, J. W. Implementation of High Slurry Concentration and Sonication to Pack High-Efficiency, Meter-Long Capillary Ultrahigh Pressure Liquid Chromatography Columns. *Journal of Chromatography A* **2016**, *1462*, 165–169. https://doi.org/10.1016/j.chroma.2016.08.002.
(144) Grinias, K. M.; Godinho, J. M.; Franklin, E. G.; Stobaugh, J. T.; Jorgenson, J. W. Development of a 45kpsi Ultrahigh Pressure Liquid Chromatography Instrument for Gradient Separations of Peptides Using Long Microcapillary Columns and Sub-2μm

Particles. *Journal of Chromatography A* **2016**, *1469*, 60–67. https://doi.org/10.1016/j.chroma.2016.09.053.
(145) Gilar, M.; Olivova, P.; Daly, A. E.; Gebler, J. C. Orthogonality of Separation in Two-Dimensional Liquid Chromatography. *Anal. Chem.* **2005**, *77* (19), 6426–6434. https://doi.org/10.1021/ac050923i.
(146) Gilar, M.; Fridrich, J.; Schure, M. R.; Jaworski, A. Comparison of Orthogonality Estimation Methods for the Two-Dimensional Separations of Peptides. *Anal. Chem.* **2012**, *84* (20), 8722–8732. https://doi.org/10.1021/ac3020214.
(147) Liu, Zaiyou.; Patterson, D. G.; Lee, M. L. Geometric Approach to Factor Analysis for the Estimation of Orthogonality and Practical Peak Capacity in Comprehensive Two-Dimensional Separations. *Anal. Chem.* **1995**, *67* (21), 3840–3845. https://doi.org/10.1021/ac00117a004.
(148) Camenzuli, M.; Schoenmakers, P. J. A New Measure of Orthogonality for Multi-Dimensional Chromatography. *Analytica Chimica Acta* **2014**, *838*, 93–101. https://doi.org/10.1016/j.aca.2014.05.048.
(149) Davis, J. M.; Stoll, D. R.; Carr, P. W. Effect of First-Dimension Undersampling on Effective Peak Capacity in Comprehensive Two-Dimensional Separations. *Analytical Chemistry* **2008**, *80* (2), 461–473. https://doi.org/10.1021/ac071504j.
(150) Nowik, W.; Héron, S.; Bonose, M.; Nowik, M.; Tchapla, A. Assessment of Two-Dimensional Separative Systems Using Nearest-Neighbor Distances Approach. Part 1: Orthogonality Aspects. *Anal. Chem.* **2013**, *85* (20), 9449–9458. https://doi.org/10.1021/ac4012705.
(151) Gertner, D. S.; Bishop, D. P.; Oglobline, A.; Padula, M. P. Enhancing Coverage of Phosphatidylinositol Species in Canola Through Specialised Liquid Chromatography-Mass Spectrometry Buffer Conditions. *Journal of Chromatography A* **2021**, *1637*, 461860. https://doi.org/10.1016/j.chroma.2020.461860.
(152) Baca, M.; Desmet, G.; Ottevaere, H.; De Malsche, W. Achieving a Peak Capacity of 1800 Using an 8 m Long Pillar Array Column. *Anal. Chem.* **2019**, *91* (17), 10932–10936. https://doi.org/10.1021/acs.analchem.9b02236.
(153) Chapel, S.; Rouvière, F.; Heinisch, S. Pushing the Limits of Resolving Power and Analysis Time in On-Line Comprehensive Hydrophilic Interaction x Reversed Phase Liquid Chromatography for the Analysis of Complex Peptide Samples. *Journal of Chromatography A* **2020**, *1615*, 460753. https://doi.org/10.1016/j.chroma.2019.460753.
(154) Stoll, D. R.; Lhotka, H. R.; Harmes, D. C.; Madigan, B.; Hsiao, J. J.; Staples, G. O. High Resolution Two-Dimensional Liquid Chromatography Coupled with Mass Spectrometry for Robust and Sensitive Characterization of Therapeutic Antibodies at the Peptide Level. *Journal of Chromatography B* **2019**, *1134–1135*, 121832. https://doi.org/10.1016/j.jchromb.2019.121832.
(155) Gray, N.; Lewis, M. R.; Plumb, R. S.; Wilson, I. D.; Nicholson, J. K. High-Throughput Microbore UPLC–MS Metabolic Phenotyping of Urine for Large-Scale Epidemiology Studies. *J. Proteome Res.* **2015**, *14* (6), 2714–2721. https://doi.org/10.1021/acs.jproteome.5b00203.
(156) Gray, N.; Adesina-Georgiadis, K.; Chekmeneva, E.; Plumb, R. S.; Wilson, I. D.; Nicholson, J. K. Development of a Rapid Microbore Metabolic Profiling Ultraperformance Liquid Chromatography–Mass Spectrometry Approach for High-

Throughput Phenotyping Studies. *Anal. Chem.* **2016**, *88* (11), 5742–5751. https://doi.org/10.1021/acs.analchem.6b00038.
(157) Shen, Y.; Tolić, N.; Piehowski, P. D.; Shukla, A. K.; Kim, S.; Zhao, R.; Qu, Y.; Robinson, E.; Smith, R. D.; Paša-Tolić, L. High-Resolution Ultrahigh-Pressure Long Column Reversed-Phase Liquid Chromatography for Top-down Proteomics. *Journal of Chromatography A* **2017**, *1498*, 99–110. https://doi.org/10.1016/j.chroma.2017.01.008.
(158) Shen, Y.; Smith, R. D.; Unger, K. K.; Kumar, D.; Lubda, D. Ultrahigh-Throughput Proteomics Using Fast RPLC Separations with ESI-MS/MS. *Anal. Chem.* **2005**, *77* (20), 6692–6701. https://doi.org/10.1021/ac050876u.
(159) Shen, Y.; Strittmatter, E. F.; Zhang, R.; Metz, T. O.; Moore, R. J.; Li, F.; Udseth, H. R.; Smith, R. D.; Unger, K. K.; Kumar, D.; Lubda, D. Making Broad Proteome Protein Measurements in 1−5 Min Using High-Speed RPLC Separations and High-Accuracy Mass Measurements. *Anal. Chem.* **2005**, *77* (23), 7763–7773. https://doi.org/10.1021/ac051257o.
(160) Rogers, B. A.; Wu, Z.; Wei, B.; Zhang, X.; Cao, X.; Alabi, O.; Wirth, M. J. Submicrometer Particles and Slip Flow in Liquid Chromatography. *Analytical Chemistry* **2015**, *87* (5), 2520–2526. https://doi.org/10.1021/ac504683d.
(161) Cintrón, J. M.; Colón, L. A. Organo-Silica Nano-Particles Used in Ultrahigh-Pressure Liquid Chromatography. *The Analyst* **2002**, *127* (6), 701–704. https://doi.org/10.1039/b203236h.
(162) Xiang, Y.; Yan, B.; McNeff, C. V.; Carr, P. W.; Lee, M. L. Synthesis of Micron Diameter Polybutadiene-Encapsulated Non-Porous Zirconia Particles for Ultrahigh Pressure Liquid Chromatography. *Journal of Chromatography A* **2003**, *1002* (1–2), 71–78. https://doi.org/10.1016/S0021-9673(03)00733-7.
(163) El-Faramawy, A.; Siu, K. W. M.; Thomson, B. A. Efficiency of Nano-Electrospray Ionization. *J Am Soc Mass Spectrom* **2005**, *16* (10), 1702–1707. https://doi.org/10.1016/j.jasms.2005.06.011.
(164) Šesták, J.; Moravcová, D.; Kahle, V. Instrument Platforms for Nano Liquid Chromatography. *Journal of Chromatography A* **2015**, *1421*, 2–17.
(165) Chetwynd, A. J.; David, A. A Review of Nanoscale LC-ESI for Metabolomics and Its Potential to Enhance the Metabolome Coverage. *Talanta* **2018**, *182*, 380–390. https://doi.org/10.1016/j.talanta.2018.01.084.
(166) Yi, L.; Piehowski, P. D.; Shi, T.; Smith, R. D.; Qian, W.-J. Advances in Microscale Separations towards Nanoproteomics Applications. *Journal of Chromatography A* **2017**, *1523*, 40–48. https://doi.org/10.1016/j.chroma.2017.07.055.
(167) Wong, J.-M. T.; Malec, P. A.; Mabrouk, O. S.; Ro, J.; Dus, M.; Kennedy, R. T. Benzoyl Chloride Derivatization with Liquid Chromatography–Mass Spectrometry for Targeted Metabolomics of Neurochemicals in Biological Samples. *Journal of Chromatography A* **2016**, *1446*, 78–90. https://doi.org/10.1016/j.chroma.2016.04.006.
(168) Zhou, R.; Guo, K.; Li, L. 5-Diethylamino-Naphthalene-1-Sulfonyl Chloride (DensCl): A Novel Triplex Isotope Labeling Reagent for Quantitative Metabolome Analysis by Liquid Chromatography Mass Spectrometry. *Analytical Chemistry* **2013**, *85* (23), 11532–11539. https://doi.org/10.1021/ac403000n.
(169) Zhou, R.; Huan, T.; Li, L. Development of Versatile Isotopic Labeling Reagents for Profiling the Amine Submetabolome by Liquid Chromatography–Mass Spectrometry. *Analytica Chimica Acta* **2015**, *881*, 107–116. https://doi.org/10.1016/j.aca.2015.04.021.

(170) Grinias, J. P.; Wong, J.-M. T.; Kennedy, R. T. Repeatability of Gradient Ultrahigh Pressure Liquid Chromatography–Tandem Mass Spectrometry Methods in Instrument-Controlled Thermal Environments. *Journal of Chromatography A* **2016**, *1461*, 42–50. https://doi.org/10.1016/j.chroma.2016.07.043.
(171) Viklund, C.; Pontén, E.; Glad, B.; Irgum, K.; Hörstedt, P.; Svec, F. "Molded" Macroporous Poly(Glycidyl Methacrylate- *Co* -Trimethylolpropane Trimethacrylate) Materials with Fine Controlled Porous Properties: Preparation of Monoliths Using Photoinitiated Polymerization. *Chem. Mater.* **1997**, *9* (2), 463–471. https://doi.org/10.1021/cm9603011.
(172) Wahab, M. F.; Patel, D. C.; Wimalasinghe, R. M.; Armstrong, D. W. Fundamental and Practical Insights on the Packing of Modern High-Efficiency Analytical and Capillary Columns. *Analytical Chemistry* **2017**, *89* (16), 8177–8191. https://doi.org/10.1021/acs.analchem.7b00931.
(173) Treadway, J. W.; Wyndham, K. D.; Jorgenson, J. W. Highly Efficient Capillary Columns Packed with Superficially Porous Particles via Sequential Column Packing. *Journal of Chromatography A* **2015**, *1422*, 345–349. https://doi.org/10.1016/j.chroma.2015.10.013.
(174) Song, P.; Mabrouk, O. S.; Hershey, N. D.; Kennedy, R. T. In Vivo Neurochemical Monitoring Using Benzoyl Chloride Derivatization and Liquid Chromatography–Mass Spectrometry. *Analytical Chemistry* **2012**, *84* (1), 412–419. https://doi.org/10.1021/ac202794q.
(175) Grinias, J. P.; Wong, J.-M. T.; Nesbitt, K. M. Using Benzoyl Chloride Derivatization to Improve Small-Molecule Analysis in Biological Samples by LC–MS/MS. *LCGC* **2017**, *35* (10), 760768.
(176) DeStefano, J. J.; Langlois, T. J.; Kirkland, J. J. Characteristics of Superficially-Porous Silica Particles for Fast HPLC: Some Performance Comparisons with Sub-2- m Particles. *Journal of Chromatographic Science* **2008**, *46* (3), 254–260. https://doi.org/10.1093/chromsci/46.3.254.
(177) Bruns, S.; Stoeckel, D.; Smarsly, B. M.; Tallarek, U. Influence of Particle Properties on the Wall Region in Packed Capillaries. *Journal of Chromatography A* **2012**, *1268*, 53–63. https://doi.org/10.1016/j.chroma.2012.10.027.
(178) Cabooter, D.; Fanigliulo, A.; Bellazzi, G.; Allieri, B.; Rottigni, A.; Desmet, G. Relationship between the Particle Size Distribution of Commercial Fully Porous and Superficially Porous High-Performance Liquid Chromatography Column Packings and Their Chromatographic Performance. *Journal of Chromatography A* **2010**, *1217* (45), 7074–7081. https://doi.org/10.1016/j.chroma.2010.09.008.
(179) Rodriguez-Aller, M.; Gurny, R.; Veuthey, J.-L.; Guillarme, D. Coupling Ultra High-Pressure Liquid Chromatography with Mass Spectrometry: Constraints and Possible Applications. *Journal of Chromatography A* **2013**, *1292*, 2–18. https://doi.org/10.1016/j.chroma.2012.09.061.
(180) Barhate, C. L.; Wahab, M. F.; Tognarelli, D. J.; Berger, T. A.; Armstrong, D. W. Instrumental Idiosyncrasies Affecting the Performance of Ultrafast Chiral and Achiral Sub/Supercritical Fluid Chromatography. *Anal. Chem.* **2016**, *88* (17), 8664–8672. https://doi.org/10.1021/acs.analchem.6b01898.
(181) Wahab, M. F.; Dasgupta, P. K.; Kadjo, A. F.; Armstrong, D. W. Sampling Frequency, Response Times and Embedded Signal Filtration in Fast, High Efficiency Liquid

Chromatography: A Tutorial. *Analytica Chimica Acta* **2016**, *907*, 31–44. https://doi.org/10.1016/j.aca.2015.11.043.
(182) Desmet, G.; de Beeck, J. O.; Van Raemdonck, G.; Van Mol, K.; Claerebout, B.; Van Landuyt, N.; Jacobs, P. Separation Efficiency Kinetics of Capillary Flow Micro-Pillar Array Columns for Liquid Chromatography. *Journal of Chromatography A* **2020**, *1626*, 461279. https://doi.org/10.1016/j.chroma.2020.461279.
(183) Patel, K. D.; Jerkovich, A. D.; Link, J. C.; Jorgenson, J. W. In-Depth Characterization of Slurry Packed Capillary Columns with 1.0-Mm Nonporous Particles Using Reversed-Phase Isocratic Ultrahigh-Pressure Liquid Chromatography. *Anal. Chem.* **2004**, *76* (19), 5777–5786. https://doi.org/10.1021/ac049756x.
(184) Haskins, W. E.; Wang, Z.; Watson, C. J.; Rostand, R. R.; Witowski, S. R.; Powell, D. H.; Kennedy, R. T. Capillary LC−MS ^{2} at the Attomole Level for Monitoring and Discovering Endogenous Peptides in Microdialysis Samples Collected in Vivo. *Anal. Chem.* **2001**, *73* (21), 5005–5014. https://doi.org/10.1021/ac010774d.
(185) Fernández-Pumarega, A.; Dores-Sousa, J. L.; Eeltink, S. A Comprehensive Investigation of the Peak Capacity for the Reversed-Phase Gradient Liquid-Chromatographic Analysis of Intact Proteins Using a Polymer-Monolithic Capillary Column. *Journal of Chromatography A* **2019**, 460462. https://doi.org/10.1016/j.chroma.2019.460462.
(186) Fairchild, J. N.; Walworth, M. J.; Horváth, K.; Guiochon, G. Correlation between Peak Capacity and Protein Sequence Coverage in Proteomics Analysis by Liquid Chromatography-Mass Spectrometry/Mass Spectrometry. *Journal of Chromatography A* **2010**, *1217* (29), 4779–4783. https://doi.org/10.1016/j.chroma.2010.05.015.
(187) Mahieu, N. G.; Patti, G. J. Systems-Level Annotation of a Metabolomics Data Set Reduces 25 000 Features to Fewer than 1000 Unique Metabolites. *Anal. Chem.* **2017**, *89* (19), 10397–10406. https://doi.org/10.1021/acs.analchem.7b02380.
(188) Shen, Y.; Zhao, R.; Berger, S. J.; Anderson, G. A.; Rodriguez, N.; Smith, R. D. High-Efficiency Nanoscale Liquid Chromatography Coupled On-Line with Mass Spectrometry Using Nanoelectrospray Ionization for Proteomics. *Anal. Chem.* **2002**, *74* (16), 4235–4249. https://doi.org/10.1021/ac0202280.
(189) Lanckmans, K.; Van Eeckhaut, A.; Sarre, S.; Smolders, I.; Michotte, Y. Capillary and Nano-Liquid Chromatography–Tandem Mass Spectrometry for the Quantification of Small Molecules in Microdialysis Samples: Comparison with Microbore Dimensions. *Journal of Chromatography A* **2006**, *1131* (1–2), 166–175. https://doi.org/10.1016/j.chroma.2006.07.090.
(190) Edwards, J. L.; Edwards, R. L.; Reid, K. R.; Kennedy, R. T. Effect of Decreasing Column Inner Diameter and Use of Off-Line Two-Dimensional Chromatography on Metabolite Detection in Complex Mixtures. *Journal of Chromatography A* **2007**, *1172* (2), 127–134. https://doi.org/10.1016/j.chroma.2007.09.075.
(191) Wilson, R. E.; Groskreutz, S. R.; Weber, S. G. Improving the Sensitivity, Resolution, and Peak Capacity of Gradient Elution in Capillary Liquid Chromatography with Large-Volume Injections by Using Temperature-Assisted On-Column Solute Focusing. *Anal. Chem.* **2016**, *88* (10), 5112–5121. https://doi.org/10.1021/acs.analchem.5b04793.
(192) Mills, M. J.; Maltas, J.; John Lough, W. Assessment of Injection Volume Limits When Using On-Column Focusing with Microbore Liquid Chromatography. *Journal of Chromatography A* **1997**, *759* (1–2), 1–11. https://doi.org/10.1016/S0021-9673(96)00753-4.

(193) Zhong, Q.; Shen, L.; Liu, J.; Yu, D.; Li, S.; Yao, J.; Zhan, S.; Huang, T.; Hashi, Y.; Kawano, S.; Liu, Z.; Zhou, T. Pre-Column Dilution Large Volume Injection Ultra-High Performance Liquid Chromatography-Tandem Mass Spectrometry for the Analysis of Multi-Class Pesticides in Cabbages. *Journal of Chromatography A* **2016**, *1442*, 53–61. https://doi.org/10.1016/j.chroma.2016.03.010.

(194) Dunn, W. B.; Erban, A.; Weber, R. J. M.; Creek, D. J.; Brown, M.; Breitling, R.; Hankemeier, T.; Goodacre, R.; Neumann, S.; Kopka, J.; Viant, M. R. Mass Appeal: Metabolite Identification in Mass Spectrometry-Focused Untargeted Metabolomics. *Metabolomics* **2013**, *9* (S1), 44–66. https://doi.org/10.1007/s11306-012-0434-4.

(195) Sumner, L. W.; Amberg, A.; Barrett, D.; Beale, M. H.; Beger, R.; Daykin, C. A.; Fan, T. W.-M.; Fiehn, O.; Goodacre, R.; Griffin, J. L.; Hankemeier, T.; Hardy, N.; Harnly, J.; Higashi, R.; Kopka, J.; Lane, A. N.; Lindon, J. C.; Marriott, P.; Nicholls, A. W.; Reily, M. D.; Thaden, J. J.; Viant, M. R. Proposed Minimum Reporting Standards for Chemical Analysis: Chemical Analysis Working Group (CAWG) Metabolomics Standards Initiative (MSI). *Metabolomics* **2007**, *3* (3), 211–221. https://doi.org/10.1007/s11306-007-0082-2.

(196) Hebert, A. S.; Richards, A. L.; Bailey, D. J.; Ulbrich, A.; Coughlin, E. E.; Westphall, M. S.; Coon, J. J. The One Hour Yeast Proteome. *Mol Cell Proteomics* **2014**, *13* (1), 339–347. https://doi.org/10.1074/mcp.M113.034769.

(197) Shishkova, E.; Hebert, A. S.; Coon, J. J. Now, More Than Ever, Proteomics Needs Better Chromatography. *Cell Systems* **2016**, *3* (4), 321–324. https://doi.org/10.1016/j.cels.2016.10.007.

(198) Webb, K. J.; Xu, T.; Park, S. K.; Yates, J. R. Modified MuDPIT Separation Identified 4488 Proteins in a System-Wide Analysis of Quiescence in Yeast. *Journal of Proteome Research* **2013**, *12* (5), 2177–2184. https://doi.org/10.1021/pr400027m.

(199) Broeckhoven, K.; Desmet, G. Advances and Innovations in Liquid Chromatography Stationary Phase Supports. *Anal. Chem.* **2021**, *93* (1), 257–272. https://doi.org/10.1021/acs.analchem.0c04466.

(200) Walter, T. H.; Andrews, R. W. Recent Innovations in UHPLC Columns and Instrumentation. *TrAC Trends in Analytical Chemistry* **2014**, *63*, 14–20. https://doi.org/10.1016/j.trac.2014.07.016.

(201) De Smet, J.; Gzil, P.; Vervoort, N.; Verelst, H.; Baron, G. V.; Desmet, G. On the Optimisation of the Bed Porosity and the Particle Shape of Ordered Chromatographic Separation Media. *Journal of Chromatography A* **2005**, *1073* (1), 43–51. https://doi.org/10.1016/j.chroma.2004.10.008.

(202) Guiochon, G. Monolithic Columns in High-Performance Liquid Chromatography. *Journal of Chromatography A* **2007**, *1168* (1), 101–168. https://doi.org/10.1016/j.chroma.2007.05.090.

(203) Horie, K.; Sato, Y.; Kimura, T.; Nakamura, T.; Ishihama, Y.; Oda, Y.; Ikegami, T.; Tanaka, N. Estimation and Optimization of the Peak Capacity of One-Dimensional Gradient High Performance Liquid Chromatography Using a Long Monolithic Silica Capillary Column. *Journal of Chromatography A* **2012**, *1228*, 283–291. https://doi.org/10.1016/j.chroma.2011.12.088.

(204) Jorgenson, J. W.; Guthrie, E. J. Liquid Chromatography in Open-Tubular Columns : Theory of Column Optimization with Limited Pressure and Analysis Time, and Fabrication of Chemically Bonded Reversed-Phase Columns on Etched Borosilicate

Glass Capillaries. *Journal of Chromatography A* **1983**, *255*, 335–348. https://doi.org/10.1016/S0021-9673(01)88293-5.
(205) Ahmed, M. A.; Felisilda, B. M. B.; Quirino, J. P. Recent Advancements in Open-Tubular Liquid Chromatography and Capillary Electrochromatography during 2014–2018. *Analytica Chimica Acta* **2019**, *1088*, 20–34. https://doi.org/10.1016/j.aca.2019.08.016.
(206) Yang, Y.; Liu, S. Non-Porous Thin Dense Layer Coating: Key to Achieving Ultrahigh Peak Capacities Using Narrow Open Tubular Columns. *Talanta Open* **2020**, *1*, 100003. https://doi.org/10.1016/j.talo.2020.100003.
(207) Vargas Medina, D. A.; Pereira dos Santos, N. G.; da Silva Burato, J. S.; Borsatto, J. V. B.; Lanças, F. M. An Overview of Open Tubular Liquid Chromatography with a Focus on the Coupling with Mass Spectrometry for the Analysis of Small Molecules. *Journal of Chromatography A* **2021**, *1641*, 461989. https://doi.org/10.1016/j.chroma.2021.461989.
(208) Xiang, P.; Yang, Y.; Zhao, Z.; Chen, A.; Liu, S. Experimentally Validating Open Tubular Liquid Chromatography for a Peak Capacity of 2000 in 3 h. *Anal. Chem.* **2019**, *91* (16), 10518–10523. https://doi.org/10.1021/acs.analchem.9b01465.
(209) Yang, Y.; Xiang, P.; Chen, A.; Liu, S. Liquid Chromatographic Separation Using a 2 Mm i.d. Open Tubular Column at Elevated Temperature. *Anal. Chem.* **2021**. https://doi.org/10.1021/acs.analchem.1c00296.
(210) Sorensen, M. J.; Kennedy, R. T. Capillary Ultrahigh-Pressure Liquid Chromatography-Mass Spectrometry for Fast and High Resolution Metabolomics Separations. *Journal of Chromatography A* **2021**, *1635*, 461706. https://doi.org/10.1016/j.chroma.2020.461706.
(211) Franklin, E. G. Utilization of Long Columns Packed with Sub-2 Um Particles Operated at High Pressures and Elevated Temperatures for High-Efficiency One-Dimensional Liquid Chromatographic Separations. The University of North Carolina at Chapel Hill 2012.
(212) Moore, S. M. Separation and Identification Techniques for Membrane Proteins Using Ultra-High Pressure Liquid Chromatography Coupled to Mass Spectrometry. *The University of North Carolina at Chapel Hill* **2016**.
(213) Blaženović, I.; Kind, T.; Sa, M. R.; Ji, J.; Vaniya, A.; Wancewicz, B.; Roberts, B. S.; Torbašinović, H.; Lee, T.; Mehta, S. S.; Showalter, M. R.; Song, H.; Kwok, J.; Jahn, D.; Kim, J.; Fiehn, O. Structure Annotation of All Mass Spectra in Untargeted Metabolomics. *Anal. Chem.* **2019**, *91* (3), 2155–2162. https://doi.org/10.1021/acs.analchem.8b04698.
(214) Chen, L.; Zhong, F.; Zhu, J. Bridging Targeted and Untargeted Mass Spectrometry-Based Metabolomics via Hybrid Approaches. *Metabolites* **2020**, *10* (9). https://doi.org/10.3390/metabo10090348.
(215) Wouters, S.; Dores-Sousa, J. L.; Liu, Y.; Pohl, C. A.; Eeltink, S. Ultra-High-Pressure Ion Chromatography with Suppressed Conductivity Detection at 70 MPa Using Columns Packed with 2.5 Mm Anion-Exchange Particles. *Anal. Chem.* **2019**, *91* (21), 13824–13830. https://doi.org/10.1021/acs.analchem.9b03283.
(216) He, Y.; Rashan, E. H.; Linke, V.; Shishkova, E.; Hebert, A. S.; Jochem, A.; Westphall, M. S.; Pagliarini, D. J.; Overmyer, K. A.; Coon, J. J. Multi-Omic Single-Shot Technology for Integrated Proteome and Lipidome Analysis. *Anal. Chem.* **2021**. https://doi.org/10.1021/acs.analchem.0c04764.

(217) Malkin, D. S.; Wei, B.; Fogiel, A. J.; Staats, S. L.; Wirth, M. J. Submicrometer Plate Heights for Capillaries Packed with Silica Colloidal Crystals. *Analytical Chemistry* **2010**, *82* (6), 2175–2177. https://doi.org/10.1021/ac100062t.
(218) Rogers, B. J.; Birdsall, R. E.; Wu, Z.; Wirth, M. J. RPLC of Intact Proteins Using Sub-0.5 Mm Particles and Commercial Instrumentation. *Analytical Chemistry* **2013**, *85* (14), 6820–6825. https://doi.org/10.1021/ac400982w.
(219) Rogers, B. J.; Wirth, M. J. Slip Flow through Colloidal Crystals of Varying Particle Diameter. *ACS Nano* **2013**, *7* (1), 725–731. https://doi.org/10.1021/nn305028f.
(220) Wei, B.; Rogers, B. J.; Wirth, M. J. Slip Flow in Colloidal Crystals for Ultraefficient Chromatography. *J. Am. Chem. Soc.* **2012**, *134* (26), 10780–10782. https://doi.org/10.1021/ja304177m.
(221) Smits, W.; Deridder, S.; Desmet, G. Theoretical Study on the Impact of Slip Flow on Chromatographic Performance. *Journal of Chromatography A* **2014**, *1366*, 120–125. https://doi.org/10.1016/j.chroma.2014.09.027.
(222) Eisenhofer, G.; Kopin, I. J.; Goldstein, D. S. Catecholamine Metabolism: A Contemporary View with Implications for Physiology and Medicine. *Pharmacol Rev* **2004**, *56* (3), 331–349. https://doi.org/10.1124/pr.56.3.1.
(223) Flak, J. N.; Goforth, P. B.; Dell'Orco, J.; Sabatini, P. V.; Li, C.; Bozadjieva, N.; Sorensen, M.; Valenta, A.; Rupp, A.; Affinati, A. H.; Cras-Méneur, C.; Ansari, A.; Sacksner, J.; Kodur, N.; Sandoval, D. A.; Kennedy, R. T.; Olson, D. P.; Myers, M. G. Ventromedial Hypothalamic Nucleus Neuronal Subset Regulates Blood Glucose Independently of Insulin. *Journal of Clinical Investigation* **2020**, *130* (6), 10.1172/JCI134135. https://doi.org/10.1172/JCI134135.
(224) Evers, S. S.; Kim, K.-S.; Bozadjieva, N.; Lewis, A. G.; Farris, D.; Sorensen, M. J.; Kim, Y.; Whitesall, S. E.; Kennedy, R. T.; Michele, D. E.; Seeley, R. J.; Sandoval, D. A. Continuous Glucose Monitoring Reveals Glycemic Variability and Hypoglycemia after Vertical Sleeve Gastrectomy in Rats. *Molecular Metabolism* **2020**, *32*, 148–159. https://doi.org/10.1016/j.molmet.2019.12.011.
(225) Armbruster, D. A.; Pry, T. Limit of Blank, Limit of Detection and Limit of Quantitation. *Clin Biochem Rev* **2008**, *29* (Suppl 1), S49–S52.
(226) Schliebs, R.; Arendt, T. The Significance of the Cholinergic System in the Brain during Aging and in Alzheimer's Disease. *J Neural Transm* **2006**, *113* (11), 1625–1644. https://doi.org/10.1007/s00702-006-0579-2.
(227) Scheja, L.; Heeren, J. The Endocrine Function of Adipose Tissues in Health and Cardiometabolic Disease. *Nat Rev Endocrinol* **2019**, *15* (9), 507–524. https://doi.org/10.1038/s41574-019-0230-6.
(228) Shackman, H. M.; Shou, M.; Cellar, N. A.; Watson, C. J.; Kennedy, R. T. Microdialysis Coupled On-Line to Capillary Liquid Chromatography with Tandem Mass Spectrometry for Monitoring Acetylcholine in Vivo. *J Neurosci Methods* **2007**, *159* (1), 86–92. https://doi.org/10.1016/j.jneumeth.2006.06.020.
(229) Jun, H.; Yu, H.; Gong, J.; Jiang, J.; Qiao, X.; Perkey, E.; Kim, D.; Emont, M. P.; Zestos, A. G.; Cho, J.-S.; Liu, J.; Kennedy, R. T.; Maillard, I.; Xu, X. Z. S.; Wu, J. An Immune-Beige Adipocyte Communication via Nicotinic Acetylcholine Receptor Signaling. *Nat Med* **2018**, *24* (6), 814–822. https://doi.org/10.1038/s41591-018-0032-8.

(230) Kennedy, R. T. Emerging Trends in in Vivo Neurochemical Monitoring by Microdialysis. *Current Opinion in Chemical Biology* **2013**, *17* (5), 860–867. https://doi.org/10.1016/j.cbpa.2013.06.012.
(231) Ngernsutivorakul, T.; White, T. S.; Kennedy, R. T. Microfabricated Probes for Studying Brain Chemistry: A Review. *ChemPhysChem* **2018**, *19* (10), 1128–1142. https://doi.org/10.1002/cphc.201701180.
(232) Ngernsutivorakul, T.; Steyer, D. J.; Valenta, A. C.; Kennedy, R. T. In Vivo Chemical Monitoring at High Spatiotemporal Resolution Using Microfabricated Sampling Probes and Droplet-Based Microfluidics Coupled to Mass Spectrometry. *Anal. Chem.* **2018**, *90* (18), 10943–10950. https://doi.org/10.1021/acs.analchem.8b02468.
(233) Valenta, A. C.; D'Amico, C. I.; Dugan, C. E.; Grinias, J. P.; Kennedy, R. T. A Microfluidic Chip for On-Line Derivatization and Application to *in Vivo* Neurochemical Monitoring. *Analyst* **2021**, 10.1039.D0AN01729A. https://doi.org/10.1039/D0AN01729A.
(234) Denisov, I. G.; Sligar, S. G. Nanodiscs for Structural and Functional Studies of Membrane Proteins. *Nature Structural & Molecular Biology* **2016**, *23* (6), 481–486. https://doi.org/10.1038/nsmb.3195.
(235) Denisov, I. G.; Grinkova, Y. V.; Lazarides, A. A.; Sligar, S. G. Directed Self-Assembly of Monodisperse Phospholipid Bilayer Nanodiscs with Controlled Size. *J. Am. Chem. Soc.* **2004**, *126* (11), 3477–3487. https://doi.org/10.1021/ja0393574.
(236) Thompson, J. D.; Carr, P. W. High-Speed Liquid Chromatography by Simultaneous Optimization of Temperature and Eluent Composition. *Anal. Chem.* **2002**, *74* (16), 4150–4159. https://doi.org/10.1021/ac0112622.
(237) Snyder, L. R.; Dolan, J. W. *High-Performance Gradient Elution: The Practical Application of the Linear-Solvent-Strength Model*; John Wiley & Sons, 2007.
(238) Snyder, L. R.; Dolan, J. W.; Gant, J. R. Gradient Elution in High-Performance Liquid Chromatography. *Journal of Chromatography A* **1979**, *165* (1), 3–30. https://doi.org/10.1016/S0021-9673(00)85726-X.
(239) Gilar, M.; Daly, A. E.; Kele, M.; Neue, U. D.; Gebler, J. C. Implications of Column Peak Capacity on the Separation of Complex Peptide Mixtures in Single- and Two-Dimensional High-Performance Liquid Chromatography. *Journal of Chromatography A* **2004**, *1061* (2), 183–192. https://doi.org/10.1016/j.chroma.2004.10.092.